HELSINKI UNIVERSITY OF TECHNOLOGY
Department of Electrical and Communications Engineering

Ville-Veikko Aallos

Spectrometer Demonstrator with Dynamic Diffraction Gratings for Space Applications

Master's Thesis submitted in partial fulfillment of the requirements for the degree of Master of Science in Technology.

Espoo, September 5, 2008

Supervisor: Prof. Martti Hallikainen, Helsinki University of Technology

Instructor: M.Sc (Tech) Kai Viherkanto, VTT Technical Research Centre of Finland

HELSINKI UNIVERSITY OF TECHNOLOGY

ABSTRACT OF THE MASTER'S THESIS

Author:	Ville-Veikko Aallos	
Title:	Spectrometer Demonstrator with Dynamic Diffraction Gratings for Space Applications	
Date:	September 5, 2008	**Number of pages:** 94 + 20
Department:	Department of Electrical and Communications Engineering	
Professorship:	S-92 Space Engineering	
Supervisor:	Prof. Martti Hallikainen	
Instructor:	M.Sc (Tech) Kai Viherkanto	

This thesis describes the feasibility of Programmable Micro Diffraction Gratings (PMDG), as they are commercially available today, to be used in optical data processing or as a spatial light modulator in spectrometers for miniature space instruments. The main goal was to characterise the component performance and restrictions and to develop a simple laboratory instrument to demonstrate its use and abilities. Compared to the traditional spectrometers in the infrared region, this instrument has no moving parts and has a very simple overall design.

The procured component was characterised and found to have restrictions to the instrument design with its very high f-number requirements. Available spatial direction was also limited to support only few spatial pixels in imaging systems. The usable spectral range is from mid visible to about 1600 nm. The instrument demonstrator was designed based on the performance of the component. It can use both a spectral line scan and a Hadamard transform for spectrum recovery as well as optical correlation with approximated spectral angle mapper method used in hyperspectral data processing.

The instrument demonstrator with very simple optical design and a single detector element was characterised in the wavelength range of 600-1060 nm with a series of tests including wavelength accuracy, spectral resolution, stability, throughput and some correlation measurements. The low throughput ($<0.1\%$) is the main weakness of the system design.

The results indicate that the PMDG devices are promising candidates for future space instruments but the technology is not quite there yet. As the technology matures and the production costs get lower, custom designed components will be more readily available.

Keywords: diffraction, spatial light modulation, PMDG, spectral imaging, spectrometry

TEKNILLINEN KORKEAKOULU DIPLOMITYÖN TIIVISTELMÄ

Tekijä:	Ville-Veikko Aallos	
Työn nimi:	Dynaamisia hiloja käyttävä spektrometridemonstraattori avaruussovellutuksiin	
Päivämäärä:	5.9.2008	**Sivuja:** 94 + 20
Osasto:	Sähkö- ja tietoliikennetekniikan osasto	
Professuuri:	S-92 Avaruustekniikka	
Työn valvoja:	Prof. Martti Hallikainen	
Työn ohjaaja:	DI Kai Viherkanto	

Tässä työssä tutkitaan nykyisten kaupallisesti saatavilla olevien ohjelmoitavien mikrohilojen toimivuutta optisessa datan käsittelyssä tai valon moduloinnissa pienissä avaruusinstrumenteissa käytettävissä spektrometreissä. Päämääränä oli selvittää hilakomponentin suorituskyky sekä tuottaa yksinkertainen laboratorioinstrumentti sen ominaisuuksien ja käyttömahdollisuuksien esittelemiseen. Perinteisiin infrapuna-alueella käytettävissä oleviin spektrometreihin verrattuna tämä laite on hyvin yksinkertainen toteutukseltaan eikä sisällä yhtään liikkuvia osia.

Hankitun komponentin suorituskyvyn määritys paljasti, ettei kyseistä komponenttia voi istuttaa kaikkiin instrumentteihin sen vaatimien korkeiden f-lukujen takia. Käytettävissä oleva spatiaalisuunta ei myöskään sovi kuvaaville instrumenteille. Käytettävissä oleva spektrialue on puolesta välistä näkyvää valoa noin 1600 nanometriin. Suorityskyvyn mukaan suunniteltu testilaite voi mitata spektrin sekä viivaskannauksella että Hadamard-muunnoksella ja kykenee myös optiseen korrelointiin hyperspektraalisen datan käsittelyssä käytettävän menetelmän approksimaatiolla.

Testilaitteen, jolla on yksinkertainen optinen rakenne ja yksi ilmaisinelementti, ominaisuudet määritettiin 600-1060 nm alueella. Testeihin kuului aallonpituustarkkuus, spektrierottelukyky, vakaus, kokonaisvalotehon läpäisy sekä joitakin korrelointimittauksia. Alhainen kokonaisvalotehon läpäisy ($<0.1\%$) on tämän rakenteen suurin heikkous.

Työn tuloksista voidaan päätellä, että ohjelmoitavilla mikrohiloilla voi olla käyttöä tulevissa instrumenteissa, mutta teknologia ei ole ihan vielä sillä tasolla. Tilaajan tarpeiden mukaan suunniteltujen komponenttien tarjonta paranee varmasti tulevaisuudessa tekniikan kehittyessä ja tuotantokustannuksien muuttuessa halvemmiksi.

Avainsanat: valon modulointi, PMDG, spektraalinen kuvantaminen, spektrometria

Acknowledgements

The work described in this Master's thesis was conducted at the Optical Sensors and Space Instruments team of VTT Technical Research Centre of Finland during 2007-2008. The team is lead by D.Sc (Tech) Heikki Saari. The work was part of the project under the contract AO/1-5196/06/NL/SFe of the European Space Agency (ESA). I would like to thank the project participants, VTT and ESA, for giving me this opportunity to work with this exciting and new technology. The work was challenging and very educational.

I would like to thank my instructor M.Sc (Tech) Kai Viherkanto for his advice and guidance during this work. I would also like to thank my supervisor Prof. Martti Hallikainen for accepting to supervise this work and for all his guidelines.

I wish to thank all my fellow workers at the Optical Sensors and Space Instruments team for their help along this educational task. Special thanks go to Mr. Christer Holmlund and Mr. Rami Mannila for their expert advice.

Finally, I would like to express my greatest gratitude to my family and friends for enduring me and for their support during my studies and during this work.

Espoo, September 5, 2008

Ville-Veikko Aallos

Contents

Notations

A	area	[m^2]
B_{noise}	noise bandwidth	[Hz]
C	capacitance	[F]
c	speed of light in vacuum	[m/s]
D	angular dispersion	[°/nm]
D_l	diameter of a lens	[m]
D_T	diagonal transmission correction matrix	
d	groove spacing of a grating	[m]
E	energy of a photon	[J]
E_e	electrostatic energy	[J]
E_g	gap energy	[eV]
E_λ	spectral irradiance	[$Wm^{-2}nm^{-1}$]
e_i	random error	
F_e	electrostatic force	[N]
f	focal length	[m]
f'	effective focal length	[m]
$f/\#$	f-number	
$FWHM$	full-width at half-maximum	[nm]

H_n	Hadamard matrix of size n	
h	Planck's constant	[Js]
I_λ	spectral radiant intensity	[$\mathrm{Wsr^{-1}nm^{-1}}$]
I_n	Identity matrix of size n	
i	integer	
i_D	dark-current	[A]
k	size of the Hadamard simplex	
L_λ	spectral radiance	[$\mathrm{Wm^{-2}sr^{-1}nm^{-1}}$]
MSE	mean square error	
m	diffraction or spectral order	
N	number of grooves illuminated	
n	size of the Hadamard matrix	
NEP	noise equivalent power	[$\mathrm{W}/\sqrt{Hz}$]
P	reciprocal linear dispersion	[nm/mm]
Q	radiant energy	[J]
R	resolving power	
R_L	feedback or load resistor	[Ω]
r	radius	[m]
$\Re$	responsivity	[A/W]
S_k	Hadamard simplex of size k	
S^{-1}	inverse matrix of S	
SNR	signal-to-noise ratio	
t	time	[s]
V	voltage	[V]

V_{PI}	pull-in voltage	[V]
x	distance	[m]
x_0	initial distance	[m]
α	incident angle	[°]
β	diffraction angle	[°]
β_m	diffraction angle for diffraction order m	[°]
δ	displacement	[m]
ϵ_0	dielectric constant of vacuum	[Fm^{-1}]
ϵ_r	relative permittivity	
η_0	diffraction efficiency for zero order	
η_i	measurement result	
κ	spring constant	[Nm^{-1}]
λ	wavelength	[m]
σ	average noise	[V]
τ_{oi}	transmission in opaque state for i^{th} spectral component	
τ_{ti}	transmission in transmissive state for i^{th} spectral component	
Φ_λ	spectral radiant flux	[W/nm]
φ	angle between incident light and plane perpendicular to the grooves	[°]
Ψ	real value of the target	
Ψ'	best estimation for the real value of the target	
ψ	angle between normal and observation direction	[°]
Ω	solid angle	[sr]

Abbreviations

CWL	Centre Wavelength
DSP	Digital Signal Processor
DTS	Digital Transform Spectrometer
DWDM	Dense Wavelength Division Multiplexing
ESA	European Space Agency
ESTEC	European Space Research and Technology Centre
FWHM	Full-Width at Half-Maximum
GEMS	Grating Electro-Mechanical System
GLM	Grating Light Modulator
GLV	Grating Light Valve
HTS	Hadamard Transform Spectrometry
IHT	Inverse Hadamard Transform
IR	Infrared
LCROSS	Lunar CRater Observation and Sensing Satellite
LVBF	Linear Variable Bandpass Filter
MCG	MEMS Compound Grating
MEMS	Micro-Electro-Mechanical System
MOEMS	Micro-Opto-Electro-Mechanical System

MSE	Mean Square Error
NASA	National Aeronautics and Space Administration
NEP	Noise Equivalent Power
NIR	Near Infrared
PCB	Printed Circuit Board
PMDG	Programmable Micro Diffraction Grating
SAM	Spectral Angle Mapper
SNR	Signal-to-Noise Ratio
SPL	Spatial Light Modulator
TDI	Time Delay and Integration
VIS	Visible
WDM	Wavelength Division Multiplexing

List of Figures

List of Tables

Chapter 1

Introduction

The number of space projects involving low-cost micro-satellites or instruments on rovers is increasing and creates stringent requirements on the cost, size, weight, reliability, and power consumption of optical instruments. The use of micro- or nano-technologies to produce application-specific microinstruments allows the production of miniaturised instruments. Micro-Electro-Mechanical Systems (MEMS) or Micro-Opto-Electro-Mechanical Systems (MOEMS) are being developed to be used in such devices. The ongoing exploitation of MEMS technology has recently surfaced a new type of device called Programmable Micro Diffraction Grating or PMDG for short. The advantages of such a device, like of all MEMS devices, are their small size, fast response time and programmability. [1]

A PMDG is a MEMS based component which is usually made of an array of long thin bendable ribbons fabricated on a silicon substrate [2]. There are different types of PMDGs, some have the ability to change blaze angle or to change grating pitch via stretching, but usually the controllable attribute is the vertical deflection of the ribbons. Some PMDGs let you tune the vertical position of each ribbon individually and some designs do not have separate ribbons but instead a fixed grating plate whose position can be deflected by applying a voltage. The depth of these deflections varies from zero or half of incident wavelength to a quarter of incident wavelength depending on the applied voltage. The zero or $\frac{\lambda}{2}$ deflection acts as a specular mirror surface and the quarter of a wavelength deflection acts as a fully diffracting surface for $0°$ angle of incidence [2]. The diffracting angle β depends on the incident wavelength λ and is described by Equation 2.20.

1.1 Background

Several instruments have been successfully developed using PMDGs and all of them are used for industrial applications on Earth. Contrarily to a static grating, with a PMDG that allows individual control over all elements, the diffraction direction can be tuned by changing the device profile in time. Thus a PMDG in principle allows a full control of the spectral content of the diffracted light on a sub-millisecond time scale. The potential of this technology for instruments used in space missions has never been investigated in Europe, although it is a promising candidate for micro-satellites and future low-cost missions' instruments. The Hadamard spectrometer from Polychromix illustrates the potential of PMDG devices. The main advantage lies in the fact that with a PMDG device only a single detector element is needed where usually a linear detector or scanning grating is required, thus increasing the cost and size of the instrument. PMDG components are also the only spatial light modulators available for the infrared domain.

The concept of micro-satellites has been around since the 1960s. From the start they have made use of the rapid development of modern electronic devices, whereas the conventional satellites mostly use electronics that have had years of working history. Typical micro-satellites weigh less than 100 kg compared to the conventional satellites that often weigh more than 1000 kg. [3, 4]

Micro-satellites can offer relatively inexpensive means of exploring well-focused, small-scale science objectives as well as working as a proof-of-concept for larger and more expensive instrumentation. They have been a real success in Earth observation. Conventional Earth-observation and remote-sensing satellite missions cost hundreds of millions of dollars and thus there are relatively few such missions. The data they provide is superb in spatial and spectral resolution but because of the low number of such instruments on orbit, the revisit period for ground targets is poor. With reduced spectral and spatial performance the micro-satellites can be launched into orbit for a few million dollars thus making it possible to have much better temporal resolution with a multiple satellite system than with their larger cousins. [3, 4]

1.2 Objectives and Contents of the Thesis

The objective of this thesis is to study the feasibility of using Programmable Micro Diffraction Gratings in various space devices that need access to spectral information. As this is only a feasibility study, the work is done by using commercially available PMDGs and the objective is not to build a PMDG component. At this

point the PMDG components are not useful enough to be used solely as a dispersive component but rather as a spatial light modulator (SPL) that will modulate the already dispersed spectra.

Remote sensing theories, optical instruments in space missions and applications for short range remote sensing, as well as classic and programmable diffraction gratings are studied in Chapter 2. Proposed instrument concepts for PMDG devices are introduced and discussed in Chapter 3. Chapter 4 describes the characterisation measurements carried out for the chosen PMDG component. The simulations carried out for the proposed concept as well as the optical design and characterisations for the whole instrument are reported in Chapter 5. Conclusions are presented in Chapter 6.

All surveys, measurements, software development, analysis and discussion in this Master's Thesis are done by the author. The concepts presented in Chapter 3, the diffraction efficiency simulator used in Chapter 4 and the detailed opto-mechanical design of the demonstrator were created by the other members of the team.

Chapter 2

Previous Work

In this chapter, the principles of remote sensing as well as the working principles of diffraction gratings are being presented. At the end of this chapter, the work previously done on PMDG components is also reviewed.

2.1 Principles of Remote Sensing

Remote sensing describes instrument-based techniques used for observation and imaging of the surface of the Earth from finite distance using various areas of the electromagnetic spectrum (Figure 2.1) either passively or actively [5]. The mostly

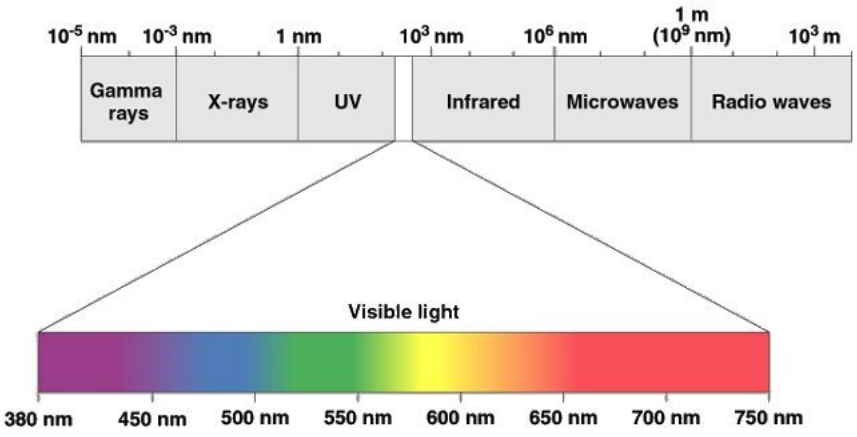

Figure 2.1. Electromagnetic spectrum between gamma rays and radio waves. The band visible to human eye is a small fraction of a whole spectrum between ultraviolet and infrared.

used bands are visible, infrared and microwaves. Active instruments, like weather

radar, measure the reflected or backscattered signal they usually transmit in the microwave region. Passive instruments, on the other hand, detect natural radiation that is emitted or reflected by the object being observed. Reflected sunlight is the most common source of radiation measured by passive instruments [4]. The radiant energy of electromagnetic radiation is defined by

$$Q = \frac{hc}{\lambda}, \tag{2.1}$$

where $h = 6.6262 \cdot 10^{-34}$ Js is Planck's constant, c is the speed of light and λ is the wavelength [6]. Optical instruments usually measure the spectral radiance which is the radiant power leaving an element of the surface, ∂A, to a certain solid angle, $\partial\Omega$, as illustrated in Figure 2.2. Spectral radiant flux Φ_λ defines the rate at which radiant energy is transferred from surface to surface and is defined by [6]

$$\Phi_\lambda = \frac{\partial^2 Q}{\partial t \cdot \partial \lambda}, \tag{2.2}$$

where Q is the radiant energy, t is time and λ is the wavelength. Spectral irradiance E_λ defines the power of the electromagnetic radiation incident on a certain surface area and spectral radiant exitance M_λ defines the power emitted from a certain surface area and are both defined by [6]

$$E_\lambda = M_\lambda = \frac{\partial \Phi_\lambda}{\partial A}, \tag{2.3}$$

where A is the area of the element. Spectral radiant intensity I_λ defines the radiant power radiating to certain solid angle and is defined by [6]

$$I_\lambda = \frac{\partial \Phi_\lambda}{\partial \Omega}, \tag{2.4}$$

where Ω is the solid angle. Spectral radiance can then be defined as [6]

$$L_\lambda = \frac{\partial^2 \Phi_\lambda}{\partial \Omega \cdot \partial A \cdot \cos\psi}. \tag{2.5}$$

where ψ is the angle between the normal of the element and the observation direction.

2.2 Optical Instruments in Space Missions

Micro-satellites and miniature instruments are typically engineered specifically to fulfill their mission objectives and nothing more with minimum costs. This means

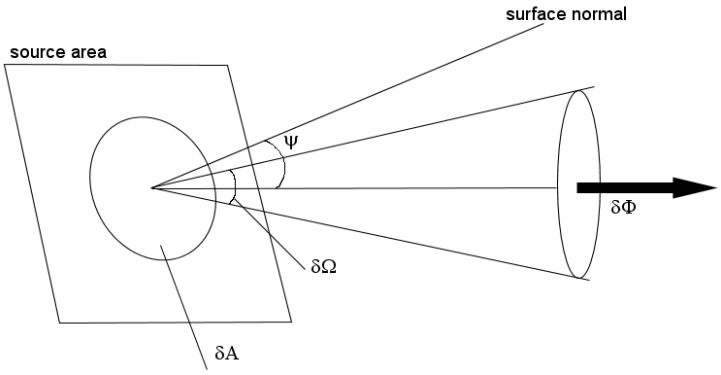

Figure 2.2. Definition of radiance. Radiance is the radiant power leaving an element of the surface, ∂A, to a certain solid angle, $\partial\Omega$. $\partial\Phi$ is the radiant flux as defined in Equation 2.2.

that the mission objectives can be carefully traded against cost to achieve this goal. Despite of low cost, micro-satellites usually tend to make maximum use of state-of-the-art technology to achieve complex functionality. Usually more onboard data processing is used to save only the essential data thus reducing the need for a large onboard storage capacity. [3, 4]

The main applications for optical instruments in space missions are as follows:

- remote sensing of planetary surfaces
- remote sensing of planetary atmospheres, impact or erupting ejecta
- space astronomy
- short range remote sensing from a lander or rover
- space station applications
- other applications (communications, attitude control etc).

The main application for a diffraction grating is spectroscopy which takes advantage of the gratings' ability to disperse light to its constituent monochromatic wavelength components. PMDGs can also be used for spatiotemporal modulation for which the applications are more diverse (image/video projection, telecom switching, spectral filtering and manipulation), but the main space application is still spectroscopy. Even though the current generation of programmable micro diffraction gratings are more suitable as spatial light modulators than as the main dispersive

element, the spectrometers are prominent candidates for this technology. For miniature instruments and single-point spectrometers, lander and rover missions are the ones that will get the most out of the new technology at this point.

2.2.1 Short Range Remote Sensing From a Lander or Rover

In these applications both long integration times and strong sources can be possible. However, the mass and power budgets of such missions are extremely stringent and compromises in instrument performances are accepted. For example the NASA Mars rovers Spirit and Opportunity weigh a total of 180 kg from which only 5 kg is for scientific payload. The Mars Science Laboratory rover, scheduled for launch in September 2009, is expected to include over ten times more payload from a total mass of about 800 kg [7].

The aperture sizes are more compatible with the current PMDG components. A reconfigurable instrument is highly desirable to gain access to larger wavelength band. In the future it will be possible to manufacture a PMDG with narrow elements so closely spaced, that with independent elements it would be possible to reconfigure a single base structure to a wide range of different gratings. Miniaturisation is possible by sacrificing performance, eliminating mechanisms and eliminating detector arrays. PMDG based digital transform spectrometers (DTS) are expected to provide a competitive alternative to traditional Fourier transform and filter based multi-band spectrometers in the 1-20 μm domain, owing to their smaller size and programmability.

For medium resolution imaging spectrometers the PMDG component could be used as a spectral correlator. The grating could be programmed with key spectral features of the searched substance. When the dispersed spectra is modulated with this kind of spectral signature weighing, the areas where the spectrum correlates with the signature of the grating will be brighter in the image. This would lead to tremendous savings in the amounts of data that is generated thus reducing the need for large onboard storage but, on the other hand, the data has no use for any other task.

2.3 Hadamard Transform Spectrometry

For spectrometers with only one detecting element there are a few possible ways to measure the full spectrum of the target. Because the detectors are blind to different wavelengths, it means that every incoming photon that has more energy, $E = hc/\lambda$,

(to a certain point) than the required gap energy E_g to excite a free electron in the detecting medium, will do so. In order to know from the measured photocurrent from which wavelength the electrons were generated, it is possible to a) let only a narrow band of the spectrum hit the detector sequentially or to b) let multiple narrow bands hit the detector in such a way that the individual bands can later on be separated from the measurements.

For a simple three-colour RGB measurement, a line scan method means that first the light passes through a red filter and the detector measures the signal value plus the noise of the detector. Then the light passes through a green filter and the detector takes another signal-noise measurement and the same goes for the blue filter. We get the following results [8]

$$\begin{cases} \eta_1 &= \Psi_1 + e_1 \\ \eta_2 &= \Psi_2 + e_2 \\ \eta_3 &= \Psi_3 + e_3 \end{cases} \tag{2.6}$$

where η_i is the measurement result, Ψ_i is the real value of the target and e_i is the random error of the detector. The best approximation for the true values of the target are the same as was measured [8]

$$\begin{cases} \Psi'_1 &= \eta_1 &= \Psi_1 + e_1 \\ \Psi'_2 &= \eta_2 &= \Psi_2 + e_2 \\ \Psi'_3 &= \eta_3 &= \Psi_3 + e_3 \end{cases} \tag{2.7}$$

The difference between the real and the measured value is the error of the detector

$$\Psi'_i - \Psi_i = e_i.$$

The mean square error is [8]

$$MSE = E\{(\Psi'_i - \Psi_i)^2\} = E\{e_i^2\} = \sigma^2. \tag{2.8}$$

It is possible to do the same measurement so that first the light passes through both the red and blue filters and the detector measures the sum signal plus noise. Then the light passes through the green and blue filters and finally through the red and green filters. The individual signals can then be solved by solving the system of equations for the measurements [8]

$$\begin{cases} \eta_1 &= \Psi_1 + \Psi_3 + e_1 \\ \eta_2 &= \Psi_2 + \Psi_3 + e_2 \\ \eta_3 &= \Psi_1 + \Psi_2 + e_3 \end{cases} \tag{2.9}$$

The best approximations for the true values are now

$$\begin{cases} \Psi'_1 &= \frac{1}{2}(\eta_1 - \eta_2 + \eta_3) &= \Psi_1 + \frac{1}{2}(e_1 - e_2 + e_3) \\ \Psi'_2 &= \frac{1}{2}(-\eta_1 + \eta_2 + \eta_3) &= \Psi_2 + \frac{1}{2}(-e_1 + e_2 + e_3) \\ \Psi'_3 &= \frac{1}{2}(\eta_1 + \eta_2 - \eta_3) &= \Psi_3 + \frac{1}{2}(e_1 + e_2 - e_3) \end{cases} \tag{2.10}$$

The detector induced noise, however, will be somewhat smaller than in the first method, because the same noise is now distributed over multiple signal measurements. The mean square error of the measurements will be [8]

$$MSE = E\{(\Psi'_i - \Psi_i)^2\} = \frac{3\sigma^2}{4}. \tag{2.11}$$

For a small number of channels, the optimum multiplexing sequence, i.e. all the channels must be measured as many times, is rather easy to come by. For measurements that include hundreds of channels, the correct, optimum multiplexing theme is not so obvious. Hadamard matrices are solutions for such optimisations, hence the name Hadamard transform spectrometry (HTS).

Hadamard matrices are $n \times n$ matrices ($n = 1, 2, 4i$, where i is a positive integer) in which half of the values equal 1 and the other half -1, and whose rows are mutually orthogonal. This means that the matrices are formed in such a way that $H_n^T \times H_n = nI_n$, where H_n is the Hadamard matrix of size n and I_n is the identity matrix. Normalised Hadamard matrices are matrices whose first row and column consists of only $+1$. For optical systems the normalised Hadamard matrices are modified to consist of only ones and zeros because the spectral components can only be turned on or off but not made negative. The modification is done so that the 1s are transformed to zeros and -1s are transformed to ones. In addition, the first row and column are removed because they now consist of only zeros. The modified matrices are called Hadamard simplex matrices, S, and for every row there is now $(k+1)/2$ ones and $(k-1)/2$ zeros [8, 9]. For a size k ($k = n-1$) Hadamard simplex S_k, the mean square error of the measurement is [8]

$$MSE = \frac{4k}{(k+1)^2}\sigma^2 \approx \frac{4\sigma^2}{k}, \tag{2.12}$$

for large k. This leads to the increase in signal-to-noise ratio (SNR) by a factor of $\frac{k+1}{2\sqrt{k}} \approx \frac{\sqrt{k}}{2}$, when k is large, which makes it a worthy scanning method for one detector systems. When photon noise (intensity fluctuations) of the target is dominant, it is better to use a single channel measurement over Hadamard method. When the noise generated in the detector is dominant, i.e. when measuring steady sources in the IR region or weak sources, better SNR can be achieved via Hadamard multiplexing [8].

The correct multiplexing pattern for each measurement point is written in the rows of the Hadamard simplex. The values of the independent channels can be solved from the size k measurement vector η by multiplying it with the inverse matrix of the used Hadamard simplex – $\Psi = S^{-1}\eta$. This is called inverse Hadamard transform (IHT) and it is true for ideal systems that pass all the light to the detector for every open channel and block all the light from closed channels independent of the wavelength. For real systems that have wavelength dependency on transmission, the demultiplexing is somewhat more complicated. [8, 10]

The T^{-1} method, described by R.A. Dyer in "Implementation problems in Hadamard transform spectrometry" [10], uses a more complicated inverse transform that is able to compensate for the nonidealities of the encoding mask. For the standard Hadamard transform the weighing scheme W is noted as $W = S$, where S is the weighing matrix (Hadamard simplex). For the T^{-1} method, the weighing scheme W is noted as $W = ST$, where S is the same as before and $T = D_T + (2/(k+1))\mathbf{1}\tau_o^T$ is based on the transmission of the encoding mask. The contents of T are [10]

$$D_T = diag(d_{11}, d_{22}, \ldots, d_{kk}) = diag(\tau_{t1} - \tau_{o1}, \tau_{t2} - \tau_{o2}, \ldots, \tau_{tk} - \tau_{ok}) \tag{2.13}$$

$$\mathbf{1} = (1, 1, \ldots, 1)^T \tag{2.14}$$

$$\tau_o = (\tau_{o1}, \tau_{o2}, \ldots, \tau_{ok})^T, \tag{2.15}$$

where τ_{ti} and τ_{oi} are transmissions in transmissive and opaque state according to proper wavelength range. T^{-1} can be written as [10]

$$T^{-1} = D_T^{-1} - qD_T^{-1}\mathbf{1}\tau_o^T D_T^{-1}, \text{ where} \tag{2.16}$$

$$q = \frac{2}{(k+1) + 2\sum_{i=1}^{k} \frac{\tau_{oi}}{d_{ii}}}, \tag{2.17}$$

and the inverse transform is now $\Psi = S^{-1}T^{-1}\eta$. [10]

2.4 Diffraction Gratings

A diffraction grating is formed of a regular pattern of parallel diffracting elements, such as a group of transparent slits in an opaque screen or reflecting grooves on a substrate, separated by a distance comparable to the wavelength of the light the grating is intended to be used on. Regardless of type, the working principle for a diffraction grating is the spatial modulation of the refractive index. When light incident on a grating is diffracted, its electric field amplitude and/or phase are modified by the grating in a predictable manner, due to the periodic variation in refractive index in the region near the surface of the grating. [11]

Diffraction gratings have found their uses in many applications including telecommunications where gratings are being used to increase the capacity of fibre-optic networks using wavelength division multiplexing (WDM), laser physics where gratings are used in tuning and spectrally shaping laser light as well as in chirped pulse amplification applications, astrophysics where gratings provide clues to the composition of and processes in stars and planetary atmospheres, and chemistry, toxicology and forensic science where grating-based instruments are used to determine the presence and concentration of chemical species in samples. The most important use of diffraction gratings is of course in spectroscopy due to its ability to separate (disperse) polychromatic light into its constituent monochromatic components. [11]

2.4.1 The Physics of Diffraction Gratings

Grating Equation

The physics of gratings are described here for reflective gratings as they are more common, but the working principle is the same for transmissive gratings as well. When monochromatic light is incident on a grating surface, it is diffracted into discrete directions. For a given spacing d between the grooves, the diffracted light from each groove is in phase with the light diffracted from any other groove, leading to constructive interference. This will lead to a unique set of separate angles where all the light is going. [11]

Diffraction by a reflecting grating is illustrated in Figure 2.3, which shows a light ray of wavelength λ incident at an angle α and diffracted by a grating along a set of angles β_m measured from the grating normal. The grating normal is shown as the dashed line perpendicular to the grating surface at its centre. The sign of the diffracted angles depends on whether the light is diffracted on the same side or the opposite side of the grating normal as the incident light. [11]

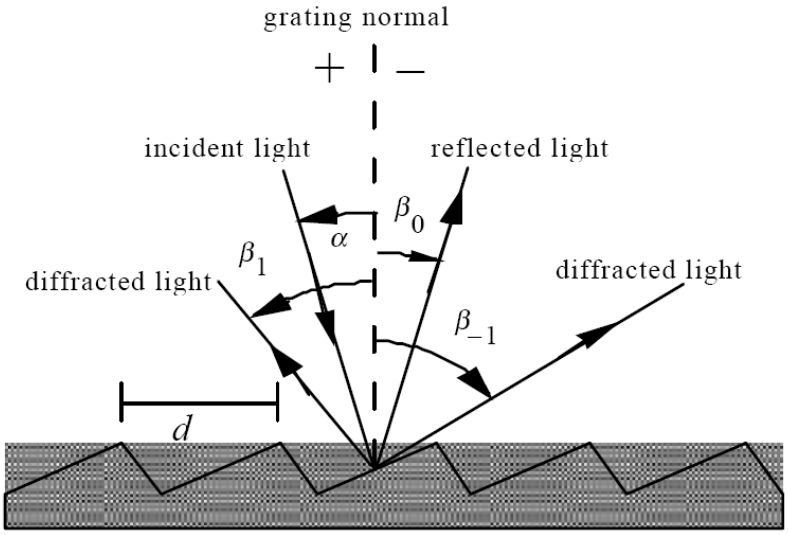

Figure 2.3. Diffraction by a reflective plane grating. A beam of monochromatic light of wavelength λ is incident on a grating and diffracted along several discrete angles. The sign convention for the angles α and β is shown by the + and − signs on either side of the grating normal. [11]

Another illustration of grating diffraction using wavefronts (surfaces of constant phase), is shown in Figure 2.4. The geometrical path difference between light from adjacent grooves is seen to be $d\sin\alpha + d\sin\beta$. The constructive interference requires that the light from adjacent grooves is in phase and that is true only when this difference or its integral multiple equals the wavelength λ of the light. At all other angles the rays originating from the groove facets will interfere destructively. [11]

The relationships between the incident light, diffracted light and groove spacing are expressed by the grating equation [11]

$$m\lambda = d(\sin\alpha + \sin\beta), \tag{2.18}$$

which governs the angular locations of the principal intensity maxima when light of wavelength λ is diffracted from a grating of groove spacing d. Here m is the diffraction order (or spectral order), which is an integer. The special case $m = 0$ leads to the law of reflection $\beta = -\alpha$ with reflective gratings. [11]

If the incident light beam is not perpendicular to the grooves, the grating equation must be modified to [11]

$$m\lambda = d\cos\varphi(\sin\alpha + \sin\beta), \tag{2.19}$$

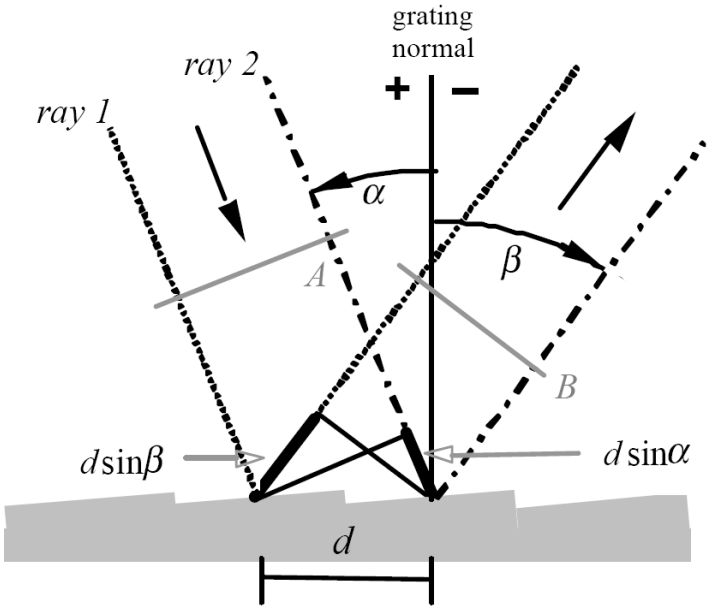

Figure 2.4. Geometry of diffraction for planar wavefronts. Two parallel rays, ray 1 and ray 2, are incident on the grating one groove spacing d apart and are in phase with each other at wavefront A. After diffraction, these rays will be in phase at diffracted wavefront B if the difference in their path lengths, $d\sin\alpha + d\sin\beta$, is an integral number of wavelength. [11]

where φ is the angle between the incident light path and the plane perpendicular to the grooves at the grating centre.

For a grating of groove spacing d, there is a purely mathematical relationship between the wavelength and the angles of incidence and diffraction. In a given spectral order m, the different wavelengths of polychromatic wavefronts incident at angle α are separated in angle [11]

$$\beta_m(\lambda) = \arcsin(\frac{m\lambda}{d} - \sin\alpha). \tag{2.20}$$

When $m = 0$, the grating acts as a mirror, and the wavelengths are not separated ($\beta = -\alpha$ for all λ). This is called specular reflection or simply the zero order. [11]

The grating equation shows that the shape of the grooves has no effect on the angles of the diffracted orders as they only depend on the groove density. The shape of the grooves does, however, have an effect on diffraction efficiency of the grating. By controlling the cross-sectional profile of the grooves, it is possible to concentrate most of the diffracted energy in a particular order for a given wavelength. A triangular

groove profile is the most commonly used. The shaping of the groove profile is called blazing. The incident angle and wavelength for which the diffraction is most efficient are often called blazing angle and blazing wavelength. [11]

As can be seen from Equation 2.20, there exists a large combination of values m and λ that satisfy the conditions for each β. These are called spectral diffraction orders and the orders of different wavelengths will overlap each other as illustrated in Figure 2.5. Overlapping orders must be filtered out if the detector is, for example, sensitive to all wavelengths.

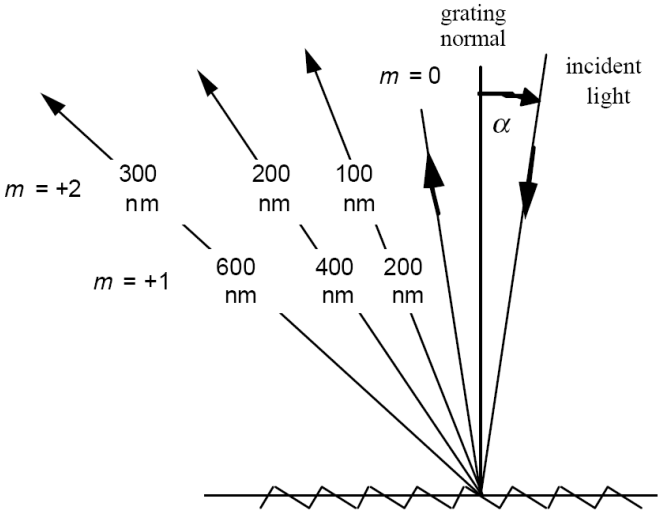

Figure 2.5. Overlapping of spectral diffraction orders. The light for wavelengths 100, 200 and 300 nm in the second order is diffracted in the same direction as the light for wavelengths 200, 400 and 600 nm in the first order. [11]

Dispersion

The primary purpose of diffraction gratings is to disperse light incident on its surface by wavelength. Monochromatic light will be diffracted into discrete angles and polychromatic light will be separated to its component wavelengths all diffracted into certain angles. The separation between diffracted light of different wavelengths is called dispersion. There are two methods to announce dispersion: angular dispersion expresses the spectral range per unit angle and linear dispersion expresses the spectral range per unit length. [11]

The angular dispersion D, that tells the angular difference $\Delta\beta$ between wavelengths λ and $\lambda + \Delta\lambda$ when the diffraction order m and the incident angle α remain

constant, can be obtained by differentiating the grating equation (2.18) [11]

$$D = \frac{\partial\beta}{\partial\lambda} = \frac{\sin\alpha + \sin\beta}{\lambda\cos\beta} = \frac{m}{d\cos\beta}. \tag{2.21}$$

The linear dispersion of a grating system is the product of the angular dispersion D and effective focal length f' of the system [11]

$$f'D = f'\frac{\partial\beta}{\partial\lambda} = \frac{(\sin\alpha + \sin\beta)f'}{\lambda\cos\beta} = \frac{mf'}{d\cos\beta}. \tag{2.22}$$

A more often used value is the reciprocal linear dispersion P [11]

$$P = \frac{d\cos\beta}{mf'}, \tag{2.23}$$

which tells the change in wavelength, in nanometres, corresponding to a change in location along the spectrum in millimetres.

Resolving Power

The resolving power R of a grating tells how well the grating can separate adjacent spectral lines of average wavelength λ. It can be defined as [11]

$$R = \frac{\lambda}{\Delta\lambda}, \tag{2.24}$$

where $\Delta\lambda$ is the difference in wavelength between two spectral lines of equal intensity. For a planar grating, theoretical R can be defined using the grating equation as [11]

$$R = mN = \frac{Nd(\sin\alpha + \sin\beta)}{\lambda}, \tag{2.25}$$

where N is the total number of grooves illuminated on the surface of the grating. Hence theoretically, a 2000 g/mm grating with a width of 60 mm that is used in first order has a numerical resolving power $R = 2000 \cdot 60 = 120000$. Therefore, at 600 nm, the bandpass is equal to

$$\Delta\lambda = \frac{600}{120000} = 0.005 \text{ nm}.$$

For real gratings, the value used for the resolving power, is usually half of the theoretical value.

2.5 Programmable Micro Diffraction Gratings

A PMDG is a MEMS based component which is usually made of an array of long thin bendable ribbons fabricated on a silicon substrate [2]. The positions of the ribbons can be actively modulated in order to provide phase shifts to an incoming light beam. The electromechanical behaviour for most PMDGs can be described by the spring-capacitor model. MEMS structures are so small that the influence of gravity can be neglected. When voltage is applied, the ribbons are being pulled down by the electrostatic force but at the same time the spring force pulls them back up. With small voltages the deflection can reach an equilibrium position but if the voltage is increased the spring force is not strong enough to balance the electric force and the ribbons will snap to the base. For some designs this will cause permanent damage. [12]

The ribbons act as parallel-plate capacitors for which applies

$$C = \epsilon_0 \frac{A}{x}, \tag{2.26}$$

where C is capacitance, ϵ_0 is the dielectric constant of vacuum (relative permittivity ϵ_r of air is ~ 1), A is the area and x is the distance between plates. The electrostatic energy E_e stored in the capacitor for a DC voltage V applied between the plates is given by

$$E_e = \frac{1}{2} C V^2. \tag{2.27}$$

The electrostatic force F_e affecting the ribbons can be defined as

$$F_e = \frac{\partial E_e}{\partial x}. \tag{2.28}$$

Combining the above equations the electrostatic force applying to ribbons can be written as

$$F_e = -\frac{\epsilon_0 A}{2} \frac{V^2}{x^2} \tag{2.29}$$

or

$$F_e = -\frac{\epsilon_0 A}{2} \frac{V^2}{(x_0 - \delta)^2}, \tag{2.30}$$

where x_0 is the initial distance between the plates and δ is the displacement. For mechanical force F_m, applies the spring force

$$F_m = -\kappa\delta, \tag{2.31}$$

where κ is the spring constant. At equilibrium $F_e = F_m$ which leads to

$$\delta^3 - 2x_0\delta^2 + x_0^2\delta - \frac{\epsilon_0 A}{2\kappa}V^2 = 0,$$

which does not have a stable solution for $\delta > \frac{x_0}{3}$ [13]. A pull-in voltage V_{PI} can be calculated when $\delta = \frac{x_0}{3}$, which leads to [12]

$$V_{PI} = \sqrt{\frac{8\kappa x_0^3}{27\epsilon_0 A}}.$$

There are several types of PMDGs under investigation throughout the world but only two of them are available commercially. The Grating Light Valve (GLV) from Silicon Light Machines and the Polychromator from Polychromix. The GLV is being used in projectors and telecommunications and the Polychromator is used in the DTS line of infrared spectrometers from Polychromix. Other interesting types of PMDGs include the MEMS Compound Grating (MCG), the Grating Electro-Mechanical System (GEMS) and the Grating Light Modulator (GLM). For these PMDGs a short description is given in the following sections. There are also many other types of dynamic diffraction gratings of which some use piezoelectric actuators to stretch the grooves, some have elements with tunable blaze angle, some are formed from soft elastomeric material and stretched by a dielectric elastomeric actuator and some are made of viscoelastic layers that change their form when voltage is applied. All of these are at their early stages of development or have some other limitations and thus are not to be included into this study.

2.5.1 Grating Light Valve

GLV is currently the commercially most successful work on PMDGs and the original device concepts were developed at Stanford University in the early 1990s. Silicon Light Machines was founded in 1994 to develop and commercialise a range of products based on the Grating Light Valve technology. The GLV is being used in projection displays, computer to plate printers and in optical communications. The structure of the GLV pixel is presented in Figure 2.6. [13, 14, 15]

The GLV consists of a linear array of dual supported ribbons formed of silicon nitride (Si_3N_4) and aluminium (Figure 2.7). The ribbons are organised in pixels of six ribbons, which share a common electrode. Every other ribbon is static and the rest can be deflected by applying a voltage. The achievable contrast ratio can be better than 4000:1. The unactuated state acts as a mirror surface and the actuated

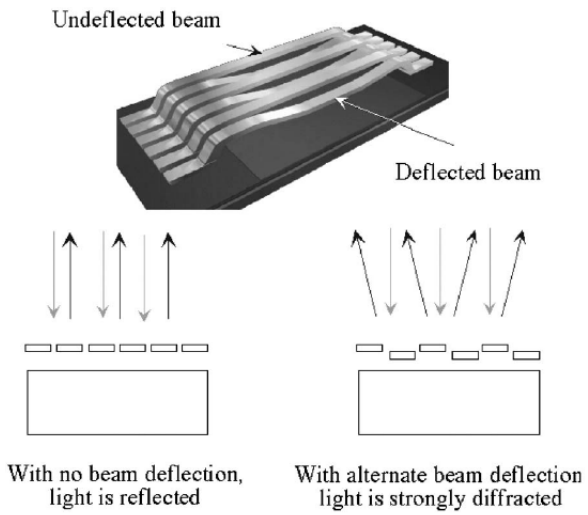

Figure 2.6. Mechanical structure of the GLV pixel [16]. This figure shows the unactuated state which acts as a mirror surface, and actuated state which is fully diffracting. The displaced beam does not remain flat and parallel for the whole length but the ribbons are longer than the usable pixel area at the centre. [17]

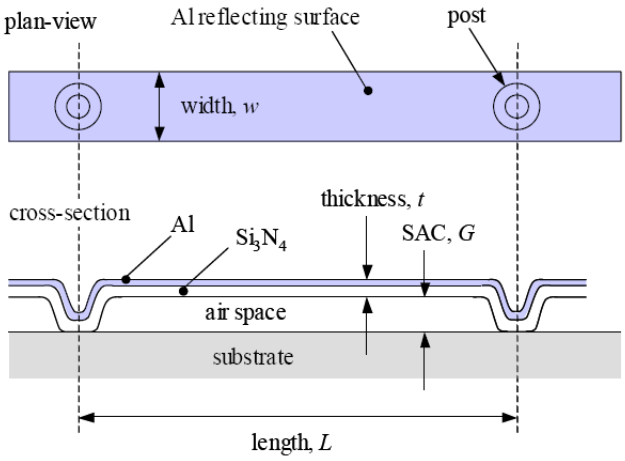

Figure 2.7. Physical structure of the GLV ribbon [18]. The GLV ribbon is made of silicon nitride and aluminium. The ribbons are 200-300 nm thick, 100-1000 μm long, 1-10 μm wide and spaced only 0.5 μm apart. [13]

state, where every other ribbon is pulled down by $\lambda/4$, is a fully diffracting surface with power transferring to the diffraction orders. GLVs can have more than 1000 pixels and can handle very fast switching speeds (20 ns) and high power (over 10 kW/cm^2). The usable area covers only 1/3 of the ribbon length at the centre. [18, 14]

Sony has continued to develop the GLV (renamed GxL) for large area laser projectors and has demonstrated a blazed GxL construction with 6480 ribbons (1080 pixels) at the 2005 World Exposition in Aichi, Japan. The blazed structure shown in Figure 2.8 has higher optical efficiency, >70% for RGB lasers, and higher contrast ratio, > 10000:1, than the flat GxL structure. [19]

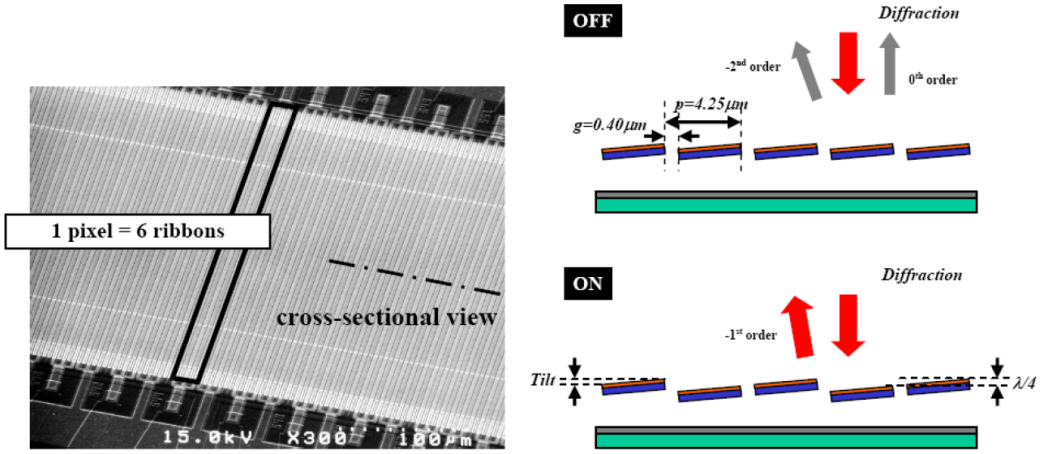

Figure 2.8. Structure and principle of blazed GxL. Sony has continued to develop the GLV (renamed GxL) for large area laser projectors and has demonstrated a blazed GxL construction, which has a higher optical efficiency than the flat GxL [19].

2.5.2 Polychromator

A variant of the GLV was developed at Sandia National Laboratories in the mid 1990s and continued at Polychromix. The Polychromator is very similar in function to the GLV but the structure is slightly more complicated as is presented in Figure 2.9. The main difference is that the reflecting surface is made to remain flat during deflection by constructing another ribbon layer on top of the bendable ribbons. With this design much longer beams are possible than in the GLV, and a prototype with 10 mm long elements has been developed. [21]

In 2005, Polychromix introduced a complete NIR spectrometer based on the Polychromator, which acts as a spatial light modulator with the grating organised into 100 groups of 12-element pixels [22]. The Polychromator has also been qualified for the NASA LCROSS (Lunar CRater Observation and Sensing Satellite) mission to look for water on the Moon [23]. Polychromix has also developed a free space optical switch product for 1.55 μm dense wavelength division multiplexed (DWDM) optical telecommunications called "Dynamic Channel Orchestrator"[16]. It uses an

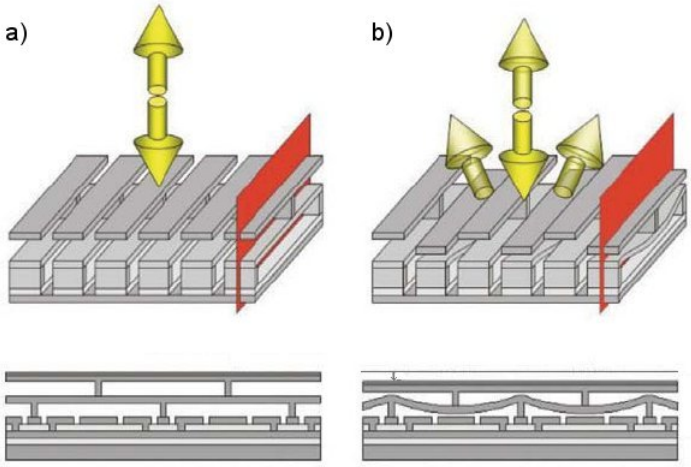

Figure 2.9. Mechanical structure of the Polychromator [20]. Figure a) on the left shows the unactuated state which acts as a mirror surface. Figure b) on the right shows the actuated state which is fully diffracting. The displaced beam remains flat and parallel to the substrate.

alternative configuration of the Polychromator where every other ribbon is initially displaced by $\lambda/2$. In this configuration there need not be any gaps between two adjacent ribbons and the reflection coefficient and dynamic range is improved. [16]

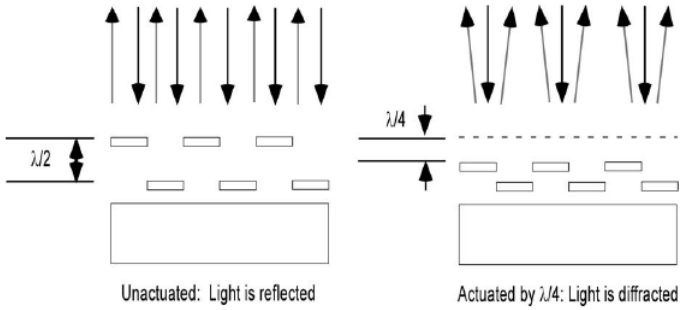

Figure 2.10. Alternate Polychromator design with beams initially displaced vertically by half a wavelength [16]. There is no need for gaps between two adjacent ribbons and the reflection coefficient and dynamic range is thus improved.

Sandia and Polychromix have also demonstrated a correlation radiometer, which uses a Polychromator with independent elements. The Polychromator diffracts a modulated "polychromatic" spectrum in a desired direction with the use of arbitrary grating profiles that have a maximum deflection of $\lambda/2$. The spectral transfer function can be reconfigured at a rate of 1 kHz. [24]

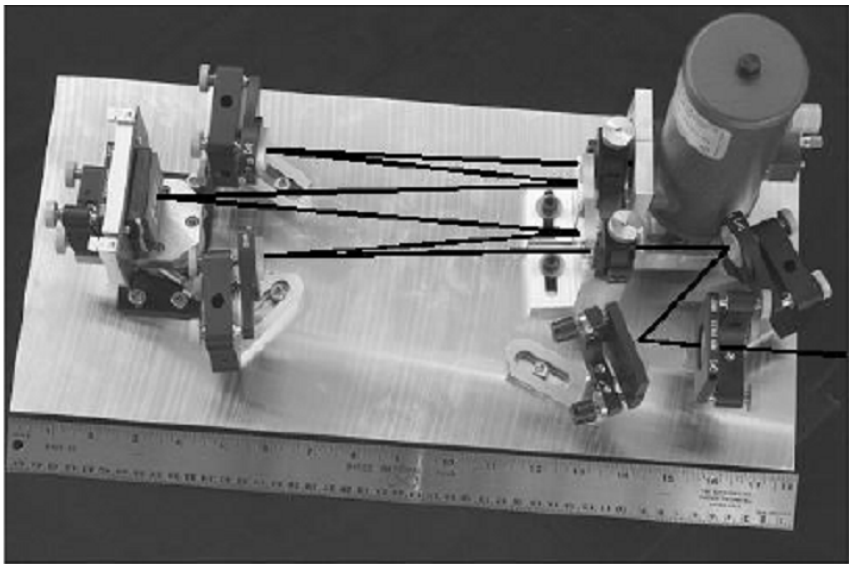

Figure 2.11. The optical layout of a Polychromator-based correlation radiometer [24]. The lines indicate the path of the infrared radiation from the entrance to the detector.

2.5.3 MEMS Compound Grating

The MEMS compound grating (Figure 2.12) is developed at the College of Nanoscale Science and Engineering (CNSE) of the University at Albany - SUNY for free space optical switching in DWDM telecommunications. The main difference compared to the GLV and the Polychromator is that there is a gap equal to the width of the ribbons between the elements. The size of the ribbons is 2x220 μm. The substrate is covered with a nitride layer that does not reflect light. The working principle is almost the same as in the GLV and the Polychromator in which the state, where the alternate ribbons are displaced by $\lambda/4$, acts as a diffractive surface but because of the wide gaps between the elements, the reflecting state is also a grating surface and the actuated state is a compound of two gratings. A 2D array has been presented but no commercial products have resulted. [25, 26]

2.5.4 Grating Electro-Mechanical System

A competitor to the GLV in laser display applications has been developed at Eastman Kodak Company, Rochester, USA [27]. The structure and working principle of the GEMS is presented in Figure 2.14. The grating elements are oriented so that the ribbons are perpendicular to the pixel line, in 90°, compared to the GLV or the Polychromator, where the ribbons of each pixels are side by side so the edge of the

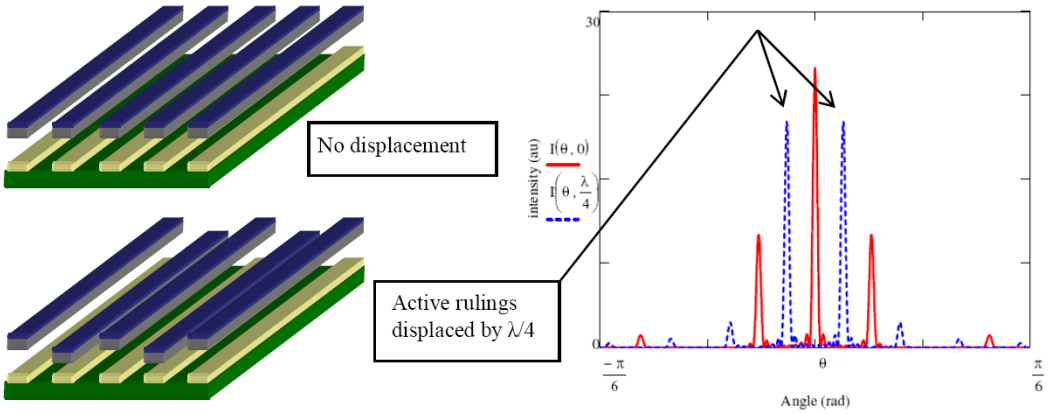

Figure 2.12. Operation of MCG. By applying a voltage, active rulings are displaced and the diffraction pattern changes. [25]

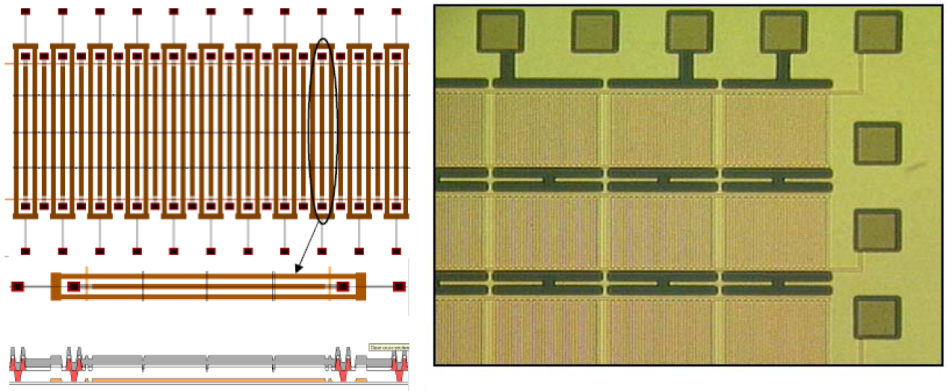

Figure 2.13. Structure of MCG. Left image shows the M63 design for the MCG ribbon and the right image shows part of a 2D MCG array. [25]

pixel can not be seen. This structure has some advantages in masking the unwanted orders in spatial light modulation because the diffraction pattern is perpendicular to the whole GEMS device. The working principle only supports a binary operation where the beam is either up or down and there are no intermediate states. Switching times can be less than 50 ns [28]. Prototype devices with 1080 pixels with 4 ribbons per pixel have been produced but no commercialisation has emerged. A programmable imaging spectrometer using GEMS has also been demonstrated by ITT Space Systems [29] (Figure 2.15). [28, 27, 30]

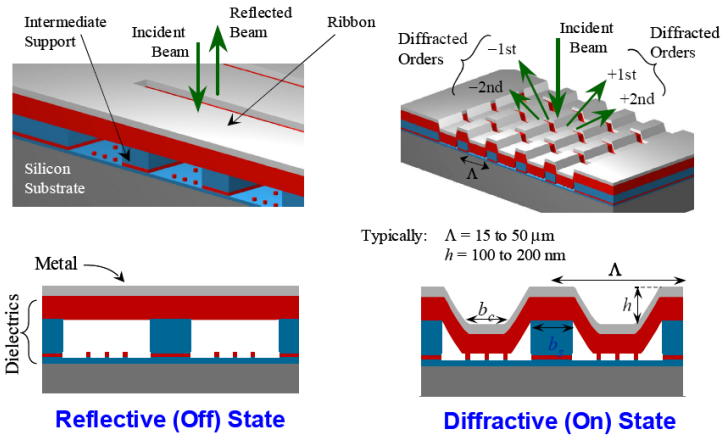

Figure 2.14. Structure of GEMS [29]. The GEMS device operates by diffraction of an incident beam on the grating surface that is formed when electrostatic forces pull down the metallized ribbons around the support structure.

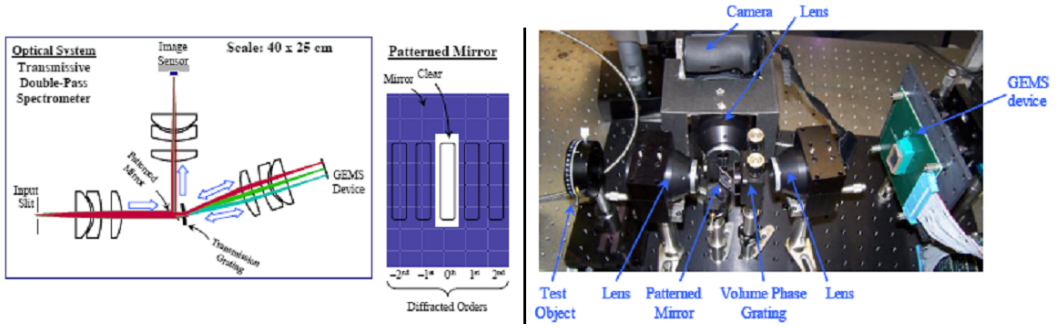

Figure 2.15. A programmable imaging spectrometer with GEMS [29]. The GEMS modulates the spectrum in the focal plane. On the left the MPSI system design is shown along side a view of the pattern mirror that acts as a selective optical stop to pass only the bands chosen by the GEMS device. On the right a laboratory demonstration with 11 spectral channels that shows the feasibility of a TDI-compatible programmable imaging spectrometer.

2.5.5 Grating Light Modulator

The Grating Light Modulator that has a completely different kind of structure compared to the aforementioned PMDGs, has been developed in the Department of Optic-Electronic Engineering at University of Chongqing in China. The GLM consists of grating plate pixels (33x33 μm) supported by four cantilevers (Figure 2.16). Each individual grating plate can be pulled down by a reflecting electrode beneath it. This structure can be easily implemented in 2D arrays in contrary to the GLV and the Polychromator, for instance. The structure has been designed to work in

binary operation mode where different shades of gray can be achieved by varying the durations of the two states. [31]

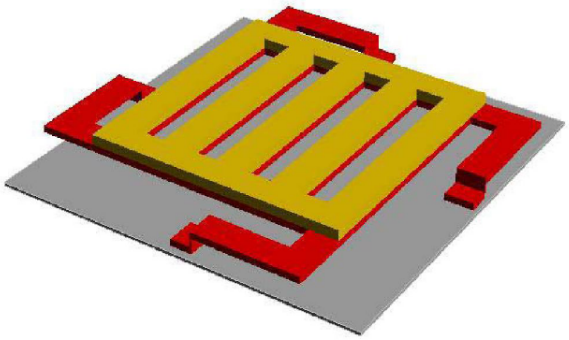

Figure 2.16. A GLM pixel. The GLM pixel consists of grating plate supported by four cantilevers. [31]

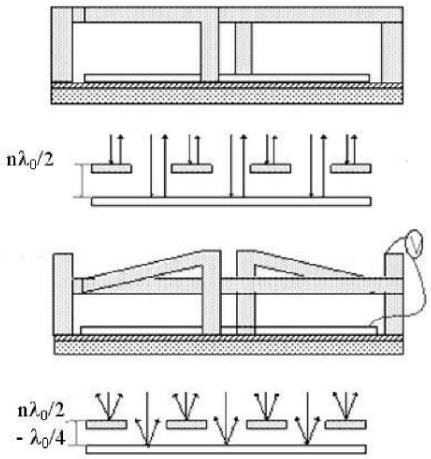

Figure 2.17. GLM working principle. Cross view of two states of GLM pixel. In the upper figure the GLM pixel is in a reflective state and in the lower figure the GLM pixel is in a diffractive state. [31]

Chapter 3

Proposed Instrument Concepts for PMDGs

In this chapter, two instrument concepts for PMDG devices are introduced. At the end of this chapter there is discussion about the presented concepts and one concept is selected for further development.

3.1 Imaging Programmable Spectrometer

A concept with an ImSpector type Prism-Grating-Prism imaging spectrograph [32] for 900-1700 nm wavelength range and the PMDG is shown in Figure 3.1. The objective focuses the image of the target on the input slit of the spectrograph. The image of the slit is dispersed and focused on the PMDG by the spectrograph optics. The PMDG is used for the selecting of wavelengths and also for intensity modulation. The selected wavelengths are reflected back to the spectrograph with zero (or $\lambda/2$) deflection and focused on a line sensor. The intensity can be modulated by controlling the deflection of the pixel between zero and $\lambda/4$. With $\lambda/4$ deflection the light is diffracted to an angle that does not propagate through the optics of the spectrograph and thus is not detected by the line sensor.

An implementation of this concept using two spectrographs and a transmissive LCD spatial light modulator has been investigated by Uula Kantojärvi with the Imaging Spectral Signature Instrument (ISSI) in his Master's Thesis "Feature-specific on-board technology for airborne spectral imaging" [33] and the end results have been reported in SPIE publication "Performance of the Imaging Spectral Signature Instrument (ISSI) breadboard" [34].

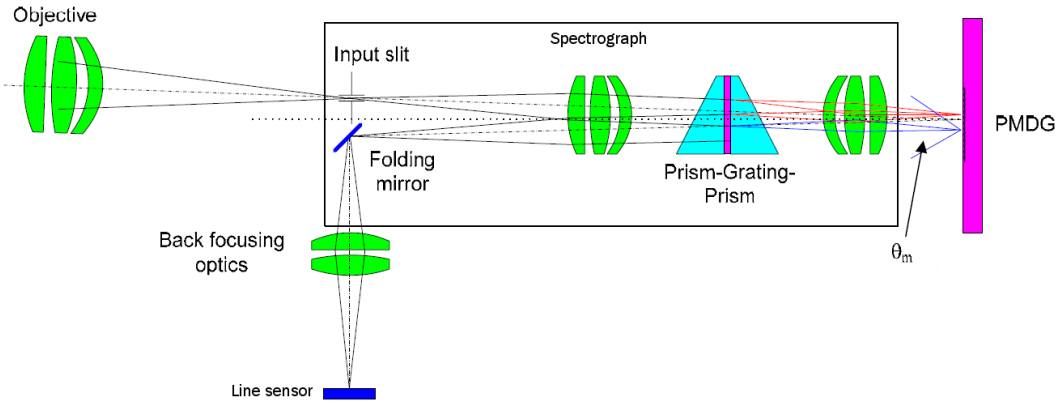

Figure 3.1. Off-axis imaging programmable spectrometer. An off-axis concept with one spectrograph and PMDG. Light rays for blue and red are shown. The wavelengths of red are selected and thus reflected back to spectrograph, but the wavelengths of blue are diffracted and are not detected by the photo sensor. This concept, even with an additional context imager as in Figure 3.2, would have the best transmission and it could use a 10/90 beamsplitter for the context imager.

A simplified, on-axis structure of the aforementioned concept with an additional context imager is presented in Figure 3.2. The transmission for this concept is lower than for the off-axis version as light would have to pass the beamsplitter twice, and for that the beamsplitter would have to be with 50/50 dividing relation.

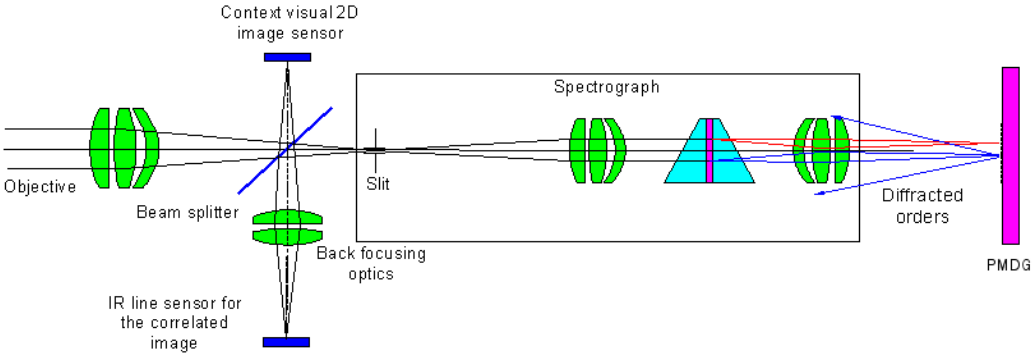

Figure 3.2. On-axis imaging programmable spectrometer. An on-axis concept with one spectrograph, PMDG and additional context imager. This simplified concept would not have as good a transmission as the off-axis version and it would have to use a 50/50 beamsplitter. However, it is simpler to build to demonstrate the feasibility of the PMDG.

The instrument concept can use spectral line scan or Hadamard transform spectral acquisition methods and it also performs optical correlation of a programmed signature with the target pixel signature. An image is formed by scanning a line across the target. The correlation method is an approximation of the spectral angle mapper (SAM) used in hyperspectral data processing.

3.2 Single-point Miniature Spectrometer

A concept of a small single-point spectrometer is presented in Figure 3.3. The fore

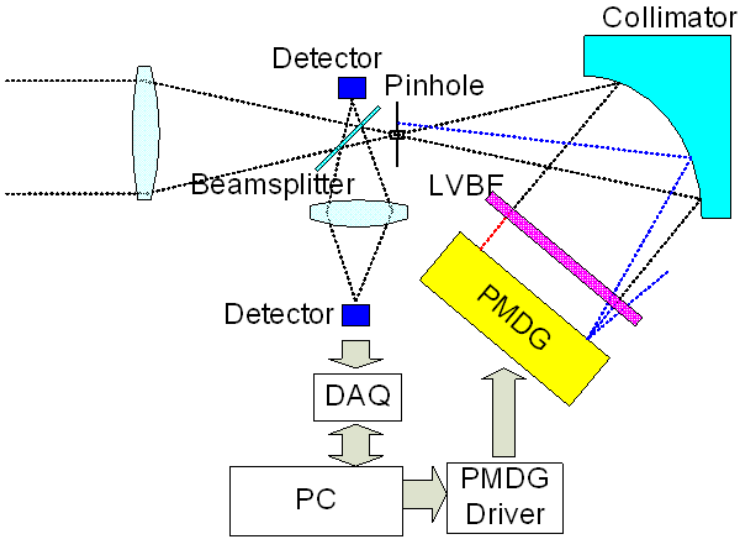

Figure 3.3. Single-point miniature spectrometer. An on-axis concept with a beamsplitter, linear variable bandpass filter and PMDG.

optics focuses the light to a pinhole through a beamsplitter which guides part of the incoming light to a monitoring detector. The light that goes through the pinhole is collimated and guided through a linear variable bandpass filter (LVBF) that passes different spectral bands on different parts of the filter thus separating the spectral elements. The PMDG does a Hadamard transform through the spectrum and the reflected light returns to the pinhole. Diffracted light does not hit the pinhole because of its slightly different incident angle on the collimator. The beamsplitter guides the reflected light through a focusing lens to a single detector element.

A modified implementation of the aforementioned concept uses a slightly tilted PMDG so that the reflected light returns to a different pinhole. A Zemax illustration, which simultaneously demonstrates the light paths of accepted (blue) and rejected

(green) rays, of the working principle of this implementation using a lens is presented in Figure 3.4. In this illustration the PMDG is tilted 1° so that we have different entrance and exit pinholes. The light enters from the uppermost pinhole with a diameter of 600 μm. The input light is then collimated using aspheric lens with a focal length of 50 mm. There is then an aperture to block light from hitting the surface around the grating which would cause unwanted reflection. For the accepted light rays the PMDG is a mirror surface and for the rejected rays a common diffraction angle based on the smallest angle is used. It can be noted that accepted rays hit the exit pinhole and are guided to the detector with a folding mirror and the rejected rays do not hit the exit slit because their light path differs by a few degrees. The tilting will cause some attenuation to the accepted light because it will hit a slightly different portion off the pass band on the LVBF than on the first pass through. Rejected light will be more attenuated due to same reason.

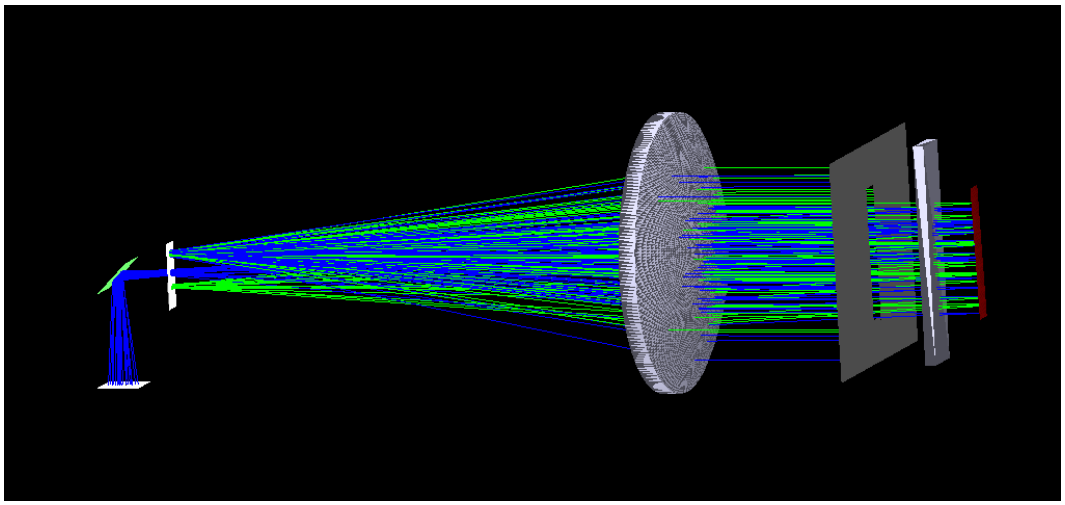

Figure 3.4. A Zemax illustration, which simultaneously demonstrates the light paths of accepted (blue) and rejected (green) rays, with tilted PMDG.

The instrument concept can use spectral line scan or Hadamard transform spectral acquisition methods for recovering the target spectrum. It is also possible to use optical correlation of a programmed signature with the target signature. The correlation method is an approximation of the spectral angle mapper (SAM) used in hyperspectral data processing.

3.3 Discussion on the Presented Concepts

It is clear that the imaging programmable spectrometer using the telecentric spectrograph is not going to work properly with this particular PMDG because the spectrograph operates with f-numbers smaller than 4. The diffraction angles are so small (see Chapter 4) that it would require very high f-numbers to prevent the diffracted orders from propagating through the spectrograph and reaching the detector. The f-number for imaging system is defined as [35]

$$f/\# = \frac{1}{2\sin\alpha}, \tag{3.1}$$

which describes the marginal ray angle that is capable of propagating through the system. For f-number of $f/\# = 4$ the largest angle is thus

$$\alpha = \arcsin\frac{1}{2 \cdot f/\#} \approx 7.18°. \tag{3.2}$$

The smallest diffraction angle is 2.2° at $\lambda = 900$ nm. The marginal angle of the system must be limited to half of that so that the light that diffracts to angle of 2.2° and has the opening angle defined by the f-number does not overlap with the acceptance angle of the system. This turns out as f-number $f/\# = 26$. Also the achievable field of view would be limited with only 1.5 mm usable area on the PMDG in spatial direction. The concept idea in itself is not a bad one, as it would work with a PMDG that is developed with the particular use in mind. To prevent diffraction orders from propagating through the spectrograph, the PMDG should have narrower beams, like 3.1 μm with 0.5 μm gaps, that results in larger diffraction angles (as defined by Equation 2.20). Alternatively the PMDG could be like the GEMS, where the elements inside the pixels are oriented differently, so that diffraction orders could be filtered out. The field of view could be improved by longer beams in the spatial direction or even by use of multiple gratings or single 2D grating even though modulation is not required in spatial direction.

The single-point miniature spectrometer will suffer from unsuitable wavelength bands of the off-the-shelf LVBFs. It is possible to order LVBFs with custom specifications but it is outside the scope of this project. Moreover, the whole concept will suffer from the throughput of the LVBF. Because the whole LVBF is illuminated with white light and only a narrow band of the incident light passes through the LVBF at any given point, the "dispersion efficiency" of the LVBF is on a scale of its relative bandwidth − merely 1 %. For a normal diffraction grating, light of a

certain wavelength will be guided to the same point from any part of the grating. Of course, the light will also go to different orders, but the efficiency for dispersion can still be much better – >0.9 for the blazed wavelength. A grating is a much better dispersing element for this kind of spectrometer but it would require more complicated optical design and longer optical paths to work. This architecture is already used by Polychromix in their DTS line of spectrometers. As the decision was to make the optical structure as simple and compact as possible to gain something new, the use of LVBFs can be sanctioned. Total throughput for the demonstrator will also suffer from the aperture in front of the LVBF which only passes through the light that will hit the grating surface. The low throughput is mitigated by the fact, that all the transmitted light is collected on a single detector pixel via Hadamard transform method compared to spectrometer architectures where the light is spread on an array of pixels. The bottom line radiometric performance value is the SNR of the detector channels. For a real instrument the LVBF could be directly integrated on the PMDG and matched to the aperture and to the spectral band per pixel. This would make the structure even more compact and would increase the throughput and resolution.

Due to the restrictions in implementation of the imaging programmable spectrometer, most of the work will be done for the single-point miniature spectrometer concept.

Chapter 4

Characterisation of the Chosen PMDG Type

This chapter is about the PMDG device that was chosen to be the heart of the project and about its characterisation. As the work was to be done with commercially available components the choices were limited.

4.1 Introduction

The chosen PMDG, shown in Figure 4.1, is a PCX Polychromator chip from Polychromix. Because PMDG components are not yet commercially available as stand-alone kits, the only way to obtain a PMDG sample was to procure a DTS-1700 spectrometer from Polychromix and remove its PMDG along with the control electronics. The Polychromator consists of 100 individually controllable pixels, each consisting ten circa 10 μm wide elements separated by circa 2 μm gaps. Each element consists of 11 segments as shown in Figure 4.2. Every other inter-pixel element is fixed and the rest are controlled by the same voltage, controllable from 0 to 14.85 V with 256 steps plus a bias voltage of 15.16 V to create a square-well grating. The area of each pixel is circa 120x2000 μm^2.

The Polychromator is controlled with the original PCB (printed circuit board) with some modifications to bypass the programmed functionality of the digital signal processor (DSP). The PCB of the DTS-1700 is shown in Figure 4.3. The PMDG is originally controlled by the DSP which controls fifty digital potentiometers that are connected in series. Every digital potentiometer controls two pixels in the PMDG using voltage range of 0 V to 14.85 V digitised with 8 bits. The contacts between the

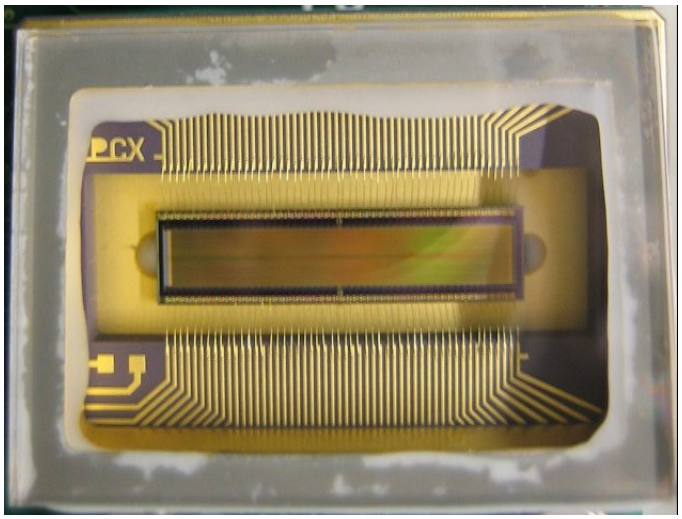

Figure 4.1. Polychromix PCX Polychromator. PCX Polychromator chip from Polychromix. The grating and the PCB it is connected to was disassembled from DTS-1700 spectrometer.

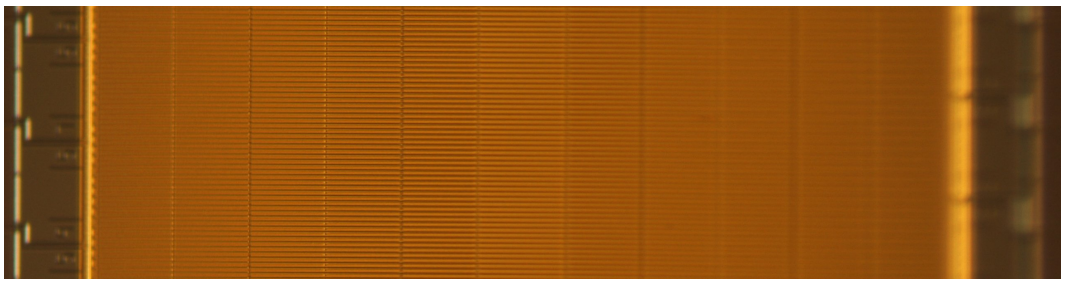

Figure 4.2. Polychromator segment structure. Eleven segments of five pixels of the Polychromator imaged with Nikon Optiphot optical microscope. The plane of the grating is slightly tilted and the space under the microscope objective is limited so that the image is out of focus on some part of the grating.

DSP and the first digital potentiometer have been cut in order to insert a bypassing control line. This makes the direct control of the pixels possible.

For the characterisation measurements, some additional equipment were needed. All the additional equipment used in characterisation measurements, except basic lenses and filters, are listed in Table 4.1 and are from the VTT laboratory.

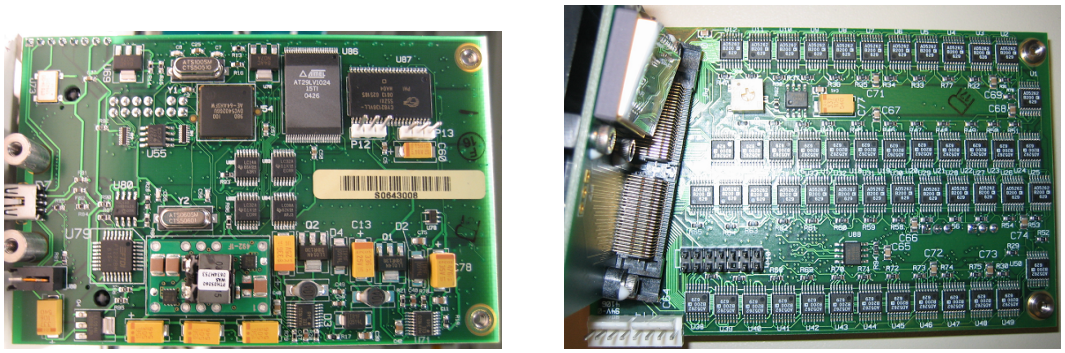

Figure 4.3. Original PCB from DTS-1700 spectrometer. Backside and frontside of the PCB which is used to control the pixels. The frontside is almost completely covered by fifty digital potentiometers. The packaging of the Polychromator can be seen on the separate PCB perpendicular to the control PCB.

Table 4.1. Additional equipment used for characterisation measurements.

Laser sources:	JDSU 1507P, HeNe 632.8 nm
	Melles Griot GreNe, HeNe 543.3 nm
Spectrometers:	Ando AQ6317 (600-1750 nm, ±0.05 nm, 0.015 nm FWHM)
	Ocean Optics HR4000 (200-1100 nm, 0.75 nm FWHM)
Monochromator:	Jobin Yvon HR-640 (±0.05 nm)
Signal Analyser:	Hewlett-Packard HP 89410A Vector Signal Analyzer
LCR meter:	Hewlett-Packard HP 4263A
Oscilloscope:	Tektronix TDS 744A
Camera:	JAI CV-A10CL
Software:	National Instruments LabVIEW 8.2 for automated measurements

4.2 PMDG Pitch and Diffraction Orders

4.2.1 Test Setup for PMDG Pitch and Diffraction Orders

The grating pitch, basic diffraction behaviour and contrast ratios were determined by directing a helium-neon (HeNe) laser beam (632.8 nm and 543.3 nm) on the grating and observing the diffraction pattern on a screen with an area sensor. The relative distribution of intensity in the orders is measured by capturing the diffraction pattern on the screen by a camera. The PMDG operation range is scanned through with every voltage step from the flat mirror to full grating configuration. The laser

spot size can be decreased to cover a subset or single pixel of the grating. The PMDG is mounted on a xyz-stage with rotation control.

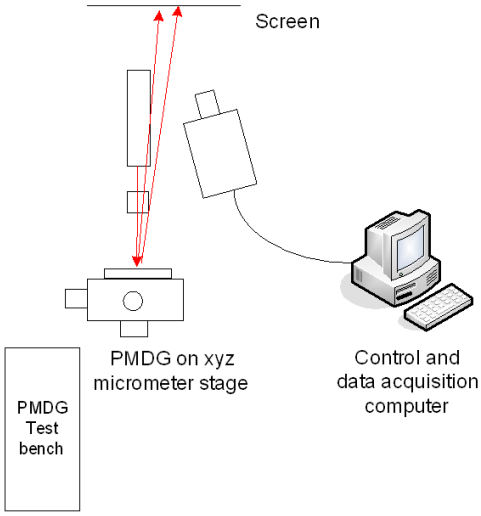

Figure 4.4. Test setup for diffraction orders.

4.2.2 Test Results for PMDG Pitch and Diffraction Orders

The pitch and diffraction orders of the PMDG were checked with different sizes and types of laser spots. PMDG pitch or groove spacing d can be determined from the grating equation (Equation 2.18). The screen was 1020 ± 2 mm from the PMDG and the locations for the first three orders were measured. The results are presented in Table 4.2. The measured grating pitch is in agreement with the estimate derived from the microscopic measurements. Furthermore an overlapping pattern with twice the spatial frequency can be seen, which corresponds to the grating formed when every second element is displaced.

Table 4.2. The groove spacing of the Polychromator.

Order	± 3	± 2	± 1
β (°)	9.26	6.13	3.09
d (μm)	11.8	11.9	11.7

Contrast ratio and basic diffraction behaviour measurements were performed with a HeNe 632.8 nm laser and two spot sizes to see if the number of modulating elements has an impact on the contrast ratio. The spot sizes used were 480 μm (about 5 pixels)

and circa 90 μm (1 pixel), which are the diameters where the beam intensity has fallen to $1/e^2$ (13.5 percent). The 480 μm spot was the laser output beam. The 90 μm spot was obtained with an OFR LMU-5x microscope objective whose focal point was imaged on the Polychromator using a lens with a focal length of 100 mm. The divergence angle for the 90 μm spot was measured to be about 12.4 mrad, even though the calculated value suggests only about 9 mrad. The reason for the difference could be that the grating resolving power has an effect on the divergence. The spot sizes were confirmed by checking how many pixels would affect the modulation. For example, for the 90 μm spot, the pixels next to the one the spot was centred on, have some effect on the contrast ratio, but that is because the full spot size (Gaussian profile) extends well beyond 1.5 times the $1/e^2$ diameter, even though the signal is minimal. The 90 μm spot was also confirmed by directly imaging the laser spot with a CCD that has 8.3 μm pixels.

The sum signal used in calculations was calculated over the spot intensity profile. The camera images the diffraction pattern (zero and first orders) from a screen as seen in Figure 4.5. The control program takes an average from the image over the diffraction spots to get an average intensity line profile as shown in Figure 4.6(a). When these line profiles from every voltage step are combined together, we get a 3D figure (Figure 4.6(b)), which shows how the pattern changes with voltage. The sum signal was calculated over the spot profile. For example for the reflected signal (the profile at the centre), the sum was calculated over the camera pixels 100 to 170. The sum signal was used so that the results are not based only on a single maximum pixel whose location on the spot could change due to laser speckle (the spot has random intensity pattern due to interference).

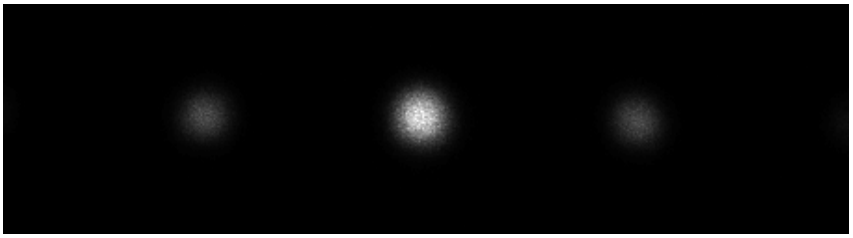

Figure 4.5. Laser diffraction intensity profile on a screen. Diffraction pattern (zero and first orders) as seen by the camera from the screen. The speckle pattern is clearly visible as a grainy spot.

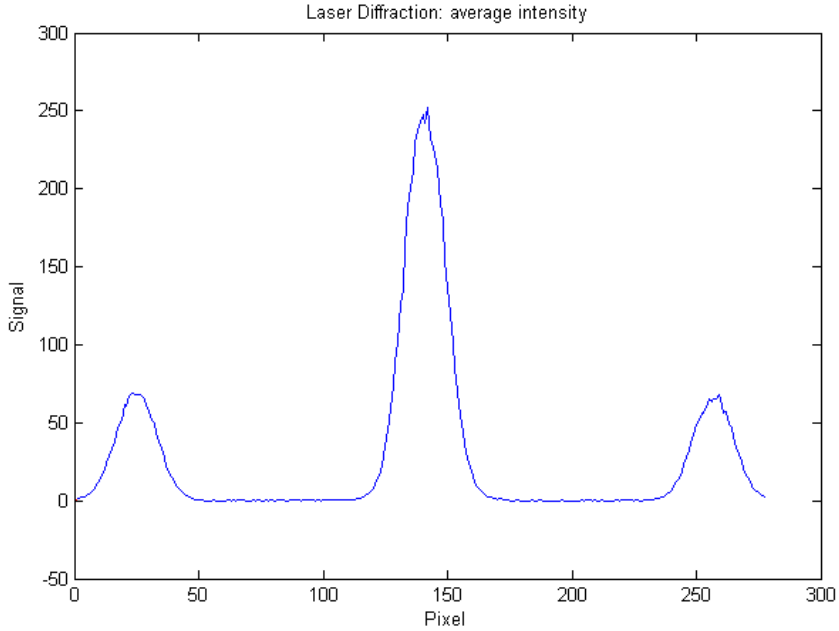

(a)

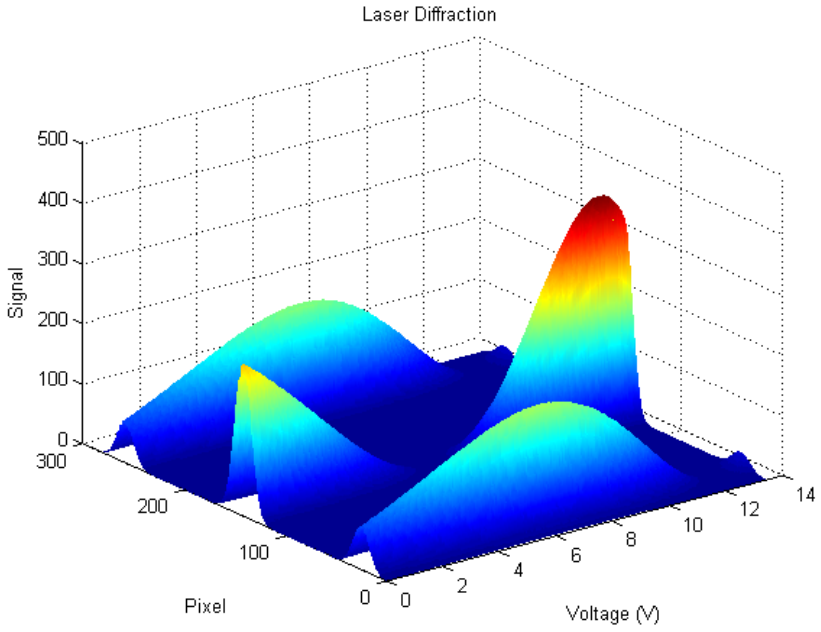

(b)

Figure 4.6. Laser diffraction intensity profile. (a) Average intensity line profile that was calculated from what the camera sees (Figure 4.5) per camera pixel line over the diffraction spot profile. (b) 3D plot which show the voltage, highlighted pixel area and signal. Dark signal was reduced at the capturing phase. The sum signal was calculated over the spot profile for example for the reflected signal (the profile at the centre) the sum was calculated over the camera pixels 100 to 170.

The results for the 480 μm HeNe 632.8 nm laser spot modulated with 5 pixels at the centre of the grating and at both ends is shown in Figure 4.7. The contrast ratios for the zero order reflection were $CR_{0-4} = 500$, $CR_{95-99} = 530$ and $CR_{48-52} = 220$ and for the 1st order diffraction twice as much. The difference between the measured contrast ratios for pixels at the centre of the grating and at the edges is probably due to some change in the ambient dark levels between the measurements, as the zero order signal minimum is twice as much as in the other measurements, even though the maximum is lower. The first order minimum has more signal as well. The results for 90 μm HeNe 632.8 nm laser spot modulated with only one pixel at the centre of the grating and at one end, is shown in Figure 4.8. The centre pixel area was modulated also with three pixels for comparison. Contrast ratios for the zero order reflection were $CR_{98} = 100$, $CR_{50} = 100$ and $CR_{49-51} = 140$. The contrast ratios for the 90 μm spots are lower because of the smaller spot size. The resolving power is lower because the spot hits fewer grating elements. The spot on the screen is much larger due to the greater divergence of the smaller waist (Gaussian laser beams have nonlinear divergence that depends on the size of the smallest beamwidth − the waist), which makes the intensity to be divided for bigger area thus causing some overlap. For both measurements, 231 voltage steps of the 256 available were used (this was the first safety limit measured from the original working spectrometer). The signal is summed over the whole spot diameter and the contrast is calculated from the summed signal. The dark signal was reduced at the capturing phase.

A measurement with 253 voltage steps (which is the maximum that Polychromix uses in their DTS-1700 spectrometer and so it was kept as a safe limit) was performed with red and green HeNe laser (632.8 nm and 543.3 nm). Results are shown in Figure 4.9, which very clearly points out how the deflection of the elements per voltage step gets bigger when the voltage increases. From Figure 4.9 the initial deflection and total deflection can be estimated to be about 80 nm and 375 nm, based on the phases of the intensity curves (maximum and minimum signals are from $\lambda/2$ and $\lambda/4$ points).

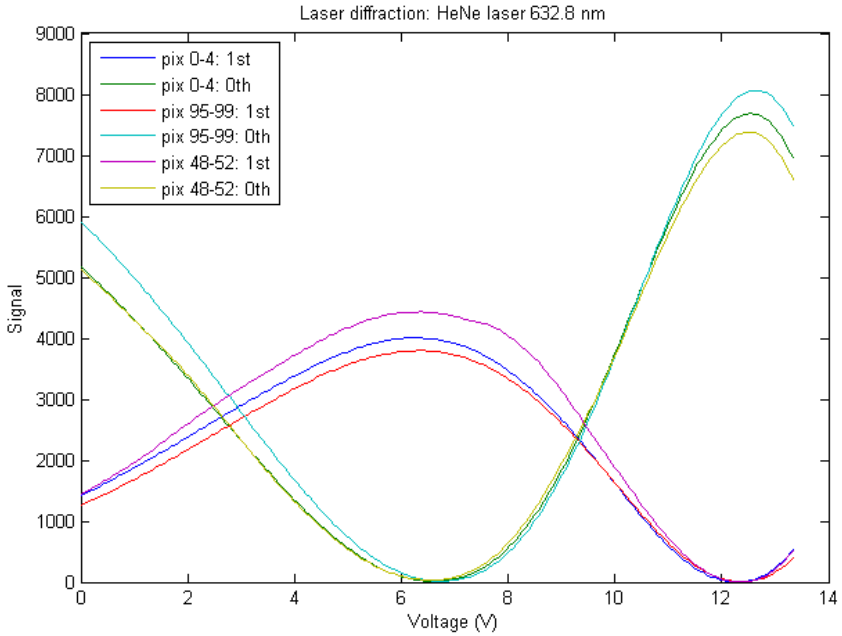

Figure 4.7. Diffraction contrast measurement for 480 μm spot. A 480 μm laser spot modulated with 5 pixels at both ends and in the centre of the Polychromator. The figure shows the intensity for zero order reflection and first order diffraction as a function of control voltage. Contrast ratios for the zero order reflection were $CR_{0-4} = 500$, $CR_{95-99} = 530$ and $CR_{48-52} = 220$. This figure suggests that the Polychromator has initial displacement caused by the bias voltage, because the zero order intensity with no voltage is lower than what is achievable with voltage.

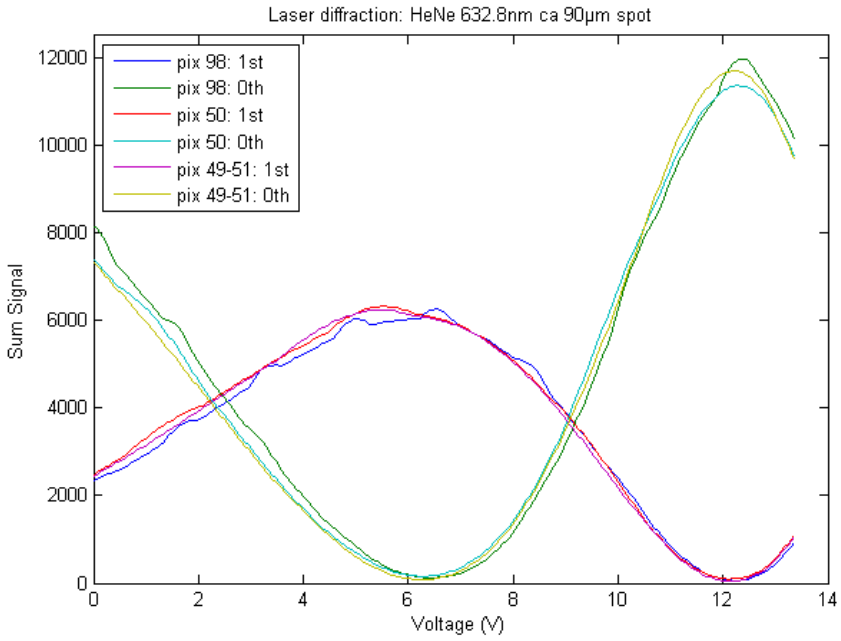

Figure 4.8. Diffraction contrast measurement for 90 μm spot. Circa 90 μm HeNe 632.8 nm laser spot modulated with 1 pixel at the centre of the grating and at the other end. The centre pixel area was modulated also with three pixels for comparison. The figure shows the intensity for zero order reflection and first order diffraction as a function of control voltage. Contrast ratios for the zero order reflection were $CR_{98} = 100$, $CR_{50} = 100$ and $CR_{49-51} = 140$. The humps that can be seen in the curve for pixel 98, could be caused by the segment structure on this scale.

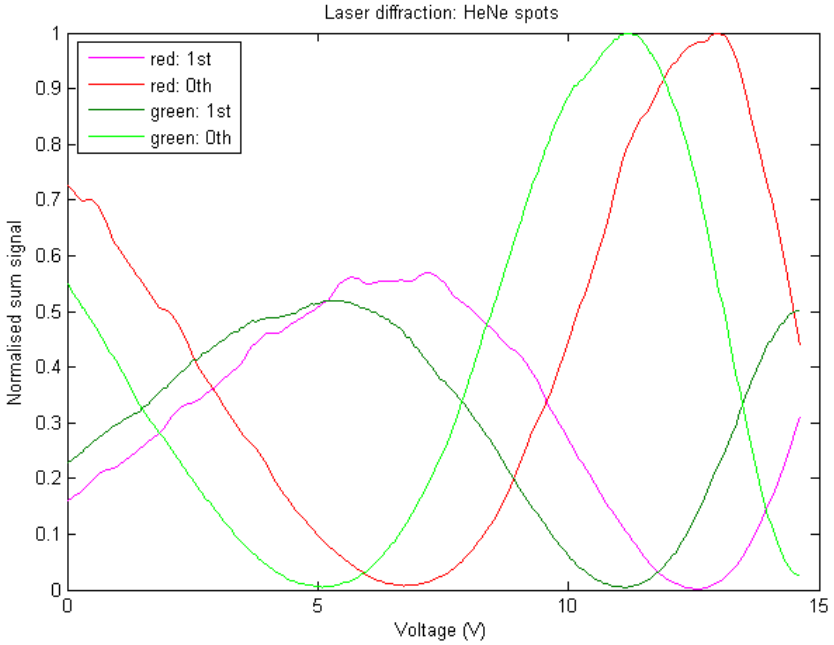

Figure 4.9. Diffraction contrast measurement for green and red laser spots. Green and red laser spots modulated with 253 voltage steps. As can be seen here from the skewing of the wave profile, the movement per voltage step with higher voltages is larger than with lower voltages.

4.3 PMDG Electrical Characteristics

4.3.1 Test Setup for PMDG Electrical Characteristics

For electrical measurements (leakage current, capacitance, frequency response, cross talk), a test PCB (Figure 4.10) was manufactured. The test PCB allows to make connections to individual pixels or to couple them in various configurations with jumpers and to control them directly.

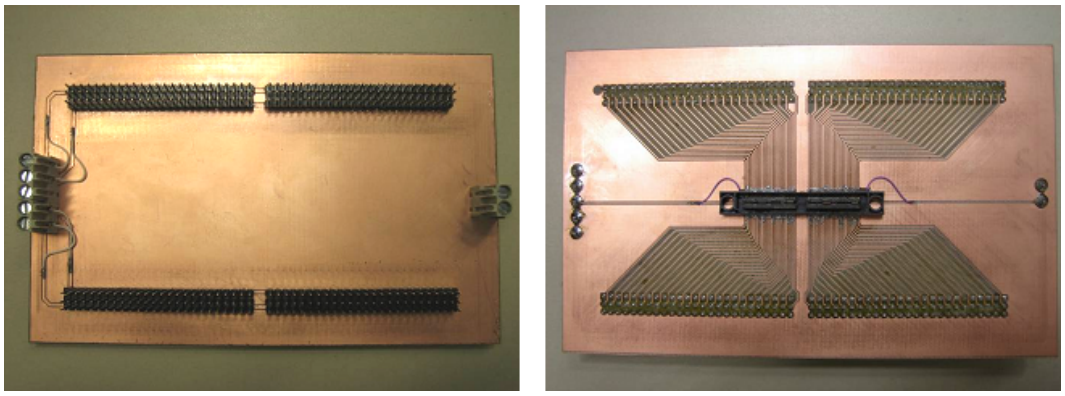

Figure 4.10. Test PCB for electrical characterisation.

For capacitance measurement, the capacitance of a single pixel and several pixels is connected in parallel with stray capacitances of the PMDG chip, the case, and above all, the circuit board onto which the PMDG is mounted. The capacitance of one pixel with five controllable grating elements is of the order of 400 fF with assumed maximum gap between the plates. Stray capacitances easily add up to several pFs. Therefore, the absolute pixel capacitance can be difficult to measure. The change in capacitance, when the pixel is actuated, can be more easily measured.

For frequency response measurements one pixel is DC-biased and excited with a signal with varying frequency. The mechanical movement is detected from the intensity of light reflected from the PMDG when illuminated by a laser. The intensity is measured using a high-speed photodiode and a spectrum or signal analyser. The excitation amplitude must probably be attenuated at frequencies close to the mechanical resonance frequency.

4.3.2 Test Results for PMDG Electrical Characteristics

First the leakage current was measured by connecting the bias to one power source with voltage controllable from 0 V to -15 V. One pixel from both sides were selected and the first was connected to an other power source with voltage range of 0 V to

14.5 V and the other pixel was connected to the common ground between the -15 V and +15 V sources. A voltmeter was connected to both lines between power source and pixel. First the bias was lowered from 0 V to -15 V slowly and the change in voltmeters was monitored. When the bias reached the -15 V, the control voltage to one pixel was increased slowly from 0 V to 14.5 V and the change in voltmeters was again monitored. The internal resistance of the voltmeters is 10 MΩ. For the whole measurement process, the leakage current stayed below 1 mV/10 MΩ = 100 pA.

The capacitance was measured with an HP 4263A LCR meter for one pixel and for 50 pixels connected in parallel. First the bias was lowered from 0 V to -15 V and the capacitance was monitored for each voltage step. Then the control voltage was increased from 0 V to 14.5 V and the capacitance was once again monitored for every voltage step. The measurement with 50 pixels was then reduced to show the capacitance for 1 pixel and the capacitances from both measurements were compared to the starting value. Figure 4.11 shows the result of the change in capacitance as a function of voltage, when the voltage was increased for the two measurements. As the capacitance depends on the gap, it can be noted that not much happens during the first 15 V, which explains the decision to use a bias voltage and a smaller range of controllable voltage instead of having the full 30 V range controllable.

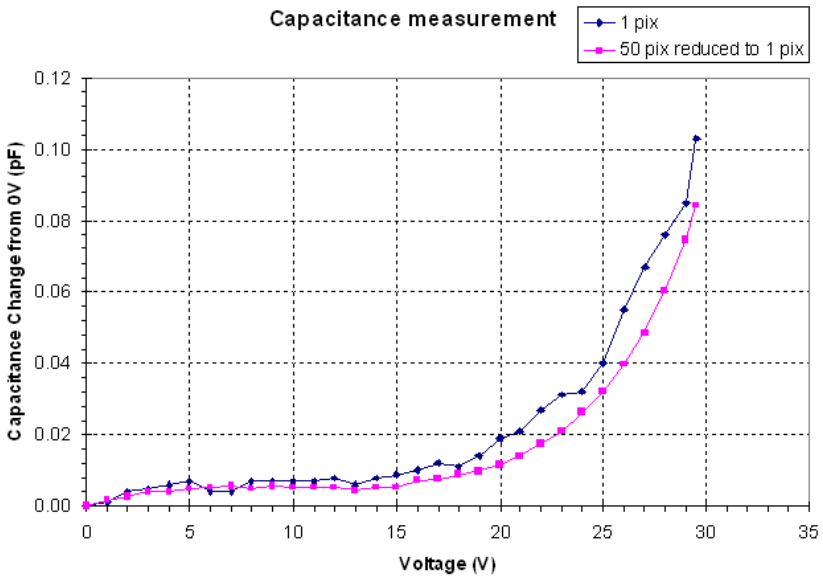

Figure 4.11. Capacitance measurement of PMDG pixels. The change in capacitance per voltage compared to the starting value. The blue curve is for the results from one pixel connected and the pink curve shows the results for 50 pixels reduced to one pixel.

During the capacitance measurements, when the power sources were switched off, an electrical surge from one of the power sources collapsed a few elements in one of the pixels which rendered the pixel unusable. Luckily the disabled pixel is near one edge. The collapsed elements are permanently fixed in down position causing short-circuit hence the pixel is cut off from the control voltage.

The frequency response was measured with an HP 89410A Vector Signal Analyzer. One pixel was modulated with the signal generated with the analyser and a laser spot was centralised on the corresponding pixel. The intensity of the diffracted 1st order spot was monitored with Si-detector connected to the same signal analyser.

First, the frequency response of the detector was measured in a way that it could be noted when the detector would be the limiting factor. For the detector, a sinusoidal excitation signal was frequency swept from 2.5 kHz to 1 MHz. An LED was used as the modulated light source. The PMDG was biased with 18 V and the excitation signal was white noise with V_{pp} = 700 mV on a frequency band from 500 Hz to 200 kHz, which was the limit set by the detector. Sinusoidal excitation was also used for the PMDG measurement but the white noise excitation resulted in a cleaner response. From the results, presented in Figure 4.12, it can be seen that the Polychromator has a resonance frequency at 47.5 kHz.

The dynamic behaviour was also monitored with a step response measurement (Figure 4.13) with and without bias voltage. The pixel was pulled down and released and the damped oscillation of the pixel was measured by following the intensity of a diffraction spot with a laser and Si-detector. This measurement gave the same resonance frequency of about 45 kHz.

To measure the coupled oscillation of the neighbour pixel, the pixel was monitored with 90 μm laser spot while the adjacent pixel was modulated with a square wave signal. Because the crosstalk between pixels is probably coupled due to the change in the surrounding gas pressure and not so much due to electrical coupling (wire lengths are so small), the expected result would be only to find out the mechanical oscillation around the base position. The laser spot was positioned in the centre of the stationary pixel and also moved further away from the modulated pixel so that the spot was definitely outside the modulated pixel. No crosstalk could be measured.

The only oscillations that could be seen was when the laser spot was still probably hitting the modulated pixel. The neighbour of the modulated pixel can not stay in any position other than the base position without the control voltage. Because all the measurements that had oscillations, showed also the input voltage step, the effect must be created by a part of the laser spot still landing on the modulated pixel (see Figure 4.14 for clarification).

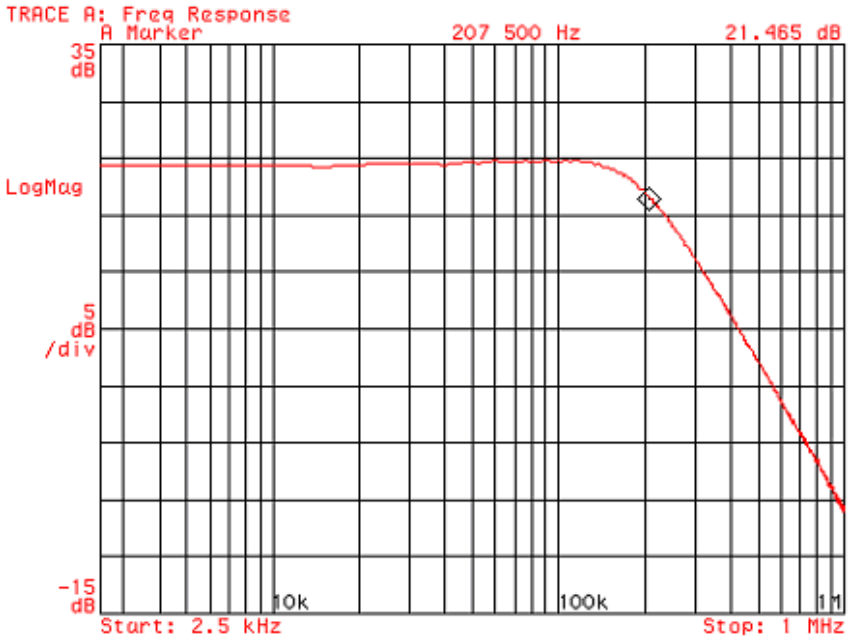

(a)

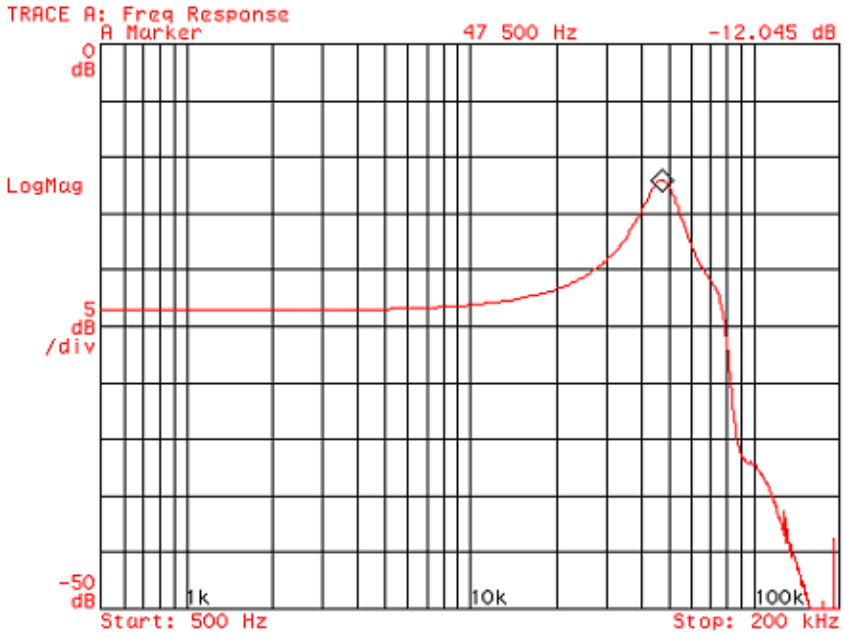

(b)

Figure 4.12. Frequency response (a) of the used Si-detector measured with sinusoidal voltage that was frequency swept from 2.5 kHz to 1 MHz. The cut-off frequency is about 207 kHz. (b) Frequency response of the PMDG measured with white noise on a frequency band from 500 Hz to 200 kHz. The Polychromator has a resonance frequency at about 47.5 kHz. Q factor ($Q = f_0/\Delta f$ for damped oscillator, where Δf is measured from the -3 dB points) can be estimated to be about $Q = 4$.

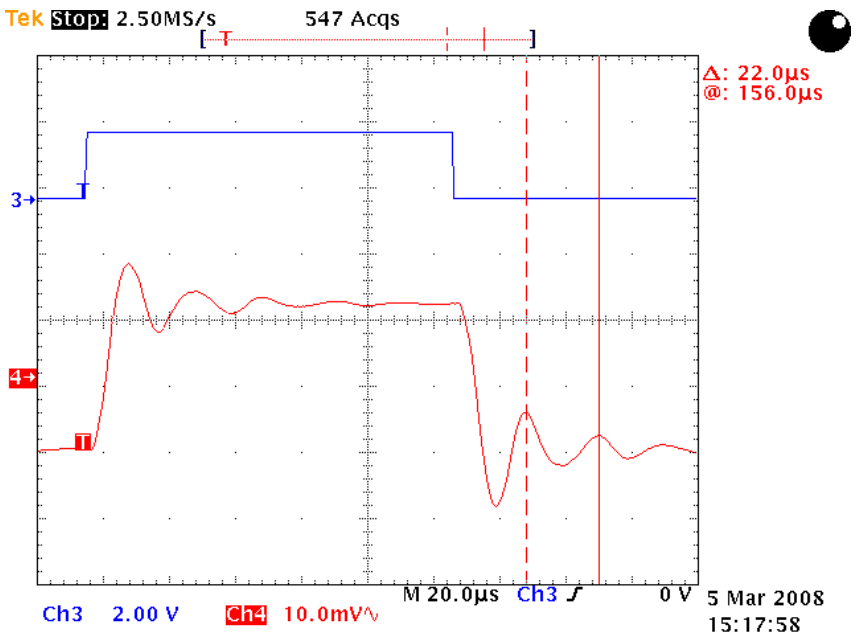

Figure 4.13. Dynamic behaviour monitored with step response. The resonance frequency can be estimated from the two markers showing Δt = 22 μs $\Rightarrow$ f_{res} = 45.5 kHz.

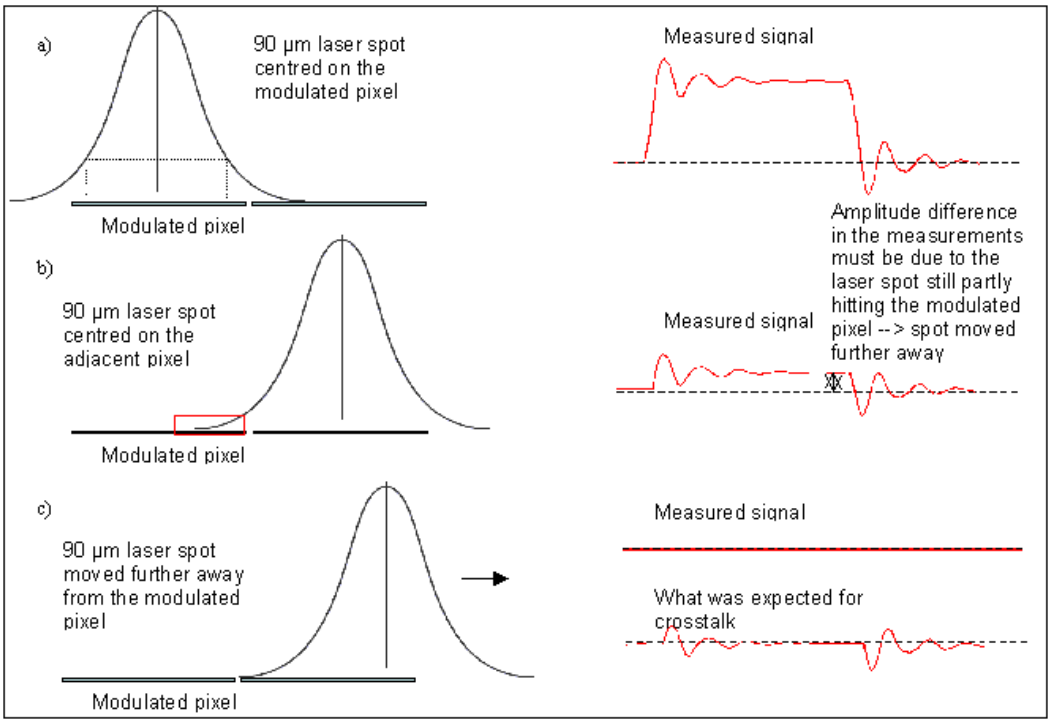

Figure 4.14. Crosstalk measurements. The first measurement (a) was for the resonance frequency. The lines inside the Gaussian spot show roughly how the 90 μm spot (measured from the 13.5 % intensity) fits the pixel. The second measurement (b) was done with the laser spot centred on the adjacent pixel. The amplitude difference between the two oscillations imply that part of the laser spot was still on the modulated pixel. For next measurements (c) the laser spot was moved further away from the modulated pixel and then the oscillations vanished altogether.

4.4 Spectral Modulation

4.4.1 Test Setup for Spectral Modulation

The DTS-1700 spectrometer is a natural test setup for measuring the spectral modulation capability of the PMDG. The original InGaAs detector was removed from the DTS and replaced by a fibre optics interface connected to a reference NIR spectrometer, which is the Ando AQ6317. The DTS was illuminated by a broad band NIR beam from the normal DTS entrance and a spectrum is dispersed across the Polychromator. Alternatively the DTS entrance was illuminated by a monochromatic beam from the Jobin Yvon HR-640 monochromator.

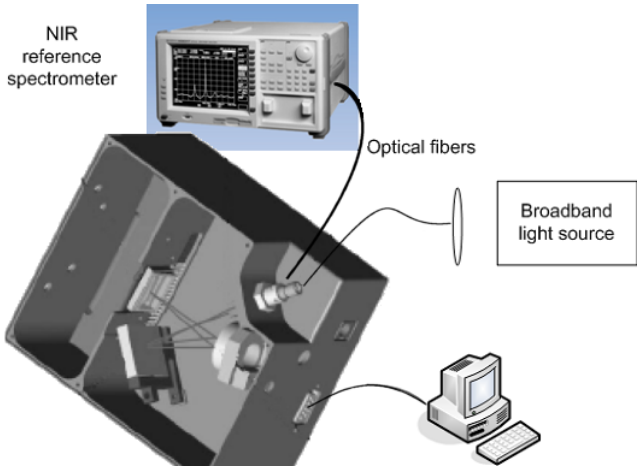

Figure 4.15. Test setup for spectral modulation.

4.4.2 Test Results for Spectral Modulation

When the NIR spectrum from a halogen lamp was modulated with the PMDG in the DTS spectrometer and the signal was measured with the AQ6317, it was noted that using one pixel was not enough to get the signal to near zero on that wavelength area. This means that the transmission for the particular wavelength would still be about 40%, as can be seen from Figure 4.16. Increasing the number of modulating pixels will improve the contrast but it will, of course, also widen the wavelength area thus worsening the achievable resolution. With two pixels the transmission decreases to about 15% and with three pixels to about 6%. When all pixels were in diffractive position for their particular wavelength area, 3% of the signal would still pass through. An explanation for this behaviour could be, that the modulated areas for each pixel will overlap each other with the three nearest pixels from both

sides, because of the dispersion of the static grating. This can be seen from the Figure 4.17, which shows a close up from 1440 nm to 1540 nm from a scan, where one pixel was pulled down in turns to maximum diffraction position and the whole spectrum was scanned with the AQ6317. The optical geometry of the system, as well as, the position of the fibre connection probably also have an effect on these results. Modulating voltages were the same as in the working DTS spectrometer.

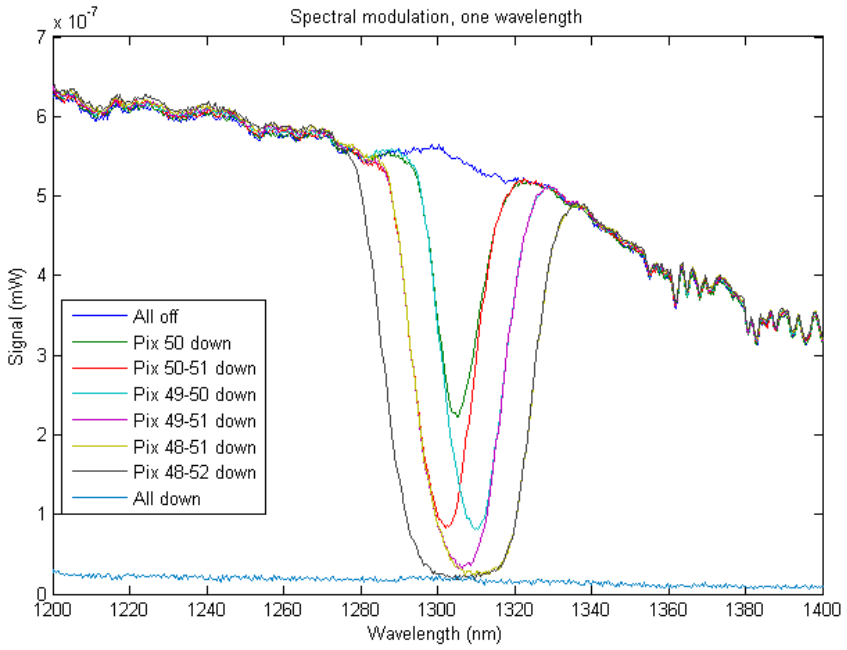

Figure 4.16. Spectral modulation. One wavelength from halogen spectrum modulated with different pixel counts and measured with the AQ6317. As can be seen the contrast with only one pixel modulating is not very good and it gets much better with two or three pixels. With one pixel modulating the transmission for the particular wavelength will still be about 40%. With two pixels the transmission drops to about 15% and with three pixels it drops down to about 6%. When all pixels were in diffractive position for their particular wavelength area, 3% of the signal would still pass through. The change of the centre wavelength position with two pixels modulating is due to the spectrum being fixed over the whole PMDG and as the adjacent pixel is pulled down, the position must shift between those two pixels.

Light from the monochromator was also connected to this test setup and the modulation capabilities were checked when the monochromator output wavelength was centered on one pixel and between two pixels. For intensity requirements the output wavelength band of the monochromator was quite wide, $FWHM = 9$ nm. The results presented in Figure 4.18(a) and Figure 4.18(b) are similar to what was measured with the whole spectral range in Figure 4.16. With non-monochromatic

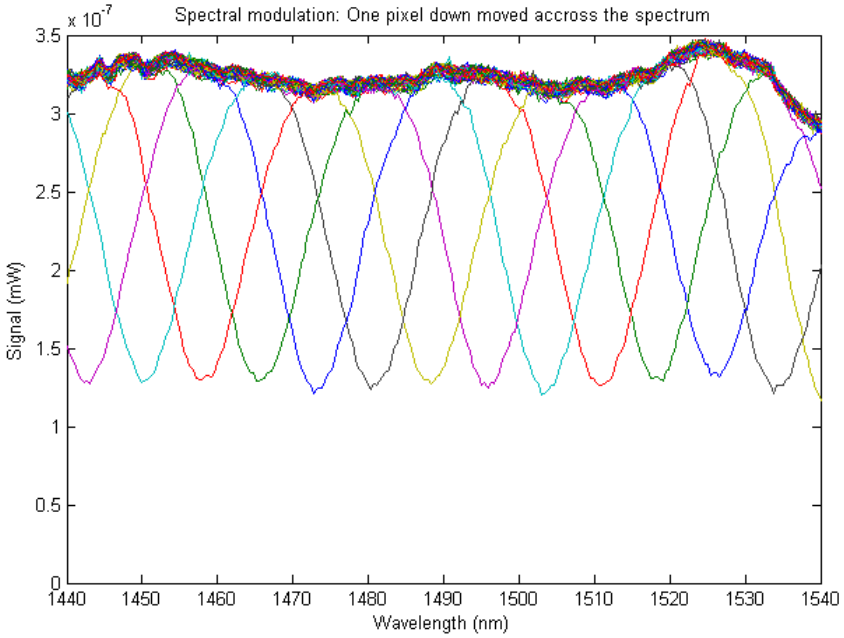

Figure 4.17. Overlapping modulation. One pixel pulled down in turns through the whole PMDG and the whole spectrum scanned between every change with the AQ6317. The resulting spectra are here plotted on top of each other to demonstrate the overlapping effects each pixel has on the spectrum. About seven pixels will have an effect on one wavelength area which is about 25 nm wide in total, depending on the dispersion of the fixed grating used to disperse the spectrum in the first place.

(FWHM $>$ 1 nm) light the achievable contrast ratio depends on the number of pixels modulating near the wavelength area. This depends on the resolving power and dispersion of the dispersing element as well as how well the optics can focus the spot on the PMDG pixel.

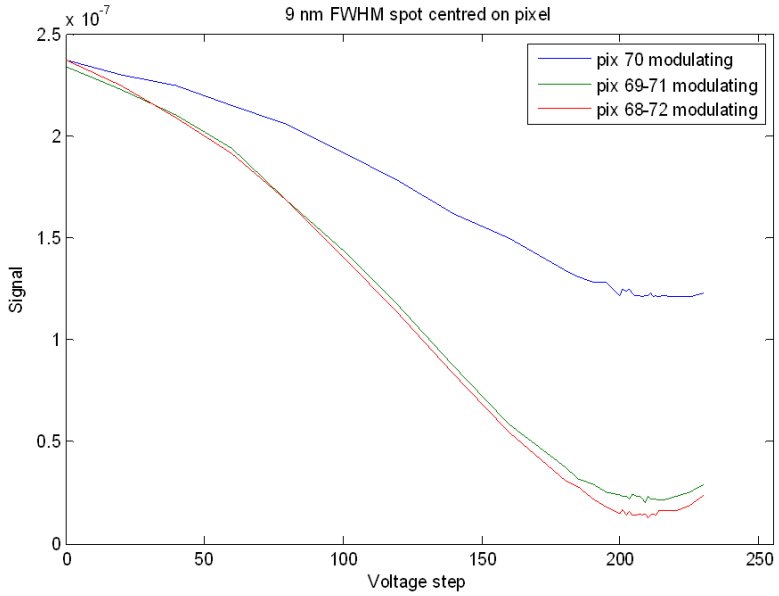

(a)

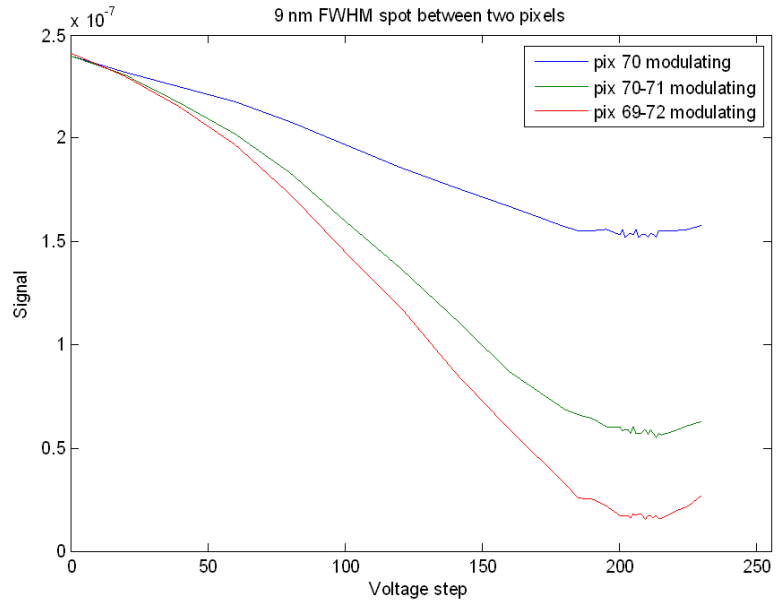

(b)

Figure 4.18. Spot from monochromator centred on a pixel and between adjacent pixels. Wide output from monochromator (FWHM = 9 nm) centred on one pixel (a) and between two pixels (b). The modulation was performed with different number of pixels. For (a) the blue curve shows the modulation only with the pixel the spot was centred on. The green curve shows the same spot modulated also with the adjacent pixels and the red curve adds the adjacent pixels to previous state. For (b) the blue curve shows the modulation only with the other of the two pixels the spot was centred between. The green curve shows the same spot modulated with both pixels and the red curve adds the adjacent pixels to previous state.

4.5 Diffraction Efficiency

4.5.1 Test Setup for Diffraction Efficiency

For diffraction efficiency measurements the output of the Jobin Yvon HR-640 monochromator was collimated with an Al-plated 90° off-axis paraboloid mirror ($\emptyset$ = 25.4 mm, focal length f = 101.6 mm). The collimated light was incident on the PMDG. The diffracted light was measured with a PbS detector (0.9-3 μm) mounted on a swing arm that was centred on the PMDG.

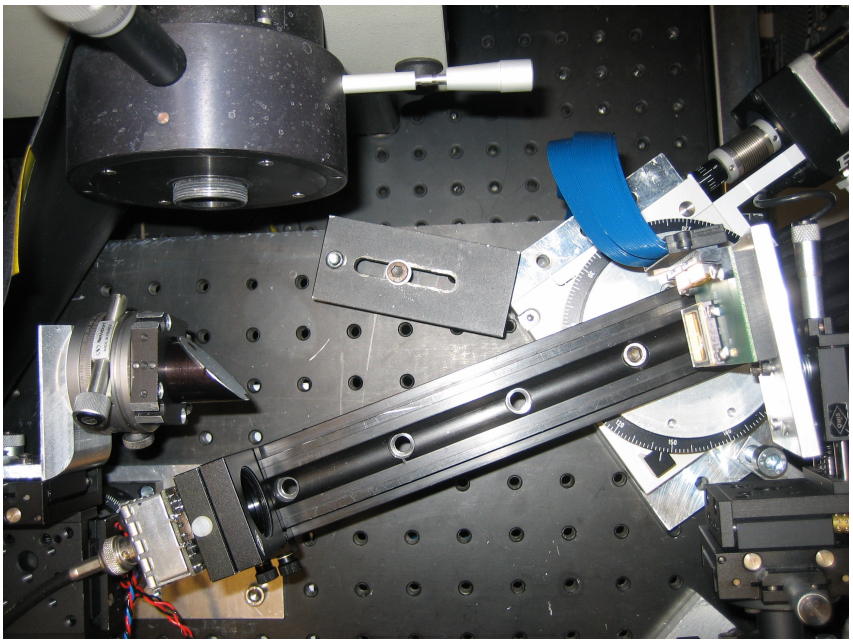

Figure 4.19. Test setup for diffraction efficiency.

A chopper and lock-in amplifier measurement system is used as the signal levels are very weak. In the NIR-range (900 - 1700 nm) a Glan-Thompson polariser was used to test the polarisation effects. Order blocking filters are used when needed. The PMDG is directly illuminated with a collimated (and polarised) monochromator beam.

From the data diffraction efficiency and angular dispersion results are calculated. The data can be presented as a 3D surface with the wavelength and modulation as the x and y-axes, and the efficiency as the z-axis. The reference intensity is measured by inserting a goldplated plane mirror instead of the PMDG.

4.5.2 Test Results for Diffraction Efficiency

The effects of polarised light on the PMDG modulation were checked with the HR-640 monochromator. First the original operation wavelength range was scanned with both TE (electric field parallel to the grooves) and TM (electric field perpendicular to the grooves) polarised light with the PMDG in reflecting state (Figure 4.20). The results were compared to a gold mirror, that represents the polarisation effects of the monochromator, and the differences between the two polarisations were rather small. The TE component seems to contain more resonances than the TM component, which is interesting, since usually the anomalies related to polarisation states are found when the electric vector is perpendicular to the grooves – the TM polarisation [36]. The effects seen in this measurement could be due to the segment structure of the Polychromator – the grating elements are not composed of single long beams (see Figure 4.2). The two polarisation states agree with the specifications for the grating used in the monochromator (see Figure B.1).

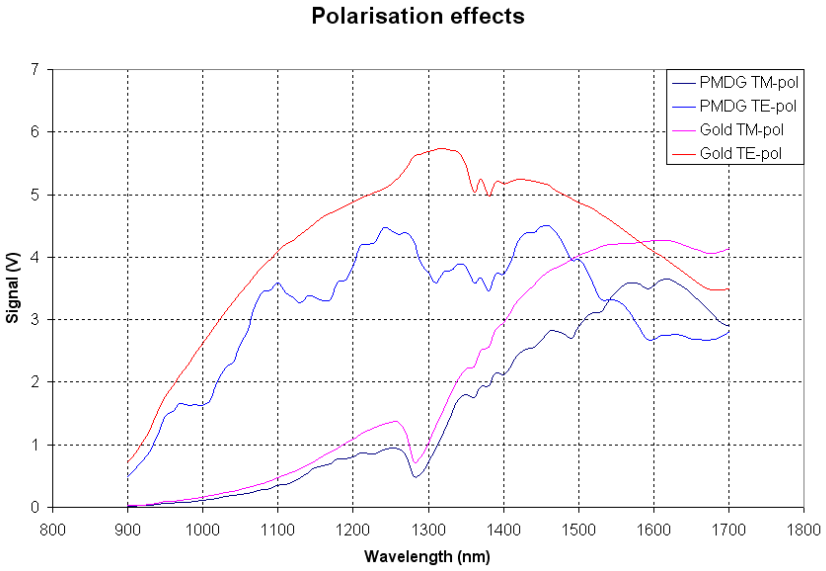

Figure 4.20. Polarisation effects. PMDG operation wavelength range scanned using polarised light. Reference values are from gold mirror. The absolute signal values are not directly comparable as the reference measurement had to be filtered with T=0.316 gray filter in order to avoid saturation.

The contrast ratio measurements with polarised light were made by positioning the detector at the location of maximum signal for the 0th and 1st orders, and gathering the signal for a sequence of element displacements. No effort was made to reduce stray light so the obtainable contrast ratio itself is not relevant. The zero

order modulation was measured with unpolarised and polarised light for comparison (Figure 4.21). The modulation with longer wavelengths was also checked (Figure 4.22) but the signal levels dropped too low after 2500 nm.

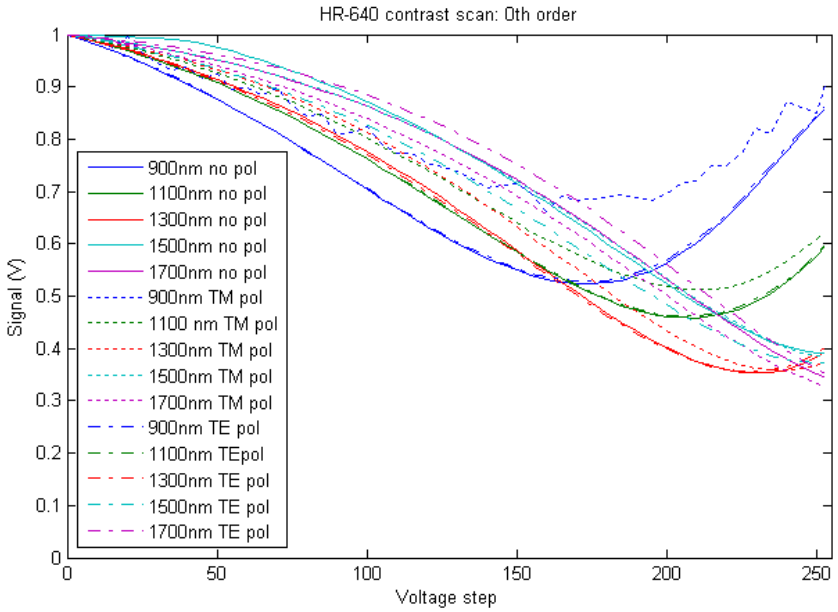

Figure 4.21. The effects of polarisation to zero order reflections measured with the HR-640 monochromator. Both polarisations act very similarly so polarisation states have no real effect on modulation. The difference with TM polarisation in shorter wavelengths is partially due to much lower signal levels from the monochromator (see Figure 4.20).

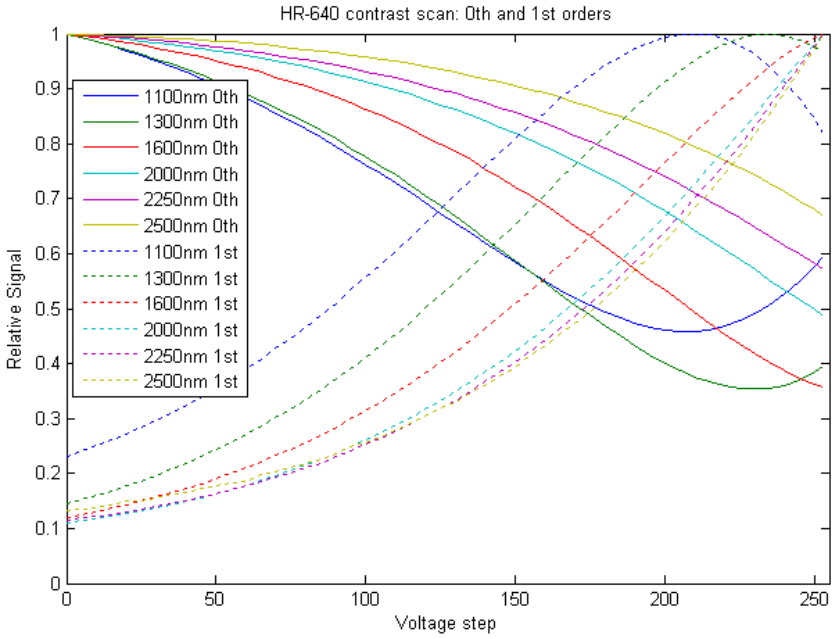

Figure 4.22. Modulation with longer wavelengths. Zero and first order contrast ratios for various wavelengths measured with the HR-640. 2500 nm was the maximum wavelength with enough signal probably due to the transmission of the cover glass of the PMDG package. As can be seen from this graph, the available modulation for wavelengths longer than 1600 nm is very limited. Even at 1600 nm the modulation is not full. This limits the usable wavelength range to 1600-1700 nm in the longer end of the spectrum. For shorter wavelengths the limiting factor will be the smaller diffraction angle, which will require larger f-numbers to separate the orders.

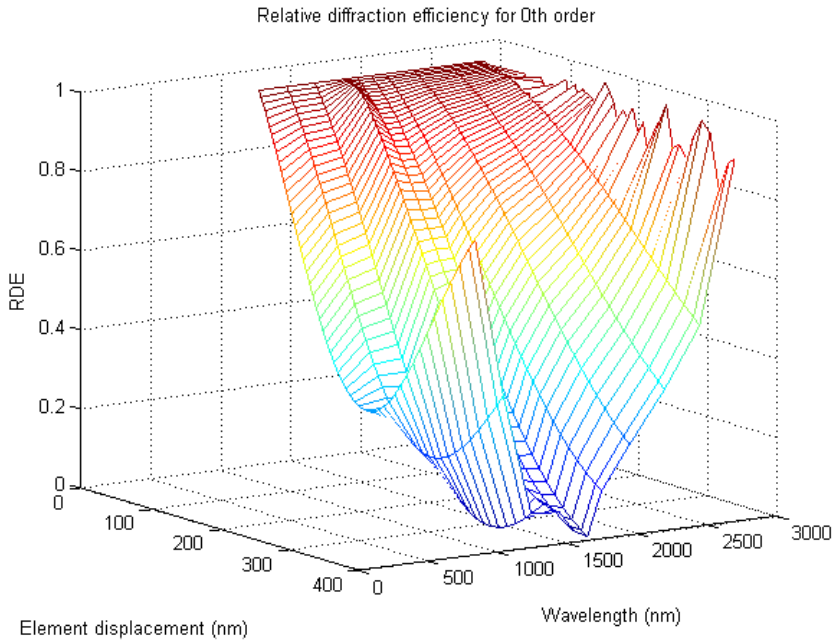

(a)

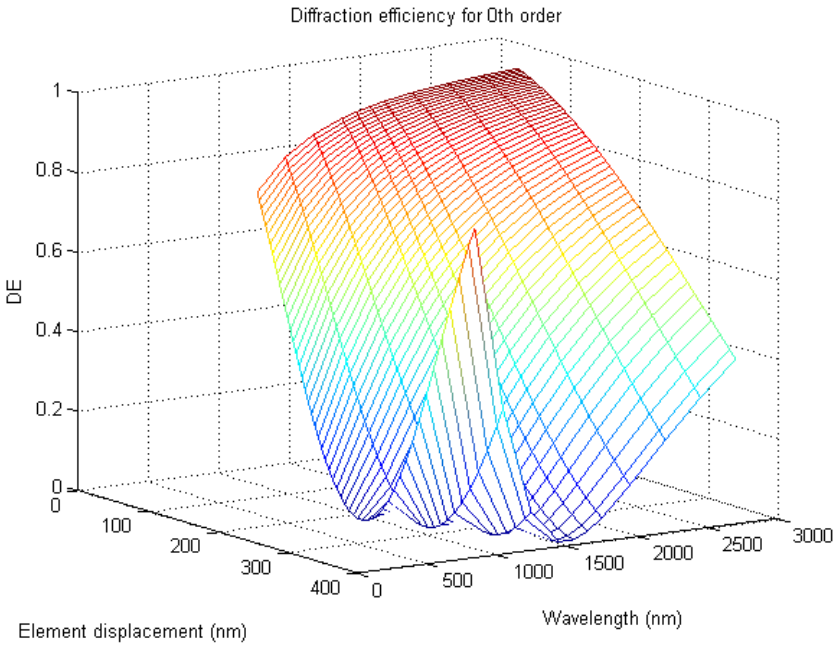

(b)

Figure 4.23. Diffraction efficiency. (a) Relative diffraction efficiency for zero order reflection measured with the HR-640 monochromator. (b) Diffraction efficiency for zero order reflection calculated from theory. ($\eta_0 = [1 + \cos(4\pi\delta/\lambda)]/2$, the fill-factor has been assumed 0.5).

The effects of different f-numbers were also measured with this setup. As the diffraction angles for the wavelength range of 900 nm to 1700 nm are only 2° to 4°, the required f-numbers to optimally distinguish the orders from each other are impracticably large. The measurement was done by reducing the aperture of a focusing lens installed between the collimating mirror and the PMDG, because increasing the focal length was not feasible within the test setup. Because of that, the measurement was done using only light at 1500 nm which provided the best signal. The results are presented in Figure 4.24 which indicate that with an f-number of 4, the reflected signal in diffraction mode does not stand out from the diffracted spot. F-number of 12.5 shows much better resolution but it still has some overlap between the diffracted and reflected spots. The required f-numbers are even larger for shorter wavelengths due to smaller diffraction angles.

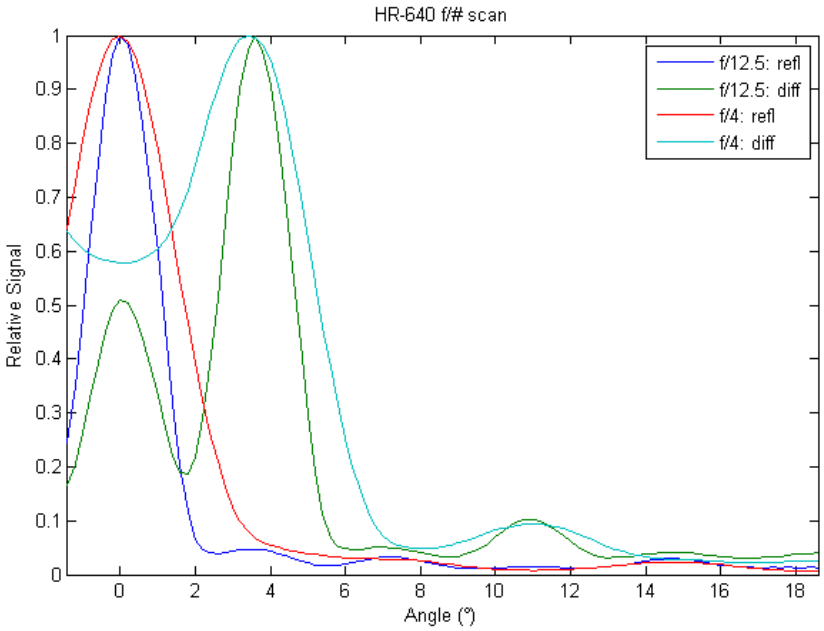

Figure 4.24. Effects of different f-numbers for 1500 nm. This measurement demonstrates the effect of f-number on angular separation of the orders. We can see that with f-number 4 the reflected signal in diffraction mode does not stand out from the diffracted spot. An f-number of 12.5 is better but still not enough. The required f-numbers are even larger for shorter wavelengths due to smaller diffraction angles.

The effect of number of modulating elements on diffraction efficiency was also measured by reducing the number of modulating pixels but no results were gained because the angular width of a spectral line, depending on the modulating elements, was smaller than the divergence of the collimated light used in the measurement.

Theoretically the angular width of a spectral line is defined by [37]

$$\Delta\beta = \frac{2\lambda}{Nd\cos\beta}, \tag{4.1}$$

where N is the total number of grooves illuminated on the surface of the grating and d is grating pitch. For $\lambda = 1500$ nm and a whole pixel, the angular width of a line is about 1.4°. The divergence of the collimated light was about 1° resulting the diameter of the collimated spot to be about 2°. Further investigations with 1-to-1 imaging of a 25 μm slit on the PMDG revealed that this would be very difficult, if not impossible, to measure. On one hand, high f-numbers are needed in order to see the effect of broadening, but on the other hand, the high f-numbers do not allow small enough spot on the PMDG which is required in order to the effect to be seen.

The radius of the smallest spot, that can be achieved due to the diffraction limit, is defined by

$$r = 1.22\frac{f\lambda}{D_l} = 1.22\lambda \cdot f/\#. \tag{4.2}$$

The diffraction angle of the 1.63 μm light is 3.96°. The broadening due to the f-number must be limited to ±1.9°, so that the orders can be separated, which means f-number of >15. In order to measure the broadening, the spot size required on the PMDG to limit the number of elements is <49 μm, which is defined by Equation 4.1. The f-number limits the spot size to 60 μm, which will cause less broadening than the f-number.

Absolute distribution of energy to orders was measured with a HeNe 632.8 nm laser spot, as it gives nice and compact spots. The results were compared to reflection from gold mirror. The measured signals are the reflection caused by the glass cover, the reflected/diffracted signal from the PMDG and the signal that has reflected from the glass cover back to PMDG and then through the glass (Figure 4.25).

As can be seen from Figure 4.26, the even diffraction orders for the diffraction mode, i.e. the same points where light diffracts in reflection mode, are missing or the signal values are much lower. This is probably due to some destructive interference caused by the two diffraction profiles – the original gaps in the grating structure and the actuated grating profile. This feature can also be seen in the simulations (see Figure 4.27).

The measurement was also repeated with 1500 nm light and the results are similar. Because the simulations also show the same behaviour for both of the wavelengths, we can draw the conclusion that the energy distribution measured with 632.8 nm is similar for the 1500 nm.

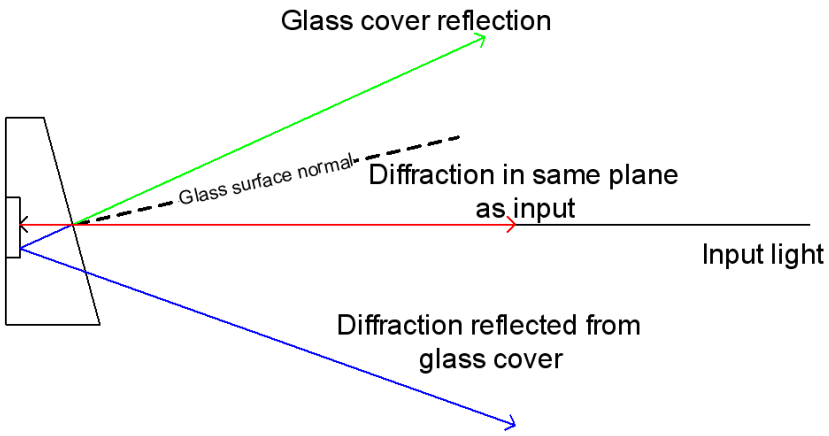

Figure 4.25. Illustration of the light paths from the PMDG component as can be seen with laser intensities. The angles are not accurate.

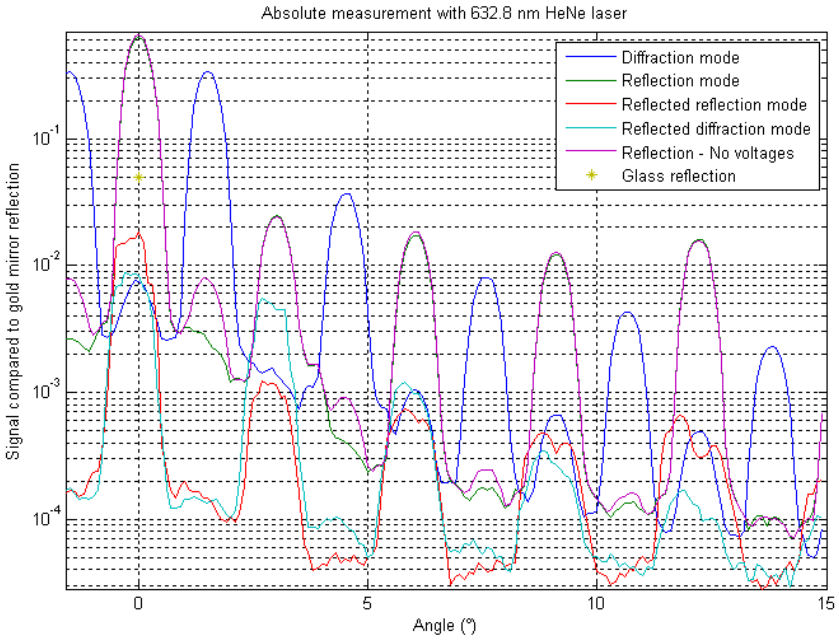

Figure 4.26. Absolute measurement with 632.8 nm HeNe laser when incident light is perpendicular to the PMDG. This graph shows the light intensities with logarithmic y-axis, compared to gold mirror reflection, that were measured from the reflected and diffracted light from PMDG and from glass cover.

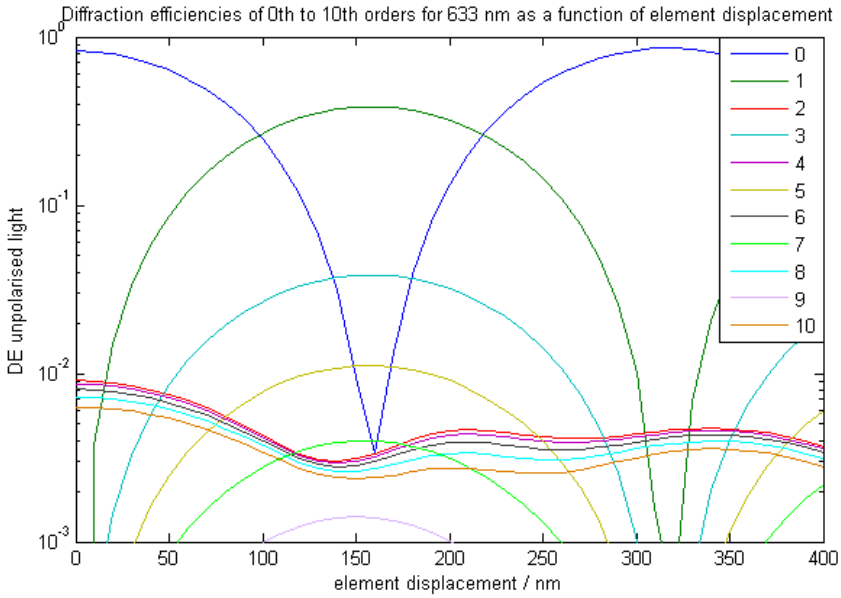

Figure 4.27. Simulated diffraction behaviour for ten first orders for 633 nm. All the even orders are suppressed when the grating is in diffractive state but they do have a maximum with zero order when the displacement is 0 nm.

Table 4.3. Distribution of incoming light intensity to different orders for 632.8 nm HeNe laser. A reflection coefficient of 0.95 was assumed for the gold mirror. Only points where >0.1% of incoming light is going, are noted separately. The values in even diffraction orders for reflection are caused by the gaps in the grating structure. They are actually the 1st, 2nd etc orders for the non-actuated grating but as they are the same points as even orders for actuated grating, it is clearer this way. The signal in the 1st order for reflection is probably due to the fact that the elements are not exactly on the same plane.

	Reflection	Diffraction
Glass reflection	4.75 %	4.75 %
0 order	60.57 %	0.72 %
1st order	0.61 %	64.96 %
2nd order	4.73 %	<0.2 %
3rd order	< 0.1 %	7.07%
4th order	3.31 %	<0.1 %
5th order	<0.1 %	1.54 %
6th order	2.28 %	<0.1 %
7th order	<0.1 %	0.82 %
8th order	3.04 %	<0.1 %
9th order	<0.1 %	0.44 %
Reflected Refl/Diff		
(0th + 1st)	1.96 %	1.87 %
Higher orders + absorption	18.36 %	17.43 %

4.6 Summary

The selected PMDG component has been characterised by a series of tests described in the previous sections. The PMDG was all the time contained in its own package behind a tilted cover glass. The overall dimensions of the PMDG itself is 2 mm x 12 mm. The grating consists of 1000 elements organised into 100 pixels consisting of 10 elements each. Every second element is static and the rest can be electrostatically displaced. The basic element pitch is circa 11.8 μm and the grating pitch formed when the elements are displaced is 23.6 μm. This gives first order diffraction angles in the range $2 \ldots 4°$ for 900-1700 nm. The elements are displaced by a voltage difference in the $15 \ldots 30$ V range with a resolution of 8 bits (using the control electronics of the DTS-1700).

Measurements of capacitance and light intensity as a function of control voltage shows that the step size increases with voltage, thus it makes sense to use a bias voltage and use the available resolution for the upper half of the control voltage range. From the laser contrast measurements and from some measurements with higher wavelengths that were done with the HR-640 monochromator, a model for deflection per voltage was fitted to the measurement points (Figure 4.28). The measurement points are from the $\lambda/4$ and $\lambda/2$ points, as these are the only fairly certain positions where one can estimate the stroke. The fitted curve is based on the simplified model for GLV that was modified and approximated as the material parameters (thickness, residual stress or spring constant) and the original gap for the Polychromator were not available. The GLV model is [13]

$$\delta(V) = \frac{x_0}{3}\left[1 - \left(1 - \left(\frac{V}{V_{PI}}\right)^{\omega}\right)^{\frac{2}{3\omega}}\right], \tag{4.3}$$

where $V_{PI} = \sqrt{\frac{8\kappa x_0^3}{27\epsilon_0 A}}$, x_0 is the original gap, κ is the spring constant, ϵ_0 is the dielectric constant of vacuum and ω is a fitting parameter. The fitting parameter used here is the same as in the original GLV model, $\omega = 1.8$. Other parameters are $x_0 = 2180$ nm and $V_{PI} = 32.2$ V.

The maximum displacement is about 400 nm. The length of the displacement limits the wavelength operation range in spatial modulation applications to $4 \times \delta = 1600$ nm. The cutoff limit is set by the transmission of the cover glass. The capacitance change of one pixel is about 100 fF for the maximum displacement. The mechanical resonance frequency of the elements is about 45 kHz, the Q-factor is circa 4 giving a step response decay time of less than 100 μs. Any static crosstalk between

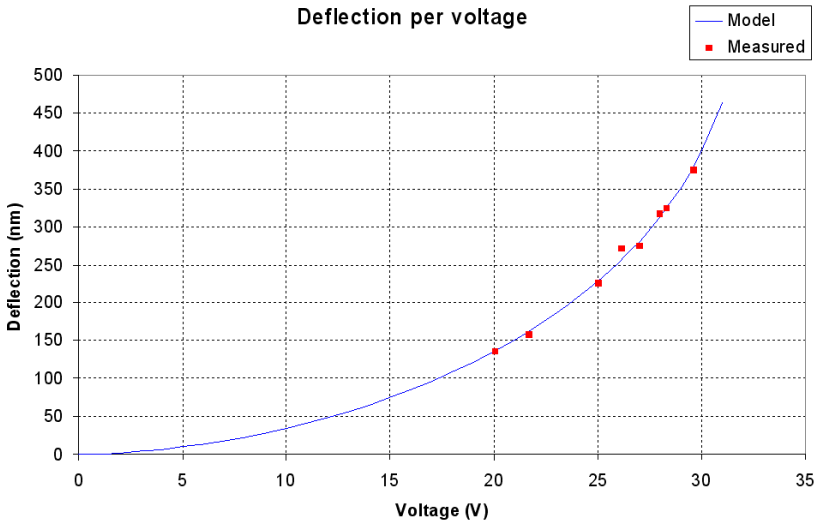

Figure 4.28. A model for predicting the deflection per control voltage. Though originally suited for the GLV, the model works really well with the test results for the Polychromator. The initial and maximum displacement with bias and control voltage from the model are the same as derived before – about 80 nm and 375 nm.

pixels could not be detected.

The absolute diffraction efficiency is circa 61 % into the zero order for maximum reflection and circa 65 % into the ±1st orders for maximum diffraction. It is noteworthy, that the even diffraction orders are suppressed in the diffractive state and that there are diffraction orders present in the reflective state, as well. Contrast ratios between min/max reflection and min/max diffraction is at least in the order of 100-500 and 200-1000 with the used test setup. The results are limited by the accuracy of the used methods and the test setup. These values should be treated carefully as more accurate measurement would probably give much higher ratios. When used in spatial light modulation applications where full order separation is required, the cone angle of the incoming monochromatic light beams must be smaller than 1.1° (for 900 nm) corresponding to an f-number of 26. When there is a finite wavelength band of light impinging on the pixel, additional dispersion induced spreading must be accounted for. The effect of the pixel width (120 μm) on the angular width of the line is rather small ($<$ 1.6° for 1.7 μm). This proved to be impossible to measure with smaller spot sizes due to required f-number limiting the smallest achievable spot. Polarisation effects were investigated in the 900 - 1700 nm range, but were found to be rather small. The TE component contains more resonances than the TM component.

Chapter 5

Instrument Detailed Design

This section is about the opto-mechanical design and characterisation of the instrument demonstrator. During the characterisation measurements of the PMDG component, it became clear that the original concept idea to demonstrate the use of PMDG with a telecentric prism-grating-prism imaging spectrograph was not going to work with this PMDG (most notably due to the f-number requirements and spatial axis length of <2 mm). Even though the main benefits of the system is in the IR region, for this thesis the demonstrator was tested mainly in the VIS-NIR region.

5.1 Opto-mechanical Design

The goal for the optical design of the demonstrator was to keep the overall structure very simple. Other important points were to avoid ghost reflections and minimising stray light. To have a system without any ghost reflections, the design was carried out without the beamsplitter. Stray light was minimised with three apertures placed into various points throughout the system. Because of the wide wavelength range (the demonstrator is to be tested with both LVBFs during the project), beam direction and collimation is performed with mirrors instead of lenses. The lens system would suffer from chromatic aberrations while mirrors are free from it.

The optical design of the demonstrator is presented in Figure 5.1. The light enters the system from a 600 μm optical fibre or from a lens assembly and a 600 μm pinhole. The input light beam is then directed with a right angle mirror to an off-axis parabolic mirror which collimates the beam. The right angle mirror was added to the system to make more space for mechanical attachment of the fibre and the detector.

Table 5.1. Specifications for single-point miniature spectrometer.

Description	Value	Rationale
Wavelength range	620 - 1080 nm	Readily available LVBFs from JDSU.
	1400 - 2500 nm	The usable wavelength range of the IR LVBF is probably feasible only at 1400 - 1700 nm due to insufficient modulation.
Spectral resolution	1-2% of CWL	Bandwidth of the LVBFs.
Throughput	max 0.07 %	Efficiency of the LVBF for "dispersion" is inherently its relative bandwidth (∼0.01). Aperture blocks most of the light.

There is an aperture in front of the PMDG to block light from hitting the surface around the PMDG active area which will cause unwanted reflection. The LVBF is mounted on the backside of this aperture, which is tilted 1 degree in order to avoid ghost reflections from the LVBF and the aperture itself. If the tilting angle of the LVBF is significantly larger, it would affect transmission through the LVBF, and if it is smaller, ghost rays would not be separated from accepted rays in the detector plane. The tilting is done in the shorter dimension of the LVBF so that the incoming light and the light reflected from the PMDG will go through the same pass band. The cover glass of the PMDG is tilted ca 5.5 degrees thus it does not cause ghost reflection. For the accepted light rays the PMDG is a mirror surface and for the rejected rays a common diffraction angle based on the smallest diffracted angle is used. Blue rays are accepted rays and green and red rays are rejected rays. There are two other apertures in the system, one after the right angle mirror limiting the input beam half cone angle and another in front of the detector allowing only wanted rays to hit the detector. Rejected rays do not hit the exit aperture because their path is different by a few degrees.

The main factor in reducing the throughput is that the efficiency of the LVBF for "dispersion" is inherently its relative bandwidth (∼0.01). Using a grating for dispersion can reach efficiencies >0.9 for the blazed wavelength. In the following table (Table 5.3) the throughput calculations for the system are presented. Because of the estimated low throughput, the signal will be amplified with transimpedance amplifier using a 500 MΩ feedback resistor.

The detailed mechanical design is performed with IronCAD and some views of the

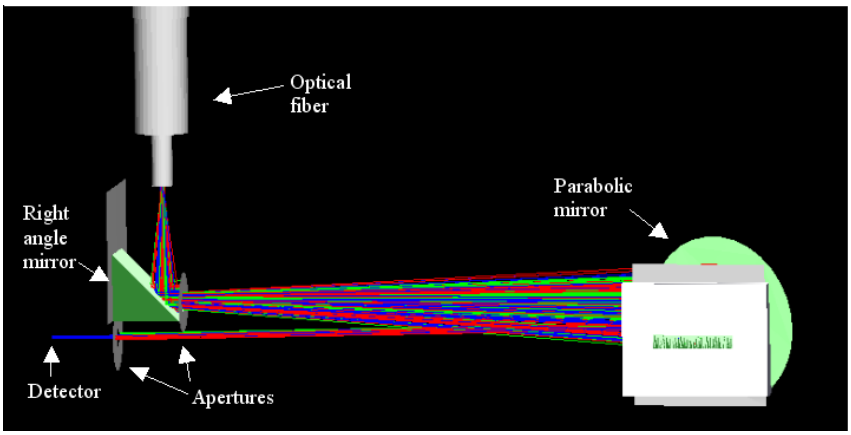

(a)

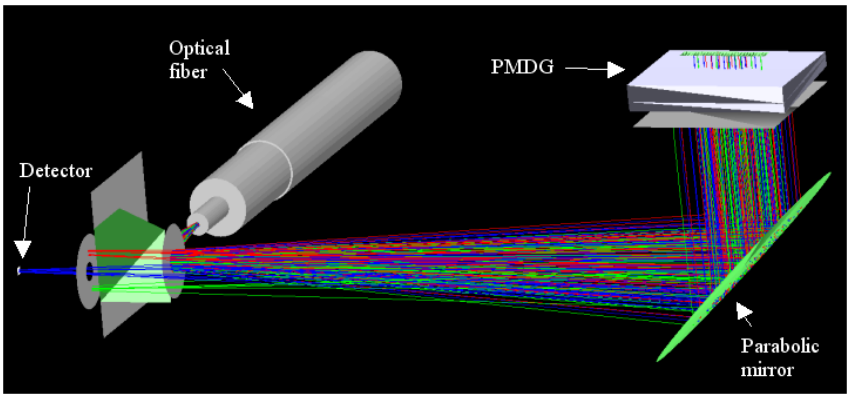

(b)

Figure 5.1. Demonstrator optical design. (a) Side view. (b) Bottom view.

Table 5.2. Optical components for the instrument demonstrator.

Component	Description
Parabolic mirror	Effective focal length = 101.6 mm, gold coated off-axis mirror (Edmund optics 47-100).
LVBF	620 - 1080 nm, BW = 1.5 % , transmission 90 % at 900 nm. 1400 - 2500 nm, BW = 0.6 %, transmission 45 % at 1400 nm.
PMDG	Polychromator disassembled from DTS-1700. Active area 2x12 mm, 100 pixels of 120x2000 μm size. Deflection range 0, 80..375 nm.
Right angle mirror	Gold coated, size of the reflecting surface is 10x14.1 mm (Edmund optics 47-028).
VIS-NIR or NIR sensor	InGaAs detector DET10C/M from Thorlabs. Si detector DET10A/M from Thorlabs.

Table 5.3. Estimated throughput of the demonstrator.

Component	Throughput	Explanation
Right angle mirror	96 %	Gold coated mirror, reflection 96 %.
Parabolic mirror	92 %	Gold coated mirror, reflection 96 %. Light goes twice through this component.
Aperture	15.5 %	Aperture in front of the LVBF pass through rays which hit to active area of the PMDG. Aperture size 1.5 mm x 12 mm.
LVBF	20 - 88 %	The transmission for the LVBF (depending on the model) is from 44.73 % to 93.86 % for one pass through. Light goes twice through LVBF.
LVBF	1 %	Because of the collimated light the LVBF passband uses only 1 % of the total beam.
PMDG	60 %	The PMDG will reflect 60 % of the incoming light to zero order.
Total	0.016 - 0.072 %	Total throughput of the demonstrator system.

3D model are shown in Figure 5.2. In order to simplify testing, the demonstrator mass and volume have not been constrained. Alignment is performed by installing the PMDG on a Pitch & Yaw Platform With Micrometer Drives (Thorlabs PY003/M) and a 1/4" Travel Translation Stage (Thorlabs MS1/M). Compact design with no moving parts and with a few optical components that will require precise positioning is desirable for harsh conditions. For example, the instrument would have to stay operational after extremely hard lift-off and even after a possible touchdown on another celestial body as repositioning would be impossible.

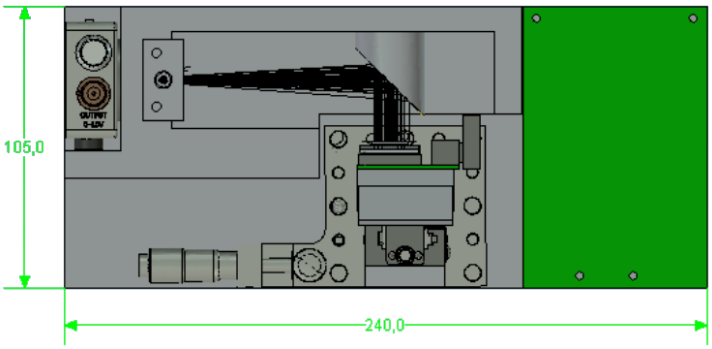

(a)

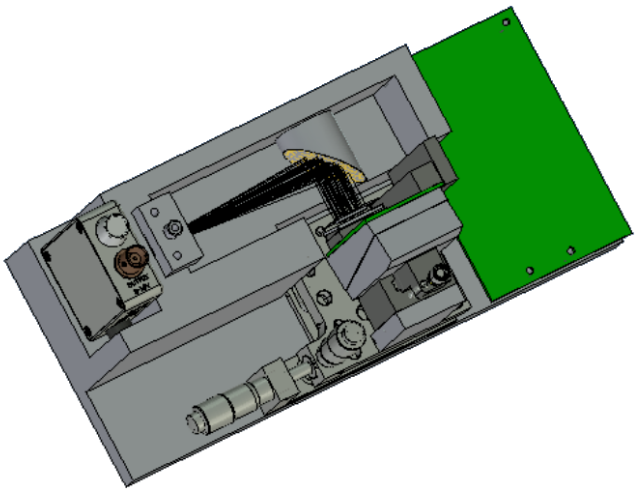

(b)

Figure 5.2. Demonstrator opto-mechanical design. (a) Main dimensions of the demonstrator. (b) Conceptual view. The green part is the PMDG controller PCB.

The control program is made with LabVIEW. The Hadamard matrices are created within the LabVIEW using mathscript. Because of the limitations in Hadamard matrix sizes that can be automatically generated (the mathscript can only form

Hadamard matrices of sizes 2^n or its multiple with 12 and 20), the first usable Hadamard matrix is of size 128.

5.1.1 Demonstrator Integration and Test Plan

The following performances will be verified by tests.

LVBF Transmission and Linear Dispersion

The LVBF is mounted on a linear stage and is illuminated with a collimated broadband beam. An input fibre to the Ando reference spectrometer is mounted behind the LVBF with an additional 50 μm slit. The LVBF transversal position is varied with the stage and the transmitted spectrum is determined. The spectrum is also measured with the LVBF removed. The transmission is determined from the signal ratio. Also the effect of tilting the LVBF on the spectrum is observed.

Si Detector Characterisation

The detector, along with the amplifier and DA-converter, is assembled. A black body source is placed in front of the detector optical axis. The irradiance at the detector is varied by changing the source distance and by changing the source electrical power. The signal level and noise is measured for each configuration. Dark signal noise, offsets and stability are also determined.

Integration

The integration is performed using the following steps:

- Fix the input fibre, input folding mirror and the aperture.
- Install the collimating mirror.
- Install the detector.
- Check with visible light that a focused spot can be formed at the detector surface. Use the PMDG pitch & yaw platform for alignment.
- Align the LVBF/aperture on the PMDG cover glass using visible light/laser to illuminate the PMDG. Use the detector for finding the maximum signal location.

The following tests are performed with the demonstrator in an integrated configuration.

Contrast Ratios

The demonstrator pinhole is illuminated with broadband light. Instead of the demonstrator detector, there is a fibre optic coupling to the HR4000 or Ando AQ6317 reference spectrometers. Different (narrowband and Hadamard) modulation patterns are programmed on the PMDG and the effect on the spectrum is observed. The obtainable contrast is determined and absolute wavelength calibration is performed.

Spectrometer Level Tests

The demonstrator is illuminated with monochromator lines and with calibration lamps (Hg, Ne, Xe, Kr) as well as with black body source. The following performance parameters are determined:

- Spectral range
- Spectral resolution
- Absolute wavelength accuracy
- Radiometric performance
- Signal to noise ratio.

The tests are performed both for the 600-1000 nm and the 1400-1700 nm configurations.

Spectrum measurements are performed with the Hadamard and line scanning method and the two methods are compared against each other. Also the correlation mode is tested. Here, in addition to the spectrally weighed measurement, a measurement of the total signal with the PMDG programmed for full transmission is needed. The ratio of these measurements is proportional to the correlation.

Also natural transmission and emission spectra are determined from various materials. It is natural to compare the performance with the Polychromix DTS-1700 spectrometer. The performance is also compared with some other spectrometer architectures.

5.2 Characterisation of Instrument Performances

5.2.1 Results for LVBF Transmission and Linear Dispersion

The LVBF6201080 was installed between collimating mirror and an output slit aperture with 50 μm slit in front of the fibre input to AQ6317 reference spectrometer. The

LVBF position was varied with linear stage and the transmission was measured from each location and the signal was compared to a measurement where the light goes past the LVBF. The FWHM of the measurements was 2-2.5% of CWL and it is most likely the collimation which has a limiting effect. The collimation was done so that the spot size would remain small, using a lens with f=20 mm and d=10 mm, in order to get enough signal through. The measured signal levels were still in the range of picowatts. The measurement was repeated with the signal coupled directly from fibre

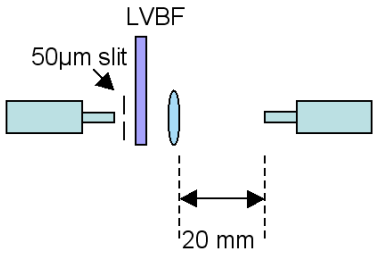

Figure 5.3. Test setup for transmission measurements.

to fibre with the LVBF in between because the transmissions for the LVBF14002500 seemed to be out of specifications. The signal values were much higher as there was no slit reducing it but the transmissions remained the same. The effect of tilting was also measured.

Measured linear dispersion for the LVBFs are about 39.78 nm/mm for the LVBF620-1080 and about 101.68 nm/mm for the LVBF14002500. Calculated bandwidths are 2-3% for both LVBFs. Tilting the LVBF shifts the wavelength band to shorter wavelengths. The effect greatly increases after a ±6° tilting angle. The vertical position inside the same pass band has no effect on transmission.

5.2.2 Results for Si Detector Characterisation

The Si detector was connected to the transimpedance amplifier with a 500 MΩ feedback resistor and the output of the amplifier was connected to the NI 9215 AD-converter. Measurements were done using the unfiltered noise bandwidth of 420 kHz of the AD converter, as well as, averaging the measurements so that the noise bandwidth dropped to about 30 Hz. The signal from a black body source was measured with three temperatures (750°C, 825°C and 900°C) and at three distances (78 mm, 350 mm and 1000 mm). The wavelength range was limited with a 766 nm band pass filter with 10 nm pass band.

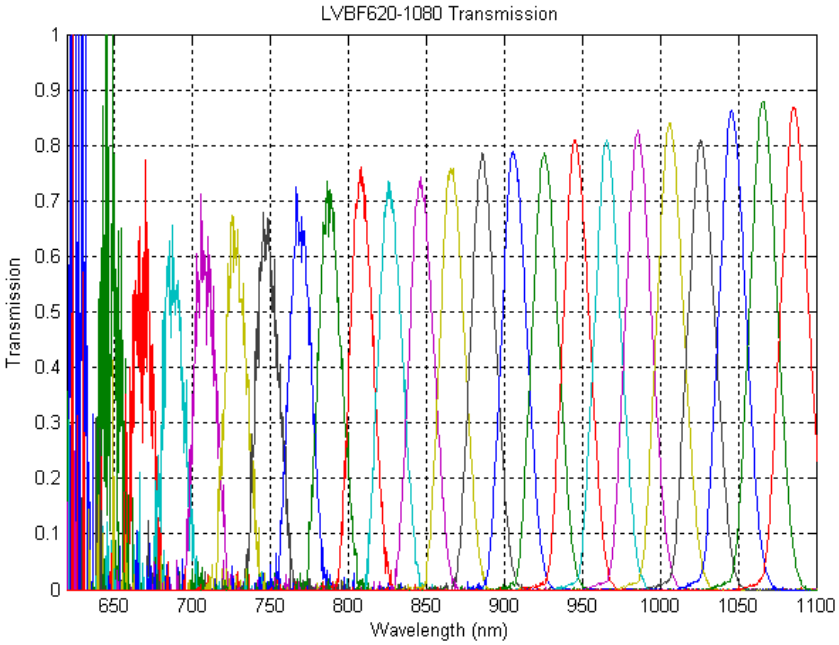

(a)

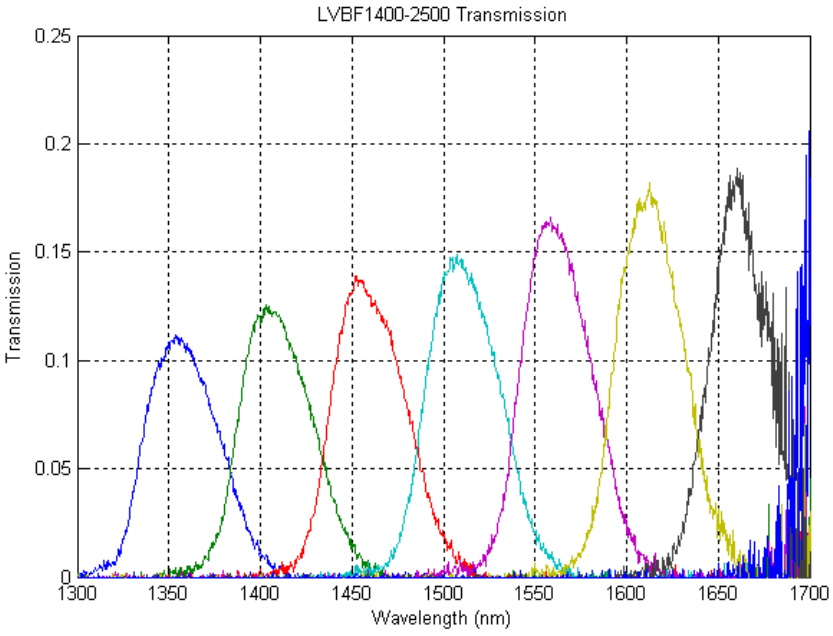

(b)

Figure 5.4. LVBF transmission measurements with collimated light and 50 μm slit. (a) Transmission for the LVBF6201080. (b) Transmission for the LVBF14002500.

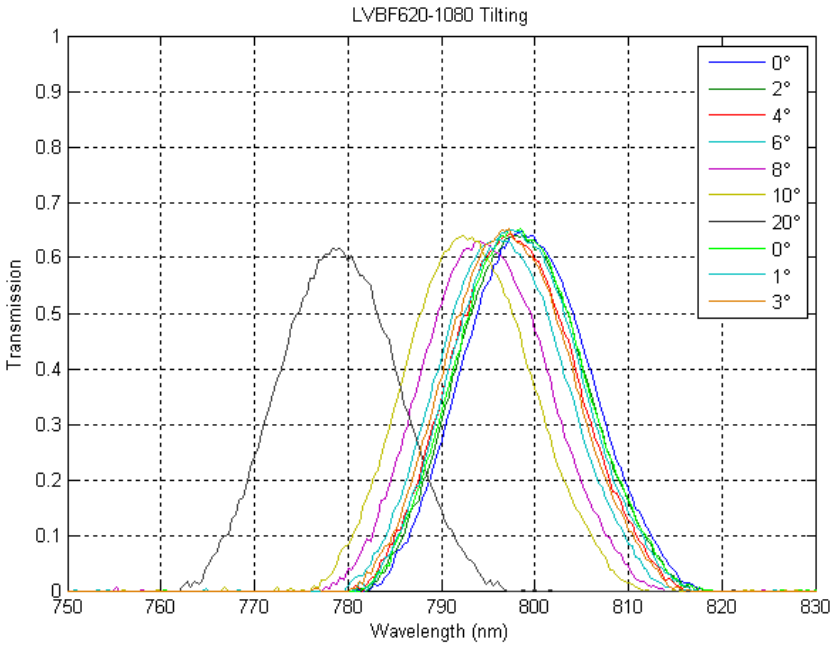

Figure 5.5. LVBF tilt measurements for LVBF6201080. If tilt is greater than ±6°, the wavelength band starts to shift more.

The average noise for these measurements are $\sigma_1 \approx 0.0011$ V for unfiltered and $\sigma_2 \approx 0.000026$ V for averaged. Using the aforementioned noise bandwidths, load resistor and average responsivity of 0.4329 A/W for the detector at 766 nm, we can calculate the NEP to be about

$$NEP = \frac{\sigma/\sqrt{B_{noise}}}{\Re \cdot R_L} \approx 2.2 \times 10^{-14} \text{ W}/\sqrt{\text{Hz}}. \tag{5.1}$$

The specifications sheet gives NEP value of 1.9×10^{-14} W/$\sqrt{\text{Hz}}$ for 750nm.

Dark signal with the detector connected was measured to be about 0.07 V and the dark signal offset with the detector disconnected was measured to be about -0.003 V. The dark current of the Si detector can thus be calculated to be

$$i_D = \frac{0.07059 \text{ V} - (-0.00294\text{V})}{500 \times 10^6 \ \Omega} \approx 0.15 \text{ nA } (@\text{T} = 20°\text{C}). \tag{5.2}$$

The specifications sheet gives dark current value of 0.3nA (2nA max) but does not specify the temperature.

5.2.3 Results for Integration

The main integration steps are glueing (fast curing epoxy adhesive) of the right angle mirror in its slot and mounting of the LVBFs in their holders with glue (optical grade epoxy adhesive). The other integration steps include components to be fastened with screws, which are reversible steps. Photos of mechanical parts and integration are presented in Appendix A. Integration was performed using the following steps:
1. The pitch & yaw platform was installed on its place
2. The collimating mirror was installed using guide pins
3. PMDG was installed on its holder and the holder was installed on the pitch & yaw table. This includes (see Appendix A for parts):
- mounting PMDG on part 3
- connecting vertical travel translation stage to part 3 after PMDG is installed on it
- mounting the package from previous steps to the holder (part 4)
4. The input folding mirror was aligned on its holding platform with light from the input fibre and the aperture. A collimated spot centred on the PMDG was used as a criterion. During this phase the frame (part 5) was tilted about 30° so that the folding mirror would rest on its back against the wall. The fibre input aperture was carefully placed on its position to show how the collimated light would hit the PMDG before glueing the mirror on its place. If the spot was misaligned the mirror position was corrected. The LVBFs were also glued on their holders.
5. The input fibre aperture was installed after the epoxy adhesive was cured
6. The detector was installed
7. The PMDG pitch & yaw platform was used for alignment with visible light to get the spot on the detector
8. The LVBF/aperture was installed and aligned on the PMDG. The alignment procedure is explained in more detail in the following section.

The alignment of the LVBF proved to be more complicated than was thought. The original idea was to align the LVBF in respect to the PMDG with maximum signal on the detector. This, however, is not recommended because the reflected signal from outside the grating area is greater than from the grating itself. Reason to this is that the whole inside area of the grating package is covered with gold layer and the area outside the grating pixels is smooth, whereas the grating has gaps. This will lead to the point that the best signal is collected when the LVBF is misaligned. Also putting the PMDG to diffraction mode and aligning with minimum signal is not practical because the alignment might be far away. One practical solution requires a fast linear-array spectrometer. The alignment was done here by using the HR4000 spectrometer

connected instead of the detector. The trick is to program some diffractive pixels, such as every fourth, on the PMDG and in addition make one larger area where all the pixels are in diffractive state (see Figure 5.6).

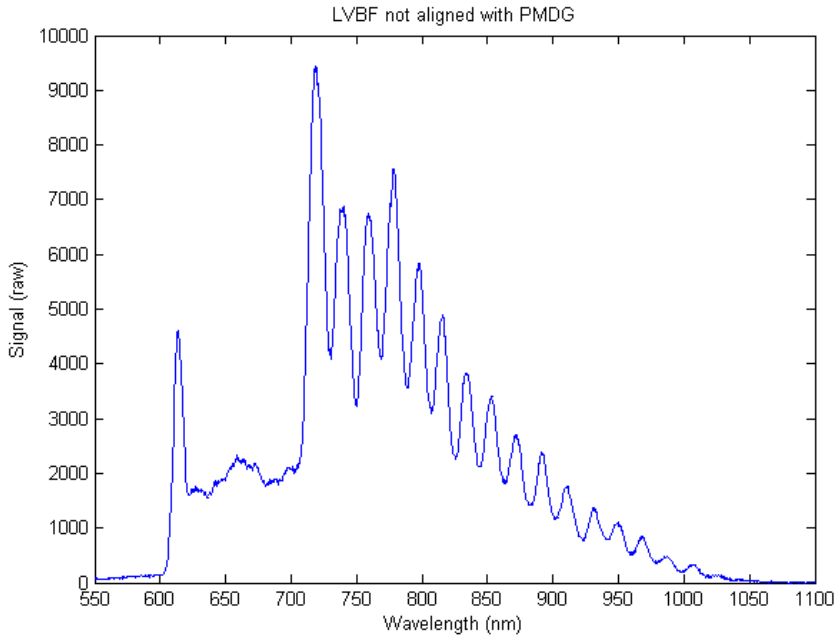

Figure 5.6. LVBF and PMDG not aligned. This figure shows a pattern of every fourth pixel in diffractive state and in addition one larger area between 620-700 nm where all the pixels are in diffractive state. The LVBF is misaligned here.

Now there should be only minimal signal from the area where all the pixels are in diffractive position (620-700 nm in Figure 5.6) since only reflected signal reaches the detector. Some signal will always come through because the pixel positions cannot be in perfect diffractive state for a given wavelength with limited control accuracy. However, the alignment should be set so that this signal is at its minimum. If the travel translation platform, that moves the PMDG up and down in respect to LVBF (spectral locations do not change), is now operated, two things can be seen. If the movement is towards the optimal alignment, the signal from the large diffractive area should get lower while the modulation pattern of every fourth (between 700-1000 nm in Figure 5.6) remains unchanged (though the signal values will drop all in all the features should be clearly visible). If the movement is towards worse alignment, the modulation patterns start to vanish (the hills and pits even out) before the signal at the diffractive area starts to get lower. For the best alignment the signal from the large diffractive area should be at its minimum (see Figure 5.7).

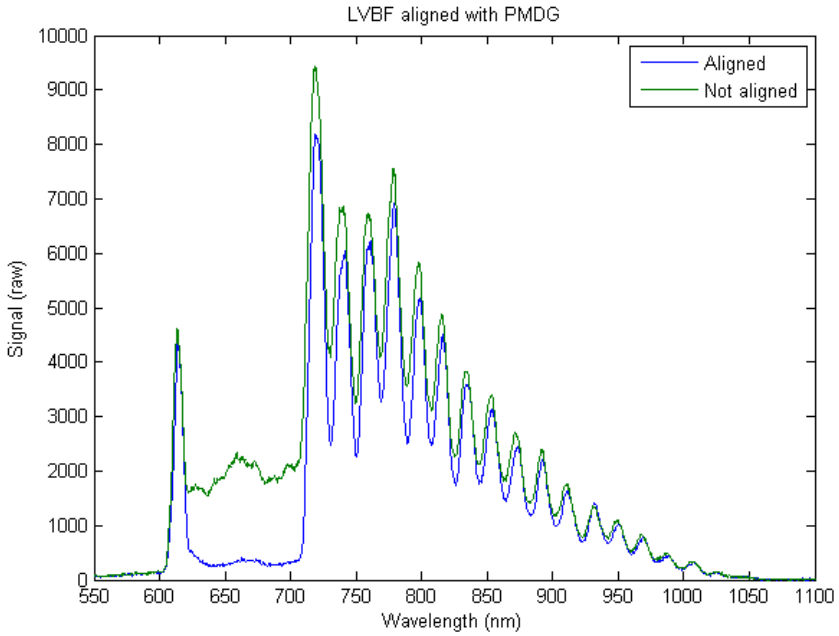

Figure 5.7. LVBF and PMDG aligned. Somewhat misaligned and then corrected LVBF position.

5.2.4 Results for Contrast Ratios

Centre wavelengths were defined with HR4000 spectrometer for the VIS LVBF. The measurements were carried out by programming a pattern with every fourth pixel in diffracting state and making four measurements to get all the pixels in diffracting state. The centre wavelengths were then checked from the modulated spectra by defining the centre point of each modulated signal minima. Using these centre wavelengths the control voltages were then calculated from the model (Equation 4.3). The control voltages were also measured and some variation between measured values and values from the model were found. There is also some variation between individual pixels on some wavelength range, meaning that some pixels require higher or lower voltages than neighbouring pixels in general. The model is of course unaware of such features. Interestingly it turned out, that the values from the model give lower signal when all the pixels are in diffraction than the ones that were measured. The values from the model are currently in use for the diffraction and the measured ones for the reflection.

Neighbouring pixels will have an effect on the contrast ratio. This is clearly visible between one and two pixels. Adding a third pixel does not add much to the contrast but will keep the centre wavelength the same (see Figure 5.8). Transmissions with

one pixel modulating is about 40 % and with two pixels about 10 %. The FWHM bandwidth of the LVBF is 1.5%, which means 10.5 nm @ 700 nm. The dispersion is almost constant at about 40 nm/mm, which turns out as about 4.8 nm shift in wavelength per pixel (120 μm). So the spectral bandwidth for each pixel is wider than the spectral shift between adjacent pixels and thus the bands will overlap. This will increase spectral resolution but may have an effect to the relative spectral features. What is actually measured is the difference in signal between reflected and diffracted states. If the modulation is not clear enough, any spectral features will remain unnoticed.

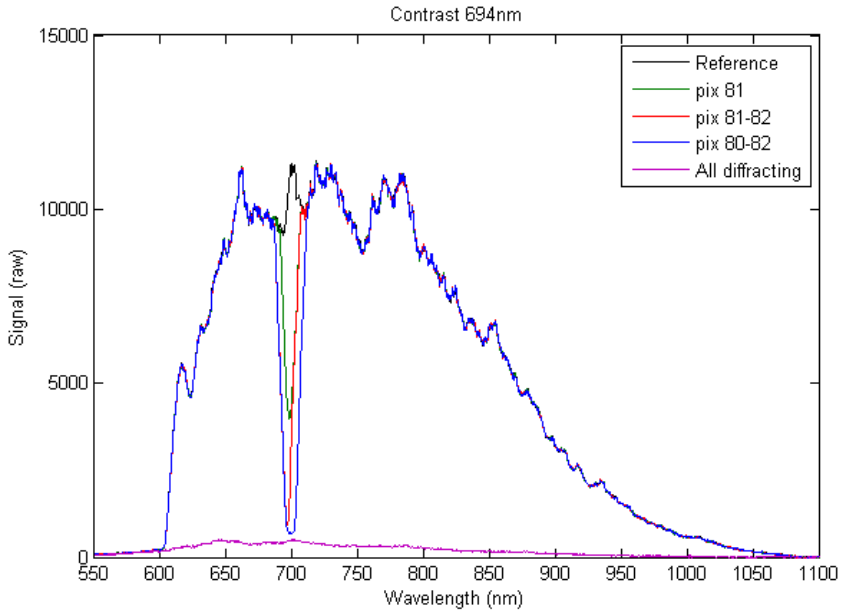

Figure 5.8. Demonstrator modulation contrast with one, two and three pixels in diffracting state. The background signal in the all diffractive state is due to somewhat diffuse ghost reflection from the LVBF aperture.

Since the transmission for certain channel depends on how many pixels in the immediate vicinity are in the same state, the transmission corrected Hadamard transform method will be almost impossible to pull through. Using some compromise value for channel transmissions only made the spectrum recovery worse. Due to this the spectrum recovery method for Hadamard technique will be using only uncorrected IHT, $\Psi = S^{-1}\eta$. The transmissions can be corrected later on with some loss in signal-to-noise ratio.

5.2.5 Results for Spectrometer Level Tests

The demonstrator input fibre was illuminated with FWHM = 4 nm monochromator lines from HR-640 and the signal was measured with line scan and Hadamard methods. The signal levels were really low and because the measurement takes time for about 2 minutes (about 1s per measurement point or pattern from which 50 ms is for signal integration and rest is for pattern change due to LabVIEW), the detector or amplifier can be seen drifting slowly throughout the measurements (probably caused by the averaging of the 1/f noise of the amplifier). The drifting is in a scale of μV but it has an effect on these signal levels. For line scan this means that the bottom line is not horizontal. Hadamard transform method will handle small drifts in a cleaner way and the drifting causes only some signal spikes, negative or positive depending on the drift, on certain locations of the spectrum that are directly related to the size of the used Hadamard matrix.

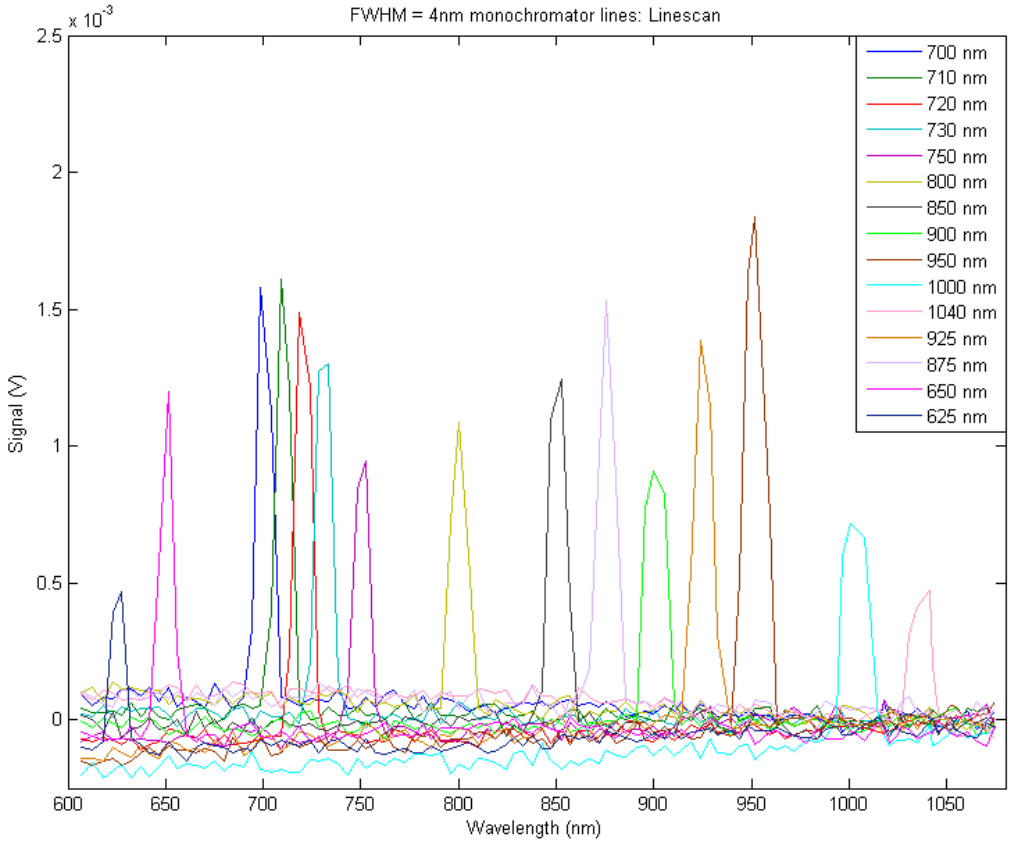

Figure 5.9. Monochromator lines from HR-640 measured with line scan method.

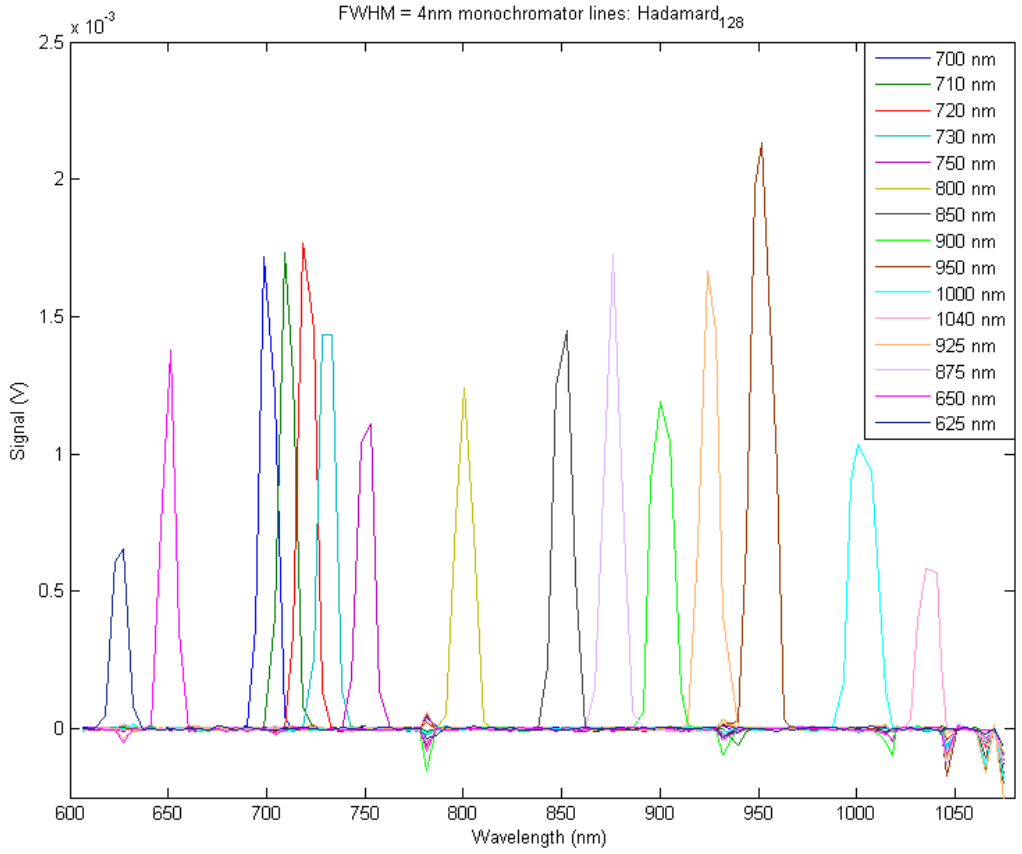

Figure 5.10. Monochromator lines from HR-640 measured with the Hadamard method. The small spikes where multiple lines can be seen are caused by the drift.

The effect of drifting with Hadamard mode is verified with the simulator (see Figure 5.11(b)). Some scans were done with the simulator with 700nm monochromator line as a test signal and with strong linear drifting to verify and emphasise the effects the drifting causes. The simulator has the same pixels (98 and 100, the last two spikes are caused by these) disabled as in the actual case. There is some additional effect in the real measurement, which increases the depth of the signal spikes caused by the bad pixels, that cannot be verified with the simulator. This could be due to the positions of the adjacent pixels as the simulator is ideal to that extent and it is a very difficult feature to simulate.

Light from 632.8 nm HeNe laser was also measured. The demonstrator measured the laser line to be at 633.2 nm and the FWHM was 6.7 nm. Stability was measured with 700 nm and 800 nm monochromator lines with the demonstrator running many hours continuously. For some reason there was a lot more noise but almost no signal

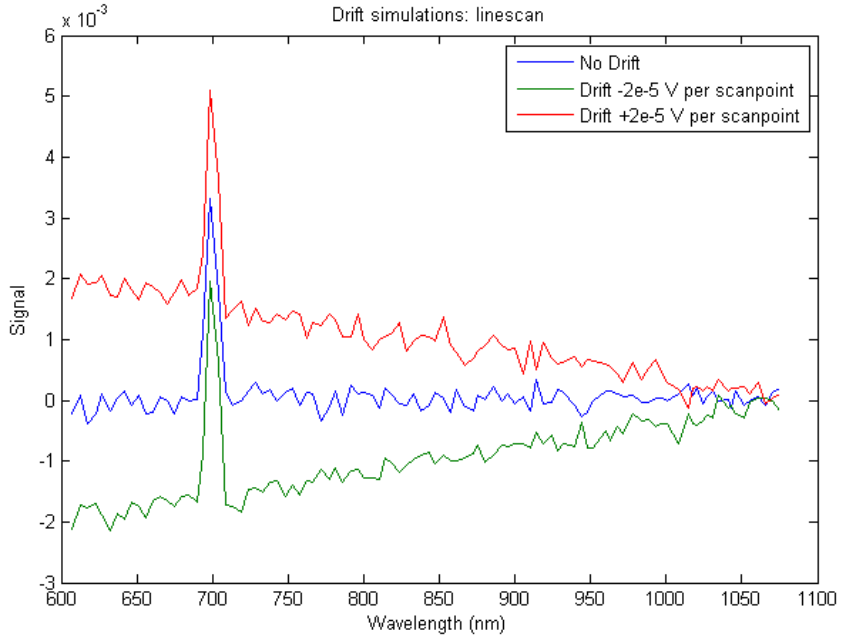

(a)

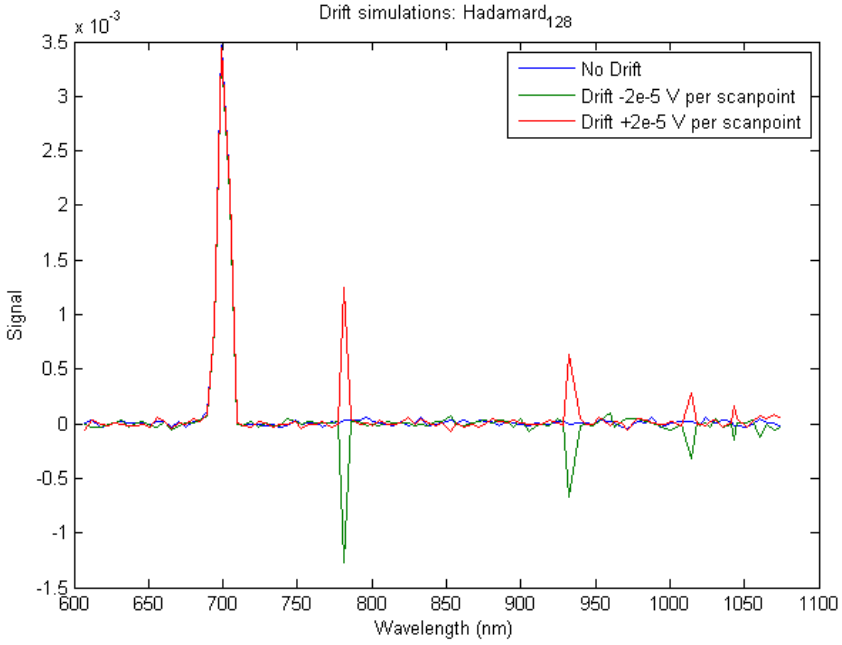

(b)

Figure 5.11. The effect of drift for a) line scan and b) Hadamard transform method as simulated for 700 nm spectral line from monochromator. The measurement goes from longer wavelengths to shorter. The simulation uses only a linearly drifting baseline but the locations of the extra spikes are the same as in the measured spectrum in Figure 5.10.

Table 5.4. Wavelength accuracy from monochromator measurements. The full-width at half-maximums for monochromator measurements with line scan and Hadamard are also reported. The monochromator output was FWHM = 4 nm. Noise has more effect on accuracy in line scan than with Hadamard transform.

Wavelength	FWHM (line)	Accuracy	FWHM (Hadamard)	Accuracy
625 nm	7.8 nm	+1.6 nm	9.2 nm	+1.3 nm
650 nm	7.5 nm	+1.7 nm	8.0 nm	+1.6 nm
700 nm	9.3 nm	+0.7 nm	9.4 nm	+0.6 nm
710 nm	9.2 nm	+0.4 nm	9.1 nm	+0.2 nm
720 nm	9.4 nm	+0.2 nm	9.6 nm	+0.1 nm
730 nm	9.4 nm	+0.6 nm	9.4 nm	+0.5 nm
750 nm	9.1 nm	+0.0 nm	9.5 nm	−0.2 nm
800 nm	11.0 nm	−1.0 nm	10.8 nm	−0.8 nm
850 nm	10.2 nm	−0.4 nm	10.6 nm	−0.1 nm
875 nm	9.4 nm	+0.1 nm	9.3 nm	+0.0 nm
900 nm	14.1 nm	+0.2 nm	14.0 nm	+0.6 nm
925 nm	10.3 nm	−0.9 nm	10.4 nm	−0.7 nm
950 nm	13.4 nm	−0.4 nm	13.9 nm	−0.6 nm
1000 nm	15.5 nm	−0.5 nm	16.3 nm	−0.5 nm
1040 nm	11.9 nm	−1.0 nm	11.8 nm	−1.0 nm

drifting compared to the measurements done on another day. Resulting spectral drift was towards shorter wavelengths at 0.1 nm/120 min.

Transmissions of various filters were also measured with line scan and Hadamard modes, and the results were compared to HR4000 spectrometer (see Figures 5.14 and 5.15). Measured filters were two high-pass filters for wavelengths >695 nm and >850 nm, and various interference filters found from the lab. Transmission bands and centre wavelengths for narrow band filters align very accurately with the high resolution reference of the HR4000 spectrometer. Hadamard transform method has some additional features caused by the drift.

The effects of polarisation were measured also with the working demonstrator by using Codixx ColorPol VIS 700 BC3 C633 polariser (Figure B.2) and measuring the output with HR4000. Glan-Thompson polariser was not used because the polariser has to be after the input inside the demonstrator and the Glan-Thompson was

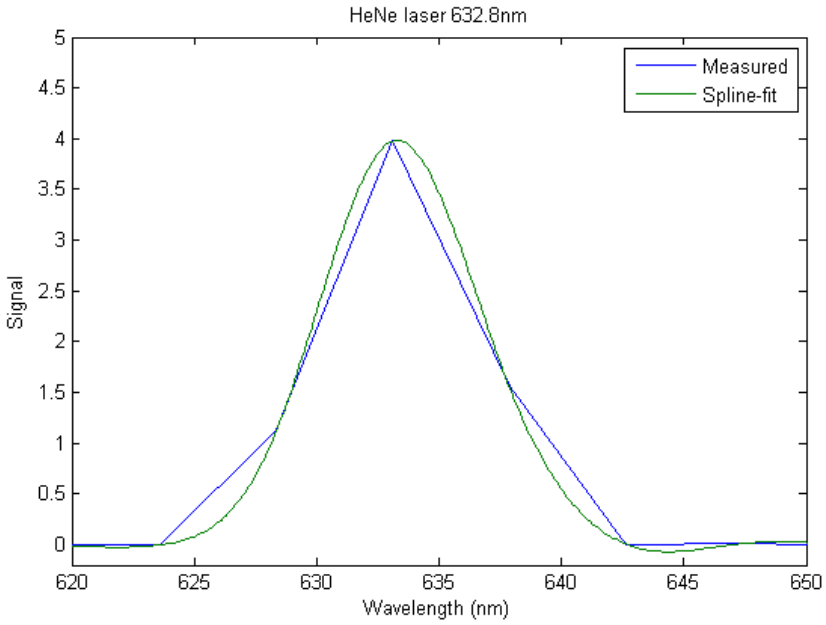

Figure 5.12. HeNe laser scan with demonstrator. Measured CWL = 633.2 nm and FWHM = 6.7 nm

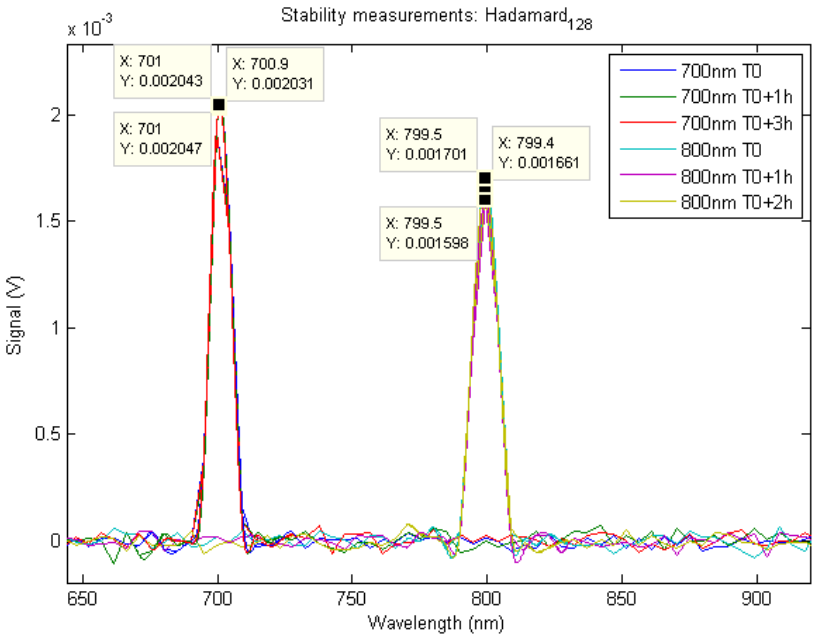

Figure 5.13. Stability measurements. Centre wavelengths for the two monochromator lines drifted only 0.1 nm in 2-3 hours. The measurements done a couple of days before gave 700.6 nm and 799.2 nm for the same wavelengths.

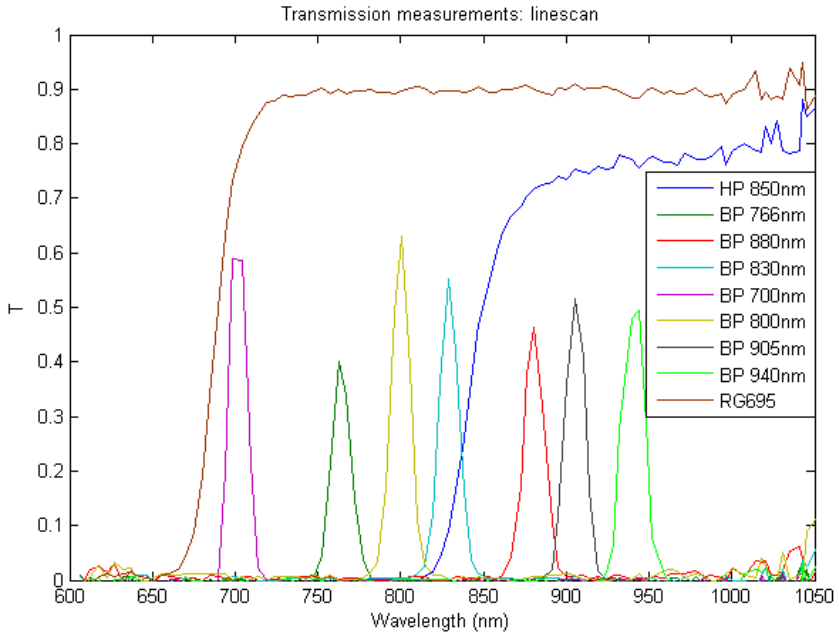

(a)

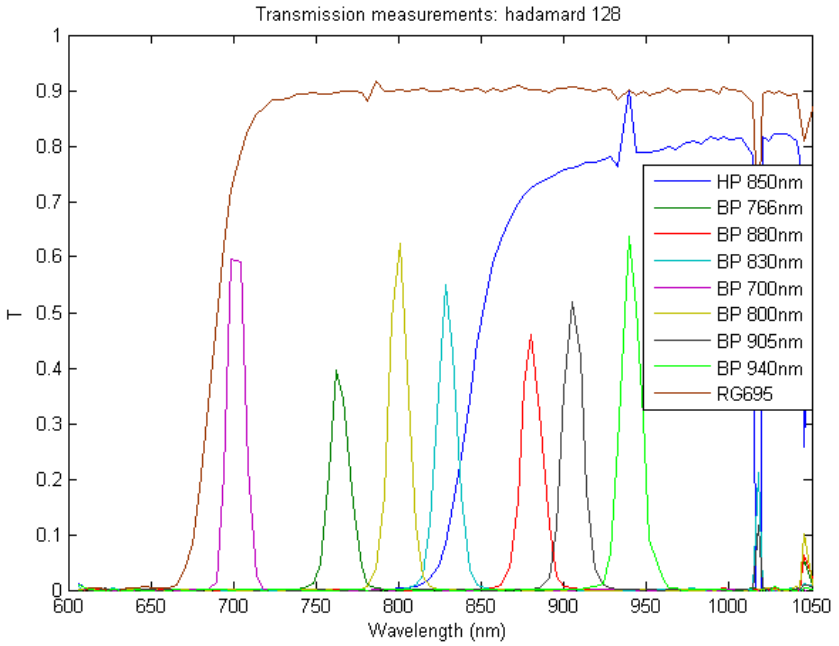

(b)

Figure 5.14. Transmission of various filters measured with a) line scan and b) Hadamard. The signal spikes in the HP850 and RG695 measurements with Hadamard are caused by the drift, the BP 940nm result gets also a bit better transmission than in line scan for the same reason.

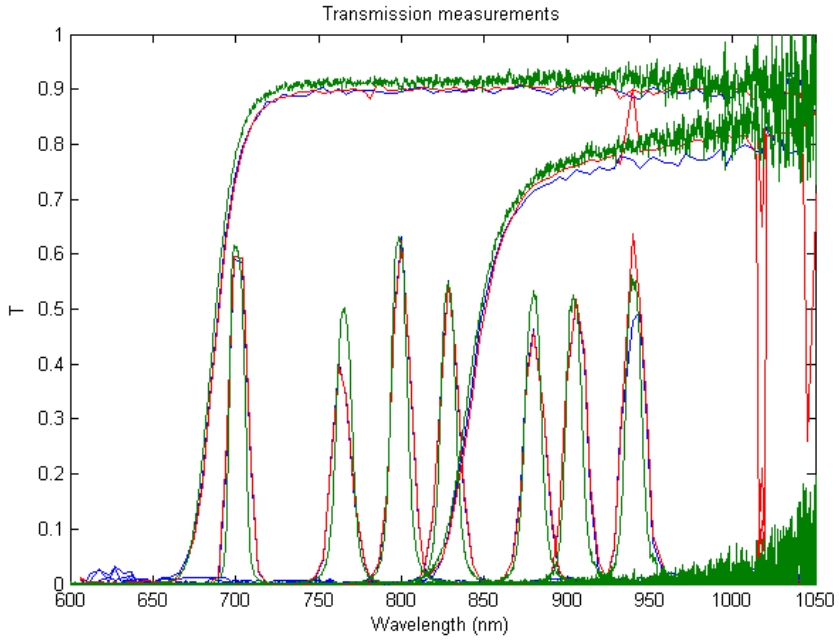

Figure 5.15. All the transmission measurements in the same figure with line scan (blue), Hadamard (red) and HR4000 (green). Transmission bands and centre wavelengths for narrow band filters align very accurately with the high resolution reference of the HR4000 spectrometer.

too large to be inserted there. Nevertheless, the results in Figure 5.16 show the same anomalies in TE polarisation that were previously measured with the PMDG component in Chapter 4.

Throughput measurements were performed with HR-640 monochromator and QED-200 absolute detector using FWHM = 4 nm source signal. Measurements were done for ten points in the spectral range of the demonstrator. The signal was coupled with fibre to the demonstrator and the QED-200 was used to determine the optical power of the fibre output to the f-number of 8.5 the demonstrator uses. The following results were gathered (see Table 5.5). The results seem to get higher than what was estimated for the demonstrator. This is probably due to the fact that the estimated calculations did not take the broadening of the LVBF transmission band into account. With longer wavelengths the signal passes through a wider area resulting in increased throughput.

Correlation measurements were done with some filter transmissions. Signature was made from 800 nm interference filter and was tested against various other filters. Another signature was made from RG695 and BG36 filters and was again tested against various other filters. The signature means that the PMDG is programmed

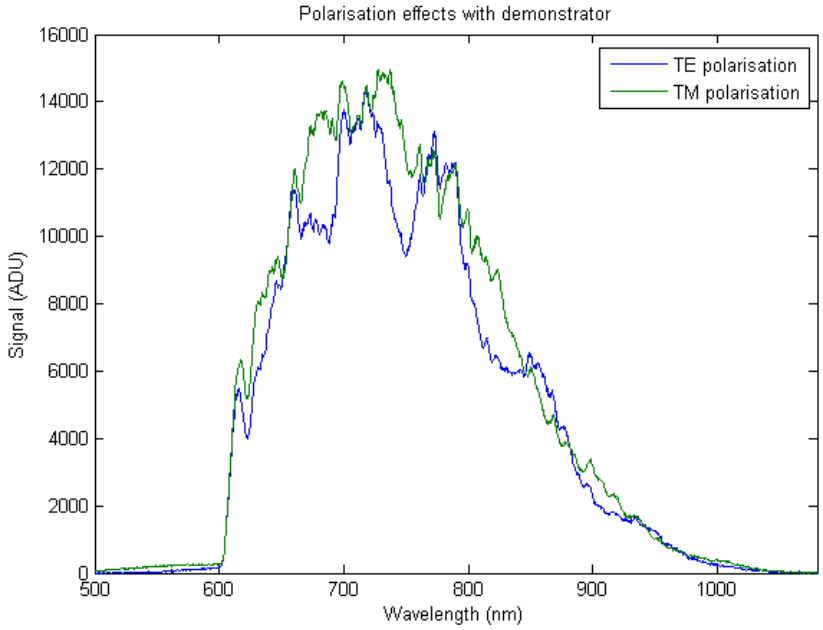

Figure 5.16. Polarisation effects with the demonstrator were measured with HR4000 and ColorPol polariser. TE polarisation shows the same anomalies as in Chapter 4.

Table 5.5. Throughput of the demonstrator. The throughput of longer wavelengths is higher than the estimated maximum throughput of 0.07%. The difference could be due to the broadening of the LVBF transmission band towards longer wavelengths.

Measurement wavelength (nm)	Throughput (%)
625	0.0265
671	0.0441
717	0.0701
763	0.0725
809	0.0883
855	0.0950
901	0.0936
947	0.0859
993	0.1225
1039	0.1341

to reflect signal according to the measured transmission spectra. The measurement takes two signal values – one with the signature and the other with fully reflecting

grating. The signature signal is then divided with the reflected signal. Correlation results are in line with what was to be expected with approximated SAM. Narrow features give much better correlation, whereas more complex signatures correlate too well with different spectra and the relative difference between right and wrong becomes small (see Table 5.6).

Table 5.6. Correlation results with signatures from 800 nm interference filter (BP800) and RG695+BG36 filters. See Figure 5.14 for the spectral features of the filters (- means untested).

	BP800	RG695+BG36
Test signal from	Correlation	Correlation
BP700	0.29	-
BP766	0.25	0.49
BP800	0.77	0.22
BP830	0.22	-
BP880	0.23	-
BP905	0.29	-
BP940	0.31	-
RG850	0.09	0.48
RG695	0.14	0.40
raw halogen	0.15	0.40
RG695+BG36	-	0.60
BG36	-	0.53

Noise measurements were done with the detector measuring the full reflection signal with no input, with narrow band illumination and with full halogen illumination to see if the photon noise of the ghost reflection would increase the noise levels. Dark signal with no input was also measured multiple times with line scan mode and Hadamard mode to assess the SNR improvement factor (see Table 5.7). The noise level of the line scan mode should be on the same scale as with the direct detector signal measurement.

The SNR improvement factor with Hadamard transform method can be calculated from the noise levels to be 6.5. Theory gives a value of 5.6. The difference is due to small drift in the line scan measurement. When corrected, the improvement factor is about 5.0.

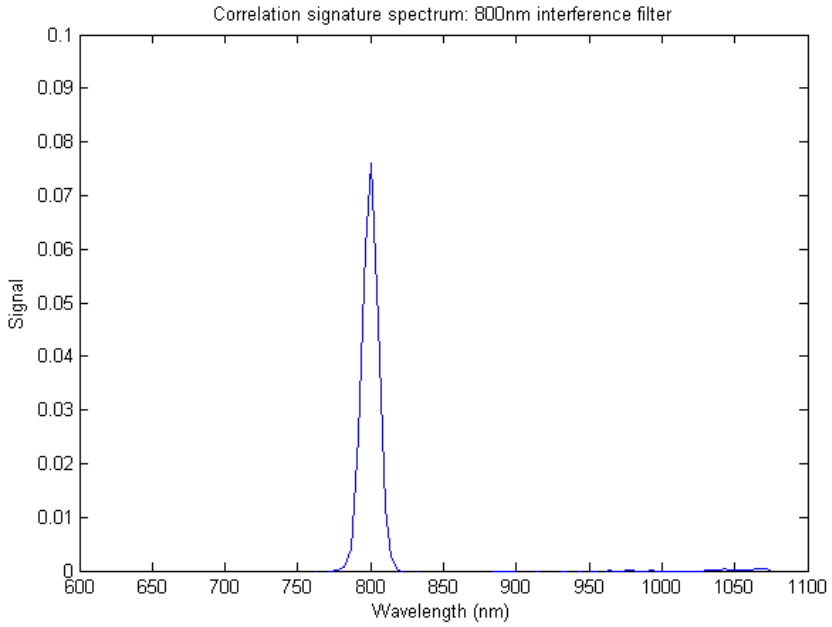

(a)

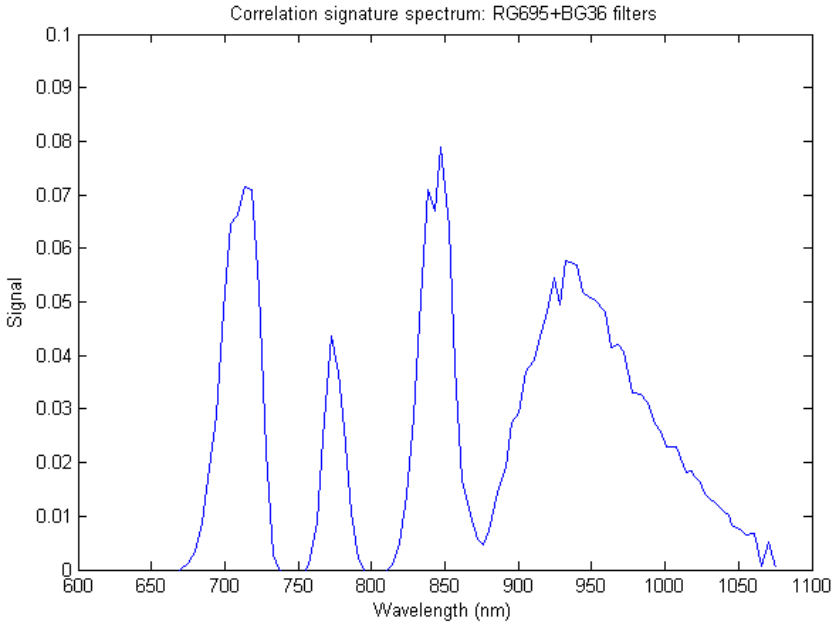

(b)

Figure 5.17. Sample spectra for correlation signatures were taken from halogen lamp through a) a 800 nm interference filter and b) RG695+BG36 filters. The signature means that the PMDG is programmed to reflect signal according to the measured transmission spectra.

Table 5.7. Noise values for certain measurements. When the demonstrator was illuminated with white light from the halogen lamp, the noise levels raised significantly because of the photon noise of the ghost reflection.

	Noise (V)
No light	2.0881×10^{-4}
Monochromator line 700 nm	1.7636×10^{-4}
Halogen lamp	0.0049
Line scan, no light	1.7484×10^{-4}
Hadamard_{128}, no light	2.7093×10^{-5}

Maximum SNR with the maximum attainable signal levels (10 V on one channel) is 2040 (66.2 dB) with photon noise. For average per-channel values (0.1 V) the SNR is 20.4 (26.2 dB). Optimised system with no ghost reflection would yield a maximum SNR of 57000 (95.1 dB) and an average per-channel SNR of 572 (55.1 dB) with line scan. Hadamard transform method will have five times better SNR compared to line scan method.

As a result from these measurements on the demonstrator with VIS LVBF, the spectral range can be determined to be 609-1060 nm, spectral resolution to be <1.5 % of centre wavelength and absolute wavelength accuracy to be ± 1.0 nm for most of the wavelength range. Throughput is <0.1 % which restricts the possible applications for this spectrometer. Hadamard transform method has about 5 times better signal-to-noise ratio than line scan.

Chapter 6

Conclusions

In this thesis, the feasibility of commercially available Programmable Micro Diffraction Gratings to be used in optical data processing or as a spatial light modulator in spectrometers for miniature space instruments was studied. The main spectrometer applications with PMDG components benefit from the fact that PMDGs are the only spatial light modulators for the IR range, they are also capable of using Hadamard transform spectral acquisition without moving parts and can be programmed for optical correlation. PMDG components are fast and can thus also be used as choppers. If every element is independently controllable, the PMDG could be used as a diffractive filter or as a reconfigurable grating. Downsides of the PMDG components are their size limitations, high control voltages and the need for large control electronics – especially for independent element control.

Some instrument concepts for PMDG devices were discussed and the selected PMDG component was characterised. An instrument demonstrator was developed based on the performance of the component, and the properties of the demonstrator were then characterised.

The built demonstrator, with only one detecting element and with a very simple optical design granted by the use of a LVBF, can measure a spectrum of the target by means of line scan or Hadamard transform methods. It can also do a single-point optical correlation measurements, that approximate spectral angle mapper technique used with hyperspectral data, to see if the target spectrum contains features programmed on the PMDG. It is true that the LVBF could be directly integrated on the top of a sensor array to make the overall structure even more compact. Such spectrometers for Si detector arrays in VIS and NIR domain (320 - 1100 nm) have been presented by JDS Uniphase. When the wavelength is increased beyond the operation range of InGaAs detectors, 1700 nm or 2500 nm for extended InGaAs,

things get more complicated. Even the standard InGaAs arrays cost many times more than Si arrays. A single detector system is very appealing for the IR range where detector materials are expensive and sensor arrays hard to manufacture. The signal-to-noise ratio can also be better than with detector arrays especially with designs using LVBFs because the throughput has the same limitations.

The goal of making the optical structure of the demonstrator as simple as possible had quite severe effects on the throughput of the system. A diffraction grating would have been a much better alternative than the linear variable bandpass filter. On the other hand, the LVBF allows much smaller dimensions and simpler optical structure than a normal static diffraction grating ever would. The original idea to use the LVBF included the use of the off-band transmission blocking to negate the diffracted signals – a feature which was later obtained with optical design. One way to utilise the best features of both components could be to use the grating to disperse the signal before collimation and then use the LVBF to enhance the off-band transmission blocking for diffracted signals. To improve the throughput using only the LVBF, the PMDG should have longer elements so that the grating area would be larger.

The intensity of the ghost reflection from the LVBF aperture came as a total surprise as the aperture is tilted and should not pass the direct reflection to the detector. Thus the reflection must be somewhat diffuse and according to this the intensity should be low. The signals of the individual channels are still much lower and thus the demonstrator tries to measure small modulation on top of huge base signal with all its noise. It does not appear as bad in the contrast measurement with the HR4000 spectrometer, but with the demonstrator utilising only a single detector element, the signal from all those individual wavelengths will be summed. To improve this, the first aperture after the right angle mirror should be made as a slit.

Another flaw in the single detector system is that it can only use a fraction of its true detecting potential for single channel. When the detector/AD converter is saturated at 10 V, the signal for single channel is on average this value divided with the number of channels – 0.1 V for a system with 100 channels. This is particularly true for the line scan. For the Hadamard transform method, the situation is better since half of the channels are measured at each measurement point. The amount of light reaching the detector is measured with all the pixels in reflective state as this method applies to all situations. Otherwise one would have to know which channel has the most signal before measuring. The dispersion of the dispersive element and the pixel width should be optimised to improve contrast. The spectral bands on adjacent pixels should have minimal overlap, although it does give a better spectral

resolution.

To better encounter the low throughput of the system design, the PMDG could also work as a chopper for a lock-in amplified measuring system. The PMDG would switch its state between the full diffracting state and the measurement pattern state, multiple times at a single measurement point. To better test this feature, the PMDG control should be on a microcontroller, which would allow much higher control rates. Using only one chop cycle per measurement point, in order to take the dark measurement before every signal measurement, should reduce the effect of drifting. This is verified with simulations but has not been tested as of yet.

Low throughput is the main factor restricting the possible space use for this instrument. Light is not usually a commodity when measuring reflected or backscattered signal from the target – especially in the IR domain. With improved design, i.e. when the active areas of the PMDG and the LVBF are larger, and with long signal integration times, the demonstrator could be used in short range remote sensing missions. Favouring attributes for these missions are the simplicity of the optical design, sturdy mechanical structure and the lack of moving parts. With the use of static diffraction gratings for dispersion, the throughput would be on a whole different level. This approach, with more complicated optical design, was already used by Polychromix in their DTS line of spectrometers and thus was not studied in this project. Even with more complicated optical design, the benefits in the IR domain are substantial and the structure of the PMDG could also be made more compatible for imaging systems.

From the overall measurements and system design it seems that the PMDG devices are a promising candidate for future instruments but the technology is not quite there yet. This does not mean that these components do not work. It just means that for better performance the PMDG must be optimised for each concept. Overall, the PMDG could use longer and narrower elements with smaller gaps, have greater deflection range and have all the elements independently controllable. However, the independent control of all elements is unnecessary in applications that use pixels. If the elements were oriented differently, diffracted orders could be filtered out. As the technology matures and the production costs get lower, custom designed components will be more readily available.

Bibliography

[1] European Space Agency, Directorate of Technical and Quality Management, "Statement of work: Instrument concepts using dynamic diffraction gratings", 5.7.2006.

[2] Araya Pothisorn and Alex J. Hariz, "Deformable grating light modulator array for use as wavelength-selective switch", in *Proc. SPIE Micro- and Nanotechnology: Materials, Processes, Packaging, and Systems III*, vol. 6415, 2006.

[3] Peter Fortescue *et al*, *Spacecraft Systems Engineering*, Third Edition, Wiley, 2003.

[4] Wiley J. Larson and James R. Wertz, *Space Mission Analysis and Design*, Second Edition, Microcosm Inc, 1992.

[5] Nicholas M. Short, *Remote sensing tutorial introduction - Part 2*, Page 1, NASA, "http://rst.gsfc.nasa.gov/Intro/Part2_1.html".

[6] P.N. Slater, *Optics and Optical Systems*, Addison-Wesley, 1980.

[7] NASA Facts - Mars Science Laboratory, Jet Propulsion Laboratory, "http://mars.jpl.nasa.gov/msl/newsroom/pdfs/MSL-200608.pdf", Oct 2006.

[8] B.K. Harms *et al*, "An introduction to Hadamard spectrometry and the multiplex advantage", *IEEE Instrumentation and Measurement Technology Conference*, IMTC-89 Conference Record, 6th IEEE, April 1989.

[9] Daryl W. Fothergill, *A prototype Hadamard imaging system*, Master's Thesis, North Carolina State University, 2005.

[10] R.A. Dyer *et al*, "Implementation problems in Hadamard transform spectrometry", *IEEE Transactions on Instrumentation and Measurement*, vol. 39, no. 1, February 1990.

[11] Christopher Palmer and Erwin Loewen, *Diffraction Grating Handbook*, Sixth Edition, Newport Corporation, 2005.

[12] Stephen D. Senturia, *Microsystem Design*, 2nd edition, Springer, 2004.

[13] Jahja I. Trisnadi, Clinton B. Carlisle and Robert Monteverde, "Overview and applications of Grating Light Valve based optical write engines for high speed digital imaging", *Photonics West 2004*, January 26 2004, San Jose, CA, USA.

[14] Robert Corrigan, Randy Cook, and Olivier Favotte, "Silicon Light Machines - Grating Light Valve technology brief", Silicon Light Machines, 2001.

[15] Eiichi Tamaki, Yoshimi Hashimoto and Omar Leung, "Computer-to-plate printing using the Grating Light Valve device", *Photonics West 2004*, January 26 2004, San Jose, CA, USA.

[16] Stephen D. Senturia, David R. Day, Michael A. Butler and Malcolm C. Smith, "Programmable diffraction gratings and their uses in displays, spectroscopy, and communications", *J. Microlith., Microfab., Microsyst.*, vol. 4, Oct-Dec 2005.

[17] David T. Amm and Robert W. Corrigan, "Optical performance of the Grating Light Valve technology", *Photonics West 1999 - Projection Displays V*, 1999.

[18] Alexander Payne, Wilhelmus DeGroot, Robert Monteverde and David Amm, "Enabling high data-rate imaging applications with Grating Light Valve technology", *Photonics West 2004 - Micromachining and Microfabrication Symposium*, January 26 2004, San Jose, CA, USA.

[19] Ito *et al.*, "High-performance blazed GxL device for large-area laser projector", *Proc. SPIE MOEMS Display, Imaging and Miniaturized Microsystems IV*, vol. 6114, 2006.

[20] Yariv Geller and Mouli Ramani, "MEMS-based digital transform spectrometers", *Laser+Photonik*, 1/2006, Carl Hanser Verlag GmbH & Co. KG, 2006.

[21] E.R. Deutsch *et al*, "A large-travel vertical planar actuator with improved stability", *IEEE: The 12th International Conference an Solid State Sensors, Actuators and Microsystems*, Boston, 2003.

[22] David R. Day *et al*, "Diffractive-MEMS implementation of a Hadamard near-infrared spectrometer", *IEEE: The 13th Intemational Conference on Solid-State Sensors, Actuators and Microsystems*, Seoul, Korea, 2005.

[23] Yariv Geller, Director of Business Development, *Polychromix partners with NASA in development of Lunar spectroscopy solution*, Polychromix News Page, "http://www.polychromix.com/viewstory.php?id=12&option=pr".

[24] Sinclair *et al*, "A MEMS based correlation radiometer", *Proc. SPIE MOEMS and Miniaturized Systems IV*, vol. 5346, 2004.

[25] Jaap Verheggen, Ganesh Panaman and James Castracane, "Characterization and fabrication of MOEMS-based diffractive optical switching elements", *Proc. SPIE MOEMS Display, Imaging and Miniaturized Microsystems IV*, vol. 6114, 2006.

[26] Ganesh Panaman, Seth Madison, Michael Sano and James Castracane, "Performance improvements of MOEMS-based diffractive arrays: address isolation and optical switching", *Proc. SPIE MOEMS and Miniaturized Systems V*, vol. 5719, 2005.

[27] J. Agostinelli *et al*, "GEMS: a simple light modulator for high-performance laser projection display", International Display Workshops (IDW '06) Paper, 2006.

[28] John Brazas and Marek Kowarz, "High-resolution laser-projection display system using a Grating Electromechanical System (GEMS)", *Proc. SPIE MOEMS Display and Imaging Systems II*, vol. 5348, 2004.

[29] Newman *et al*, "MEMS programmable spectral imaging system for remote sensing", *Proc. SPIE Spaceborn Sensors III*, vol. 6220, 2006.

[30] Marek W. Kowarz, James G. Phalen and Chris J. Johnson, "Line-scanned laser display architectures based on GEMS technology: from three-lens three-chip systems to low-cost optically efficient trilinear systems", SID 06 DIGEST, The Society for Information Display, 2006 SID.

[31] Zhihai Zhang *et al*, "Fabrication improvement of the Grating Light Modulator", *Proceedings of the 1st IEEE International Conference on Nano/Micro Engineered and Molecular Systems*, January 2006.

[32] Mauri Aikio, *Hyperspectral Prism-Grating-Prism Imaging Spectrograph*, ser. VTT Publications 435, VTT Technical Research Centre of Finland, Espoo, 2001, Ph.D. dissertation.

[33] Uula Kantojärvi, *Feature-specific on-board technology for airborne spectral imaging*, Master's Thesis, Helsinki University of Technology, Department of Electrical and Communications Engineering, Oct 23, 2006.

[34] Uula Kantojärvi *et al*, "Performance of the Imaging Spectral Signature Instrument (ISSI) breadboard", *Proc. SPIE Sensors, Systems, and Next-Generation Satellites XI*, vol. 6744, 2007.

[35] W.J. Smith, *Modern Optical Engineering*, McGraw-Hill, 2000.

[36] M.C. Hutley, *Diffraction Gratings*, Academic Press, 1982.

[37] Eugene Hecht, *Optics*, 4th Edition, Addison Wesley, 2002.

Appendix A

Mechanical Parts and Integration

Some photos of the mechanical parts as well as some photos from the integration are shown in the following.

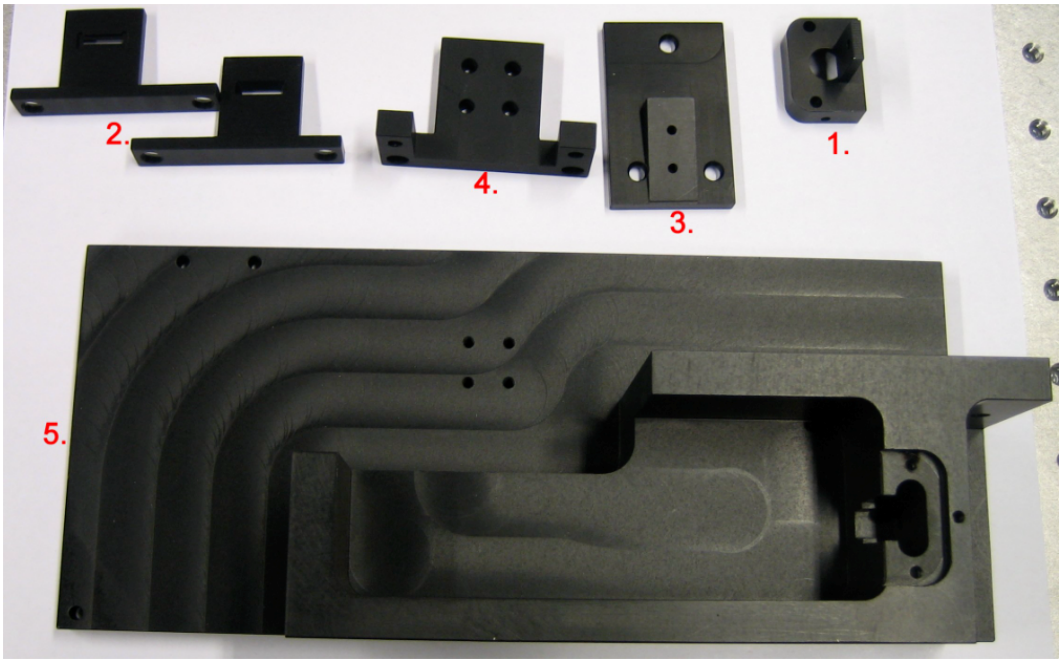

Figure A.1. Mechanical parts of the demonstrator. The pitch & yaw platform as well as the travel translation stage are missing from this shot. The shown parts are: 1. the fibre/lens input adapter with aperture, 2. the mounting apertures for the LVBFs, 3. the mounting platform for the PMDG, 4. the holder for the travel translation stage, on which the PMDG is mounted using part 3, 5. the frame.

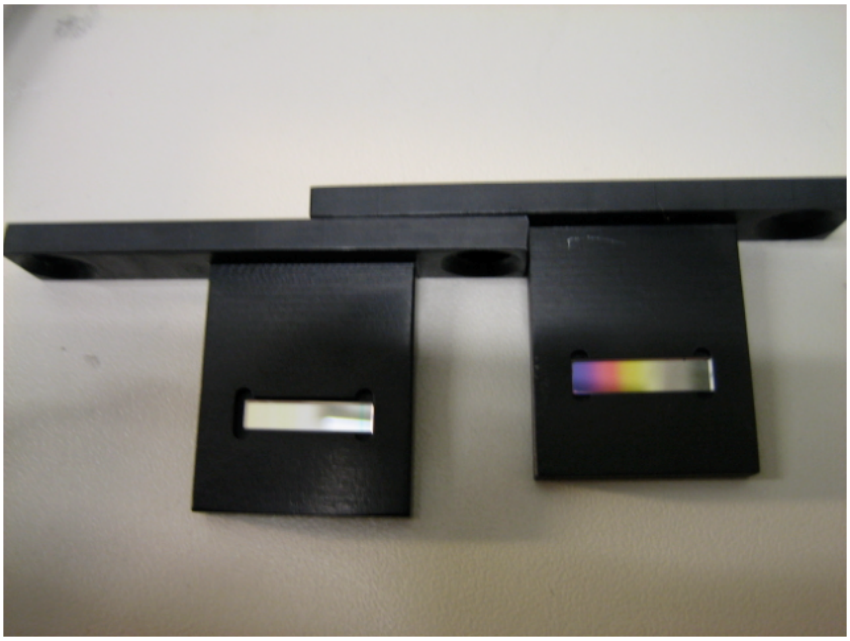

Figure A.2. Mounting apertures for the LVBFs with the visual and NIR LVBFs mounted in their holders.

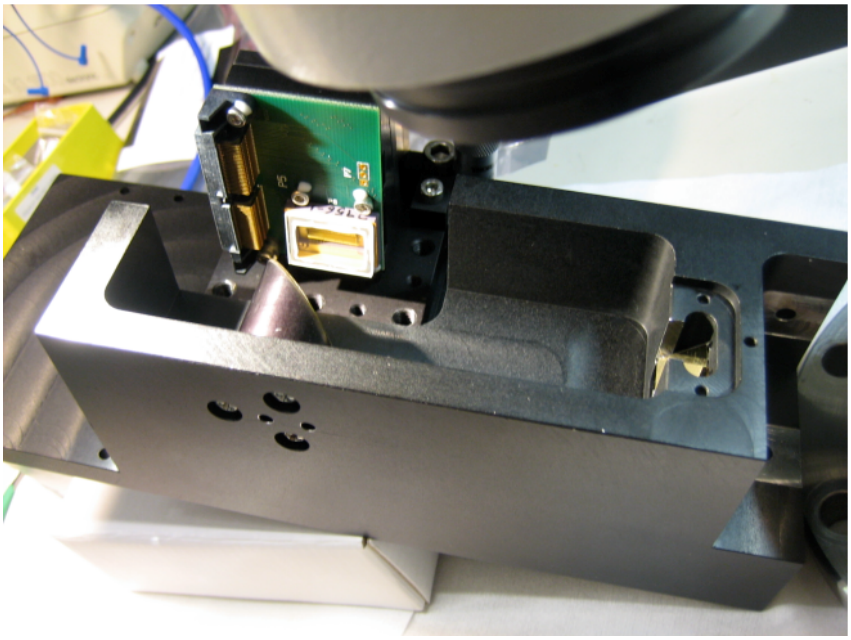

Figure A.3. Glueing of the right angle mirror. Glueing was done under a microscope and with the whole frame tilted.

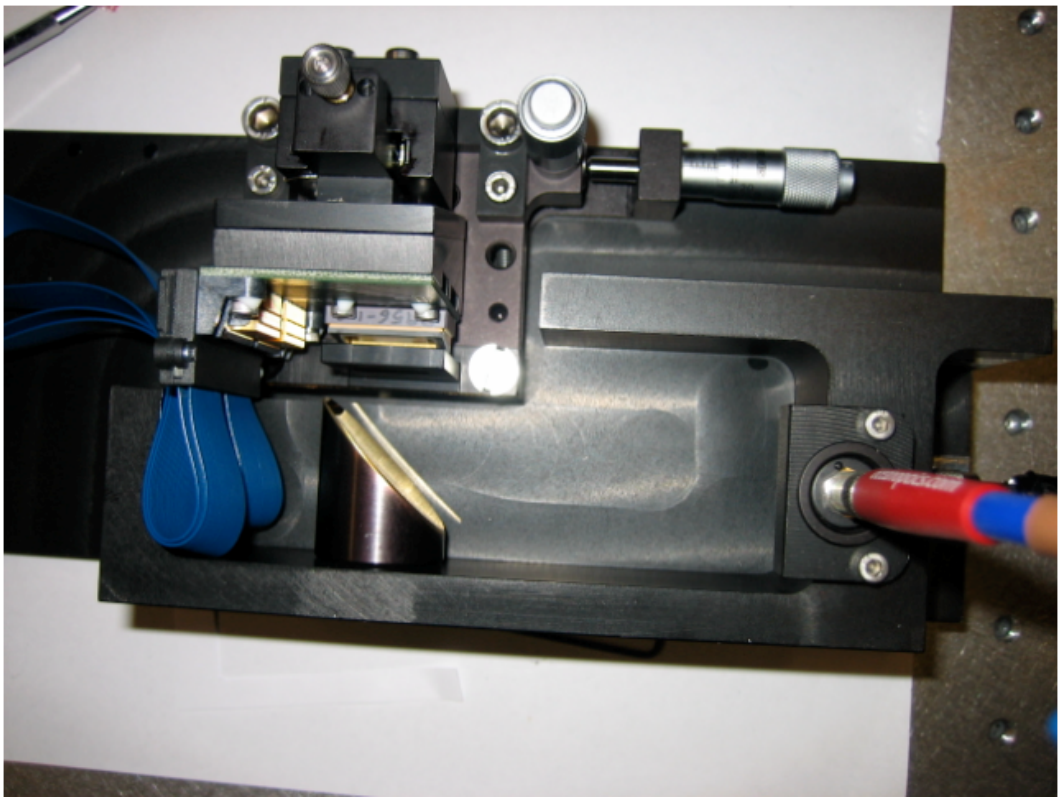

Figure A.4. Integrated demonstrator with the fibre optics connection. There is also fibre optic connection to a reference spectrometer instead of the detector.

Appendix B

Specifications for Certain Components

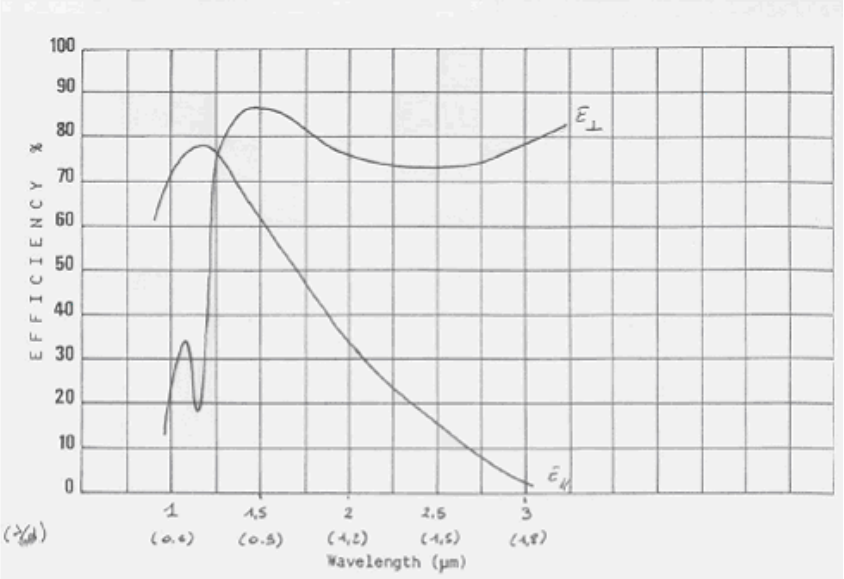

Figure B.1. Specifications for the grating used in the HR-640 monochromator.

colorPol® VIS 700 BC3 C633	
Spectral range	VIS-NIR
Wavelength range with **contrast > 1 000 : 1** (1) Transmittance (antireflection coating 633 nm)	550 to 900 nm > 81 % up to 92 % > 90 % at 633 nm
Filter size Filter thickness (2)	up to 50x30 mm² 220 ± 20 µm
Acceptance angle Polarization axis Operating temperature	± 20° < 0.5° to indicated edge -50 to +400 °C

(1) contrast: ratio of parallel to perpendicular transmittance
(2) other thicknesses on request

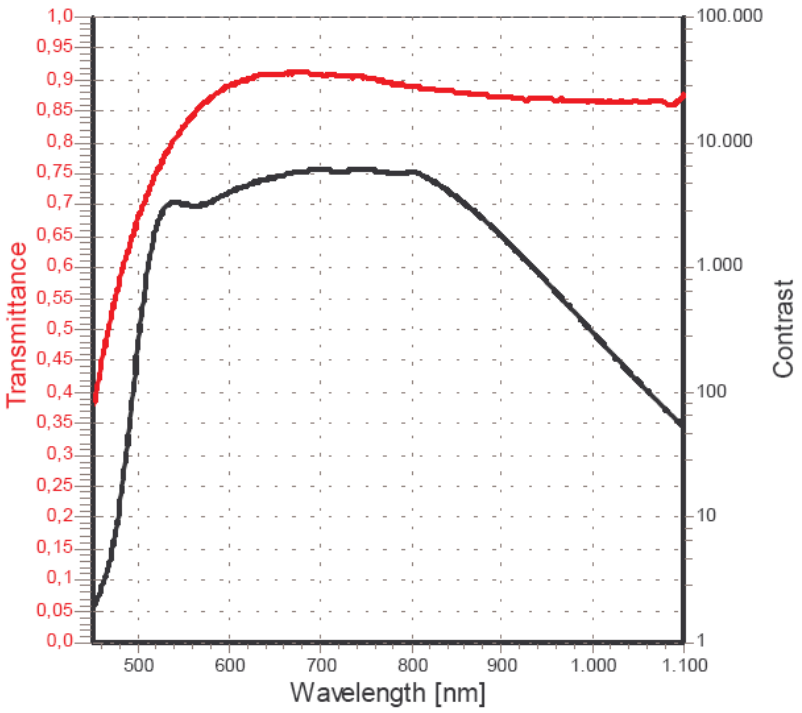

Figure B.2. Specifications for the ColorPol VIS 700 BC3 C633 polariser.